



JOSUÉ LABAKI SILVA

**Vibration of Flexible and Rigid Plates on
Transversely Isotropic Layered Media**

*Vibração de Placas Flexíveis e Rígidas em Meios
Estratificados Transversalmente Isotrópicos*

118/2012

CAMPINAS
2012



UNICAMP

UNIVERSIDADE ESTADUAL DE CAMPINAS
FACULDADE DE ENGENHARIA MECÂNICA

JOSUÉ LABAKI SILVA

Vibration of Flexible and Rigid Plates on Transversely Isotropic Layered Media

Orientador: Prof. Dr. Euclides de Mesquita Neto

Vibração de Placas Flexíveis e Rígidas em Meios Estratificados Transversalmente Isotrópicos

Doctoral Thesis presented to the School of Mechanical Engineering, University of Campinas, to obtain the Ph.D. degree in Mechanical Engineering, in the area of Solid Mechanics and Mechanical Design.

Tese de Doutorado apresentada à Faculdade de Engenharia Mecânica da Universidade Estadual de Campinas, para obtenção do título de Doutor em Engenharia Mecânica, na área de Mecânica dos Sólidos e Projeto Mecânico.

ESTE EXEMPLAR CORRESPONDE À VERSÃO
FINAL DA TESE DEFENDIDA PELO ALUNO
JOSUÉ LABAKI SILVA, E ORIENTADA PELO
PROF. DR. EUCLIDES DE MESQUITA NETO.


ASSINATURA DO ORIENTADOR

CAMPINAS
2012

FICHA CATALOGRÁFICA ELABORADA PELA
BIBLIOTECA DA ÁREA DE ENGENHARIA E ARQUITETURA - BAE - UNICAMP

L111v Labaki, Josué, 1982-
 Vibração de placas flexíveis e rígidas em meios
 estratificados transversalmente isotrópicos / Josué Labaki
 Silva. --Campinas, SP: [s.n.], 2012.

 Orientador: Euclides de Mesquita Neto.
 Tese de Doutorado - Universidade Estadual de
 Campinas, Faculdade de Engenharia Mecânica.

 1. Fundações (Engenharia). 2. Placas (Engenharia).
 3. Interação solo-estrutura. 4. Anisotropia. 5. Green,
 Funções de. I. Mesquita Neto, Euclides de, 1956-. II.
 Universidade Estadual de Campinas. Faculdade de
 Engenharia Mecânica. III. Título.

Título em Inglês: Vibration of flexible and rigid plates on transversely isotropic
layered media

Palavras-chave em Inglês: Foundations, Plates (Engineering), Soil-structure
interaction, Anisotropy, Green's functions

Área de concentração: Mecânica dos Sólidos e Projeto Mecânico

Titulação: Doutor em Engenharia Mecânica

Banca examinadora: Renato Pavanello, Pérsio Leister de Almeida Barros, Ney
Augusto Dumont, Nimalsiri Dharmakeerthi Rajapakse

Data da defesa: 18-07-2012

Programa de Pós Graduação: Engenharia Mecânica

UNIVERSIDADE ESTADUAL DE CAMPINAS
FACULDADE DE ENGENHARIA MECÂNICA
COMISSÃO DE PÓS-GRADUAÇÃO EM ENGENHARIA MECÂNICA
DEPARTAMENTO DE MECÂNICA COMPUTACIONAL

Ph.D. THESIS

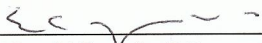
**Vibration of Flexible and Rigid Plates on
Transversely Isotropic Layered Media**

*Vibração de Placas Flexíveis e Rígidas em Meios
Estratificados Transversalmente Isotrópicos*

Author: Josué Labaki Silva

Advisor: Prof. Dr. Euclides de Mesquita Neto

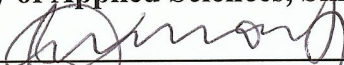
The following members of the Defense Committee have approved this Thesis:



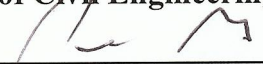
Prof. Dr. Euclides de Mesquita Neto, President
Department of Computational Mechanics, Unicamp



Prof. Dr. Nimalsiri Dharmakeerthi Rajapakse
Faculty of Applied Sciences, Simon Fraser University



Prof. Dr. Ney Augusto Dumont
Department of Civil Engineering, Pontifical Catholic University PUC-RJ

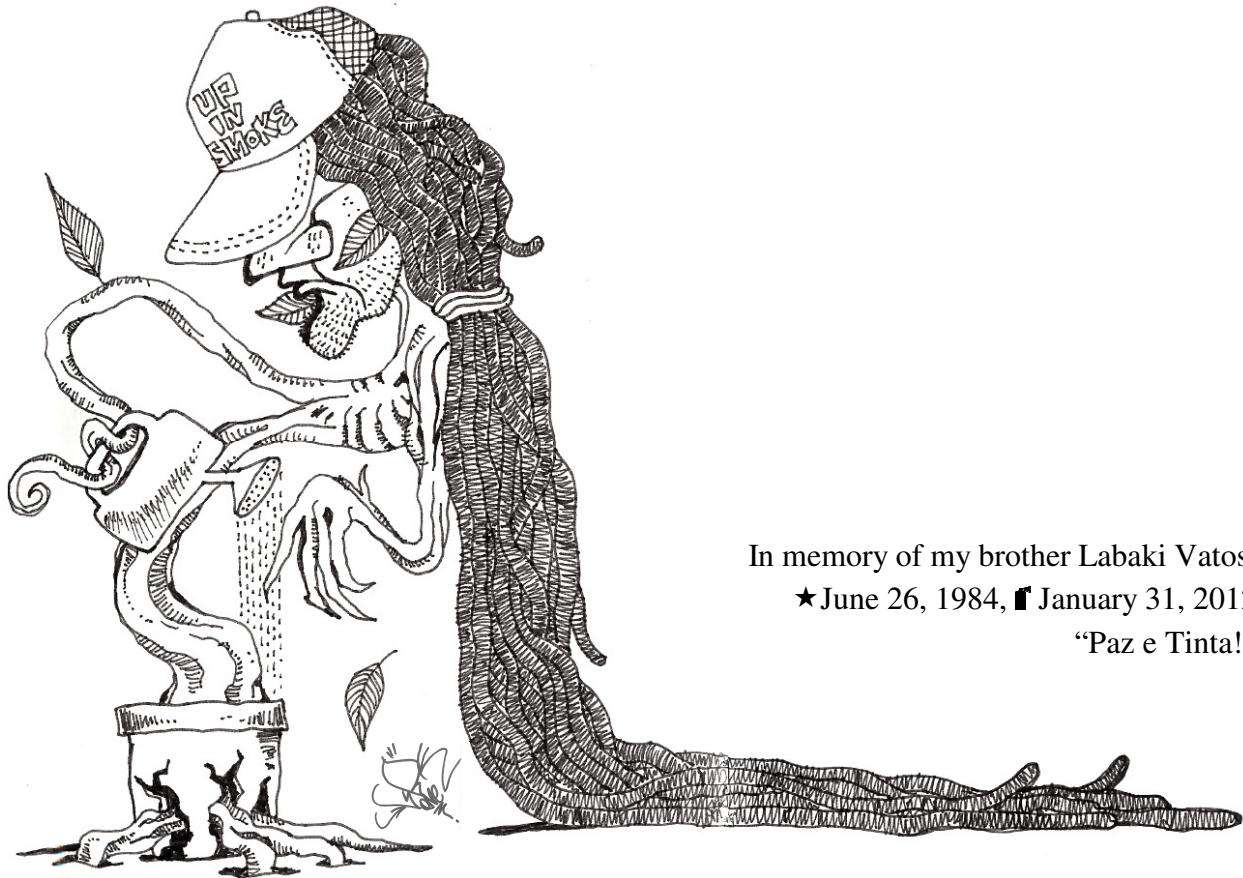


Prof. Dr. Pêrsio Leister de Almeida Barros
Department of Geotechnics and Transportation, Unicamp



Prof. Dr. Renato Pavanello
Department of Computational Mechanics, Unicamp

Campinas, 18 de julho de 2012



In memory of my brother Labaki Vatos.
★ June 26, 1984, † January 31, 2012
“Paz e Tinta!”

Acknowledgements

I acknowledge that the long process of producing a Ph.D. thesis is not a one-man job. I would like to express my deepest gratitude to all the people who have directly or indirectly helped me along this process.

I am grateful to my Ph.D. advisor, Prof. Euclides de Mesquita Neto, for all the patience, guidance and encouragement along these six years in which we have been working together. He has taught me a great deal of physics, of how to present scientific communication, and of how to focus my drive on a productive end.

My deepest gratitude to Prof. Nimal Rajapakse, who so kindly accepted to supervise me during my stay in Canada, despite his very busy life as dean of the Faculty of Applied Sciences at Simon Fraser University. Prof. Rajapakse has been instrumental in introducing me to the field of study of plates which comprises this thesis.

I am thankful for having such nice friends to work with. I would like to mention especially the friendship of my siblings of the Aquarium (our lab), Daniela Andrade and Danilo Froner.

Special thanks to Denise and her co-workers of the secretariat of the Graduate Program of Mechanical Engineering for putting up with me through all these years.

I am grateful to the Brazilian government for encouraging and believing in young researchers such as me, furnishing financial support through its Coordination for the Improvement of Higher Education Personnel (Capes).

Most importantly, none of this would have been possible without the love and patience of my family. I thank my parents for giving up so much for me, and for loving me more than I deserve.

“I’m just one hundred and one, five months and a day.”

“I can’t believe that!,” said Alice.

“Can’t you?,” the Queen said in a pitying tone. “Try again: draw a long breath, and shut your eyes.”

Alice laughed. “There’s no use trying,” she said: “one can’t believe impossible things.”

“I daresay you haven’t had much practice,” said the Queen. “When I was your age, I always did it for half-an-hour a day. Why, sometimes I’ve believed as many as six impossible things before breakfast.”

Lewis Carroll’s “Alice’s Adventures in Wonderland”

So I hope you can accept Nature as She is – absurd.

I’m going to have fun telling you about this absurdity, because I find it delightful... and I hope you will be as delighted as I am when we’re through.

Richard Feynman’s “QED: The Strange Theory of Light and Matter”

Abstract

This work presents new models to describe the time-harmonic behavior of rigid and flexible circular plates embedded in layered media. Deep embedments of the plates are represented by bi-material viscoelastic transversely isotropic interfaces. Shallow embedments are represented by multilayered viscoelastic transversely isotropic media. The models of surrounding media are derived according to classical models available in the literature, which are in cylindrical coordinates. The method used to derive these models involves Hankel transforms, in order to bring the equations of motion to a domain in which they can be dealt with algebraically. A few functions of interest are expanded in Fourier series, in order to describe quantities such as displacements, stresses and loadings in terms of axisymmetric or antisymmetric components. In the model of rigid plate, the embedded plate is described by considering that a circular surface within the surrounding medium is rigid. A set of coupled integral equations, which relate the displacements and the unknown tractions across this surface, is solved by discretizing the surface into concentric annular disc elements. Kirchhoff theory of thin elastic plates is used to describe the flexible plate. A trial function to describe the deflection profile of the plate is defined in terms of a power series. An energy functional is established, which involves the strain energy of the plate and of its surrounding medium. The minimization of this functional, under the restriction that it must satisfy the boundary conditions at the plate edge, results in the deflection profile of the embedded plate. The models of embedded plates are compared with previous results from the literature for the case of different embedments in isotropic media. New research results are provided for the case of shallow and deep embedments in layered viscoelastic transversely isotropic media, under time-harmonic vertical and transverse loads and rocking moments. The results of this work contribute to the study of embedded foundations and anchors in layered soil.

Keywords

Soil-Foundation Interaction, Rigid Plates, Flexible Plates, Transversely Isotropic Media.

Resumo

Este trabalho apresenta novos modelos para descrever o comportamento harmônico de placas rígidas e flexíveis incrustadas em meios estratificados. Incrustações profundas das placas são representadas por interfaces bi-materiais de meios viscoelásticos transversalmente isotrópicos. Incrustações rasas são representadas por meios estratificados viscoelásticos transversalmente isotrópicos. Os modelos de meios circundantes são obtidos com base em modelos clássicos disponíveis na literatura, que estão em coordenadas cilíndricas. O método usado para obter esses modelos envolve transformadas de Hankel, com o objetivo de obter as equações de movimento em um domínio no qual elas possam ser manipuladas algebricamente. Algumas funções de interesse são expandidas em séries de Fourier, para decompor grandezas como deslocamentos, tensões e carregamentos em termos axissimétricos e antissimétricos. No modelo de placa rígida, a incrustação da placa é descrita assumindo que uma superfície circular do meio circundante é rígida. Um conjunto de equações integrais acopladas, que relaciona deslocamentos e força de superfície atuantes nesta superfície, é resolvido por meio de discretização da superfície em discos anulares concêntricos. A teoria de Kirchhoff para placas finas é usada como modelo de placa flexível. Uma tentativa de solução para o perfil de deflexão da placa é definido em termos de série de potência. Uma função envolvendo as energias de deformação da placa e do meio é definida, cuja minimização, sob as restrições impostas pelas condições de contorno da placa, resulta no perfil de deflexão da placa incrustada. Os modelos de placa rígida e flexível incrustadas são comparados com resultados da literatura para incrustações em meios isotrópicos. Novos resultados são fornecidos para os casos de incrustações rasas ou profundas em meios viscoelásticos estratificados transversalmente isotrópicos, sob a ação de forças harmônicas verticais e transversais, assim como momentos. Os resultados deste trabalho contribuem para o estudo de fundações e âncoras em solos estratificados.

Palavras-chave

Interação Solo-Fundação, Placas Rígidas, Placas Flexíveis, Meios Transversalmente Isotrópicos

Table of Contents

Abstract	vii
Resumo	viii
1 INTRODUCTION	1
1.1 Literature review	1
1.2 Objectives of this work	6
1.3 Organization of the text	7
2 GREEN'S FUNCTION FOR TRANSVERSELY ISOTROPIC MEDIA	9
2.1 Transversely isotropic materials	9
2.2 Transversely isotropic three-dimensional full-space	13
2.3 Elastodynamic three-dimensional bi-material interface	21
2.3.1 Displacement boundary conditions	23
2.3.2 Stress boundary conditions	23
2.3.2.1 Vertical load	24
2.3.2.2 Transverse load	29
2.3.2.3 Pure moment loading	39
2.4 Description of the loadings	41
3 EXACT STIFFNESS METHOD FOR MULTILAYERED MEDIA	45
3.1 Underlying half-space	48

3.2 Stiffness matrix of the layers and half-space	49
3.3 Stiffness matrix of the multilayered medium	50
3.4 Example	52
4 MODEL OF AN EMBEDDED RIGID CIRCULAR PLATE	58
4.1 Problem statement	58
4.2 Governing equations	59
4.3 Vertical load	60
4.4 Transverse and moment loading	63
4.5 Validation	72
4.5.1 Numerical implementation and convergence	73
4.5.2 Bi-material interface	75
4.5.2.1 Vertical vibrations	75
4.5.2.2 Transverse and rocking vibrations	76
4.5.3 Multilayered system	77
4.6 Numerical results	78
4.6.1 Influence of the inner radius	79
4.6.2 Bi-material interface	81
4.6.3 Multilayered system	86
4.6.4 Influence of the damping	88

5 MODEL OF AN EMBEDDED ELASTIC CIRCULAR PLATE	90
5.1 Problem statement	90
5.2 Governing equations and boundary conditions	91
5.3 Variational formulation	96
5.3.1 Strain energy of the flexible plate	99
5.3.2 Strain energy of the surrounding medium	99
5.3.3 Variational formulation of the embedded plate	105
5.4 Implementation	107
5.5 Validation	108
5.5.1 Convergence	109
5.5.2 Bi-material interface	109
5.5.3 Multilayered medium	111
5.6 Numerical results	113
5.6.1 Bi-material interface	113
5.6.2 Multilayered system	116
6 CONCLUDING REMARKS	120
6.1 Further developments	124
7 REFERENCES	125

List of Tables

Table 2.1 Effect of the anisotropy index on the properties of transversely isotropic materials	12
Table 2.2 Example of transversely isotropic materials	13
Table 4.1 Summary of the terms of direct and crossed compliance presented in this chapter	72
Table 4.2 Comparison of results with analytical solution for the static problem	75
Table 4.3 Transversely isotropic materials used in the results of Figs. 4.23 to 4.25	83
Table 4.4 Multilayered media configurations	87
Table 4.5 Material properties	87
Table 5.1 Multilayered media configurations	116
Table 5.2 Multilayered media configurations	116
Table 6.1 Models of embedded plates which have been presents in the present work	123

List of Figures

- Figure 2.1 Illustration of the coordinate system and the state of stress of a point $P(r,\theta,z)$. 10
- Figure 2.2 Definition of coordinate system, domains and loading area. 21
- Figure 2.3 Internal loading configurations considering (a) vertical loads (b) transverse loads along x and (c) varying vertical load representing a concentrated moment about the y -axis. 22
- Figure 2.4 Definitions and sign conventions for tractions, stresses and external loads, considering the normal vectors at the free surfaces of each medium. The subscript m is omitted for conciseness. 27
- Figure 2.5 Decomposition of the transverse load \wp_x into an axisymmetric term \wp_0 in the radial direction and an antisymmetric term \wp_1 in the θ -direction. 29
- Figure 2.6 Decomposition of the transverse load \wp_x into an axisymmetric term \wp_0 in the radial direction and an antisymmetric term \wp_1 in the θ -direction. 30
- Figure 2.7 Decomposition of the distorting load \wp_d into an axisymmetric term \wp_0 in the radial direction and an antisymmetric term \wp_1 in the θ -direction. 31
- Figure 2.8 Load configurations for antisymmetric vertical loads which vary only with θ and not with r (a, c and d) and which vary linearly with x (b, e and f). 43
- Figure 3.1 Geometry and notation of a multilayered system. 45
- Figure 3.2 Directions of stresses and tractions at the n^{th} interface from the point of view of the (a) top and (b) bottom surfaces of the n^{th} layer when the normal vector to each surface is considered. 48
- Figure 3.3 Definitions and sign conventions for tractions, stresses and external loads, considering the normal vectors at the free surfaces of each layer. The subscript m is omitted for conciseness. 51

Figure 3.4 Layer and interface numbering, tractions and external forces, for a reduced example of $N=3$ layers plus an underlying infinite half-space.	53
Figure 4.1 (a) Circular plate of radius a buried in the interface of two media and (b) reference surface S of radius a within the interface.	58
Figure 4.2 Discretization of the region S into concentric annular disc elements for the case of $M=4$.	60
Figure 4.3 Discretization of the region S , showing the annular disc elements i and k .	61
Figure 4.4 (a) Undisturbed media and rigid surface S , (b) pure transverse displacement of the surface S , (c) pure rotation and (d) combined translation and rotation.	63
Figure 4.5 Illustration of the terms of transverse and vertical displacement u_{xx} and u_{zx} due to a uniformly distributed transverse load of unit intensity.	64
Figure 4.6 Illustration of the transverse and vertical displacement v_{xz} and v_{zz} due to a non-axisymmetric vertical load.	65
Figure 4.7 Scheme of forces and moments resulting from the antisymmetric traction t_z .	68
Figure 4.8 Illustrations of a rigid plate inside an isotropic full-space under (a) vertical, (b) transverse and (c) moment static loads.	74
Figure 4.9 Normalized vertical compliance of a rigid plate on an isotropic full-space.	75
Figure 4.10 Configuration investigated by Luco and Westmann (1971) – rigid plate resting on the surface of an isotropic half-space under (a) transverse load and (b) rocking moment.	76
Figure 4.11 Normalized transverse compliance of a rigid plate on an isotropic full-space.	76
Figure 4.12 Normalized rocking compliance of a rigid plate on an isotropic full-space.	77

Figure 4.13 Configurations of a rigid plate subjected to vertical loads (a) between a half-space and two layers of the same material and (b) at an arbitrary embedment H inside a half-space.	78
Figure 4.14 Normalized vertical dynamic compliance of a rigid plate between two isotropic layers of unit thickness and an isotropic half-space.	78
Figure 4.15 Annular plate embedded at the interface of two infinite half-spaces.	79
Figure 4.16 Influence of the inner radius b in the normalized compliance of the disc for the case of vertical load.	79
Figure 4.17 Influence of the inner radius b in the normalized compliance of the disc for the case of transverse load.	80
Figure 4.18 Influence of the inner radius b in the normalized compliance of the disc for the case of rocking moment.	80
Figure 4.19 Illustration of different bi-material configurations with an embedded rigid plate subjected to (a) vertical and (b) transverse loads and (c) rocking moments.	81
Figure 4.20 Vertical dynamic compliance of the rigid plate for different bi-material constructions. Medium 1 has anisotropy indices $n_2=n_3=1$.	81
Figure 4.21 Transverse dynamic compliance of the rigid plate for different bi-material constructions. Medium 1 has anisotropy indices $n_2=n_3=1$.	82
Figure 4.22 Rocking dynamic compliance of the rigid plate for different bi-material constructions. Medium 1 has anisotropy indices $n_2=n_3=1$.	83
Figure 4.23 Vertical dynamic compliance for the rigid plate for different bi-material constructions. Medium 1 has anisotropy indices $n_1=n_2=n_3$.	84
Figure 4.24 Transverse dynamic compliance for the rigid plate for different bi-material constructions. Medium 1 has anisotropy indices $n_1=n_2=n_3$.	84

Figure 4.25 Rocking dynamic compliance for the rigid plate for different bi-material constructions. Medium 1 has anisotropy indices $n_1=n_2=n_3$.	85
Figure 4.26 Crossed compliance $C_{XM}(\omega)$ of the rigid plate for different bi-material constructions. Medium 1 has anisotropy indices $n_2=n_3=1$.	85
Figure 4.27 Crossed compliance $C_{MX}(\omega)$ of the rigid plate for different bi-material constructions. Medium 1 has anisotropy indices $n_2=n_3=1$.	86
Figure 4.28 Illustration of different layered system configurations with an embedded plate subjected to vertical loads.	87
Figure 4.29 Vertical dynamic compliance of the rigid plate for three layered systems.	88
Figure 4.30 Influence of the damping coefficient on the frequency behavior of the rigid plate.	88
Figure 5.1 Elastic solid circular plate of radius a and thickness h buried in the interface of two transversely isotropic media.	90
Figure 5.2 Elastic solid circular plate under the effect of distributed and/or concentrated vertical loads.	91
Figure 5.3 Deflection patterns assumed by the Kirchhoff theory: (a) undeformed plate and (b) deformed plate, showing the undeformed middle surface and that normals to it remain normals after deflection.	92
Figure 5.4 Illustration of the moment $M_r(r)$ and the shear force $Q(r)$ acting on an arbitrary section of the elastic plate. Part (a) shows the surface of the whole plate, part (b) shows an arbitrary cross-section which passes through the center of the plate and part (c) shows an element of the body of the plate.	93
Figure 5.5 Different boundary conditions at the plate edge, showing (a) clamped edge, (b) simply supported edge and (c) free edge.	94

Figure 5.6 (a) Each of the terms of the power series involved in Eq. 5.12, for the case of $a_0=\alpha_n=1$ ($n=0,N$), and (b) the resulting deflection profile from the summation of all these terms.	97
Figure 5.7 Illustration of a flexible plate inside an isotropic full-space under (a) concentrated and (b) distributed static vertical loads.	109
Figure 5.8 Normalized displacement and differential deflection of a flexible plate under concentrated load.	110
Figure 5.9 Normalized displacement and moment of a flexible plate under uniformly distributed load.	111
Figure 5.10 Configuration of a flexible plate subjected to (a) concentrated and (b) distributed vertical loads between a half-space and two layers of the same material.	111
Figure 5.11 Behavior of an elastic plate at different embedments within an isotropic half-space, due to a centrally applied point load P_0 .	112
Figure 5.12 Behavior of an elastic plate at different embedments within an isotropic half-space, due to a uniformly distributed load q_0 .	112
Figure 5.13 Illustration of different bi-material configurations with an embedded flexible plate subjected to a uniformly distribute vertical load.	113
Figure 5.14 Deflection profile of a flexible plate for different bi-material constructions for the frequencies $\omega=0.2$ and $\omega=1.0$, for the case of a uniformly distributed load.	114
Figure 5.15 Deflection profile of a flexible plate for different bi-material constructions for the frequencies $\omega=2.0$ and $\omega=4.0$, for the case of a uniformly distributed load.	114
Figure 5.16 Central displacement of a flexible plate for different bi-material constructions, for the case of a uniformly distributed load.	115
Figure 5.17 Illustration of different layered system configurations with an embedded plate subjected to vertical loads.	116

Figure 5.18 Deflection profile of a flexible plate for different layered systems for the frequencies (a) $\omega \approx 0.0$ and (b) $\omega = 4.0$. 117

Figure 5.19 Moment $M_r(r)$ acting on a flexible plate for different layered systems for the frequencies (a) $\omega \approx 0.0$ and (b) $\omega = 4.0$. 117

Figure 5.20 Shear force $Q(r)$ acting on a flexible plate for different layered systems for the frequencies (a) $\omega \approx 0.0$ and (b) $\omega = 4.0$. 118

1 INTRODUCTION

Scientific methodology involves the construction and analysis of models of the subjects of physics under study. As Baran and Sweezy (1968) accurately pointed out, the purpose of such models is not to provide a mirror image of nature's reality, nor to comprise every single element of it in their sizes and proportions, but rather to single out and to provide an intensive comprehension of those elements which are decisive. Creation of models implies necessarily the abstraction of non-essential parts of reality, in order to furnish a deeper, unobstructed insight of the quantity of interest. "A model is [...] unrealistic in the sense in which the word is most commonly used. Nevertheless, paradoxically [...] it provides the key to understanding reality". Baran and Sweezy (1968) were talking about modern capitalism when they provided this justification for the use of models, but their justification holds just as fine for engineering analysis.

In real-world engineering analysis, it is rarely possible to fully understand the influence of all the variables involved in the behavior of an object of study. This is especially true for geotechnical engineering analysis (Wood, 1990). Soil materials, which are one of the objects of study of geotechnical engineering analysis, largely differ from continuum media because they are made up of discrete particles, the size of which varies considerably (Wood, 1990). A significant proportion of the volume of a soil material is made up of voids. These voids may be filled with fluids, such as oil and natural gas, and water. When a soil material is deformed, considerable and often irreversible changes in volume may occur as the relative position of the soil particles changes (Wood, 1990; Mitchell and Soga, 2005).

On the other hand, most geotechnical structures are large in comparison with the scale of the soil particles, and stress and strain quantities can be considered as averaged over volumes of soil containing many particles. This hypothesis holds especially for geotechnical analysis involving large wavelengths, and it allows the soil to be modeled as a continuum medium (Wood, 1990; Mitchell and Soga, 2005).

Different models of continua have been presented in the last century. The models

comprising the behavior of unbounded continua (full-spaces), unbounded continua possessing a free surface (half-spaces) and laterally unbounded layers of finite thickness provide representations of wave propagation in soil media. Section 1.1 presents a review of some models of full- and half-spaces and layers developed in the past decades.

1.1 Literature review

A representative portion of the models of full- and half-spaces has been produced by the research group in which the author of this thesis is enrolled, of the Department of Computational Mechanics of Unicamp. The first work of the group was presented by Mesquita (1989), which comprised non-singular auxiliary states for two- and three-dimensional viscoelastic isotropic half-spaces under time-harmonic loads. The corresponding solution for the displacement and stress fields of a two-dimensional isotropic full-space was provided by Romanini (1995). Romanini (1995) also studied the case of a layer over a rigid surface and a layer over an elastic half-space. Solutions for two-dimensional isotropic media under distributed linear, quadratic or singular loadings were derived by Barros and Mesquita (1999b) and Barros and Mesquita (2000). Efficient computation of these solutions in the frequency domain, together with Fourier transforms, allowed Mesquita et al. (2002) and Thomazo (2004) to obtain solutions of the transient response of two-dimensional isotropic half-spaces. An extension to the case of a layer over a rigid base was presented by Mesquita et al. (2003). After the development of these computationally efficient two-dimensional solutions, the group started investigating the three-dimensional problems. Mesquita, Romanini and Labaki (2012) provided an extension of the solution presented by Romanini (1995) for the three-dimensional case. The solutions comprise the displacement fields of a three-dimensional isotropic viscoelastic full-space. Time-harmonic loading uniformly distributed on a rectangular area within the full-space were considered. Double Fourier transforms were used in the solution. The resulting implementation, however, has proved to be very computationally expensive (Labaki, Romanini and Mesquita, 2012). An analogous solution has been presented by Adolph in his Ph.D. thesis (Adolph, 2006; Adolph et al, 2007), in which Radon transforms were used. All the above mentioned solutions correspond to the case of isotropic media. However, because of the way sedimentary soil is formed, the most accurate models to represent it are the ones which represent transverse anisotropic continua (Mitchell and Soga, 2005). This group of research has also derived solutions for anisotropic media, as shown

later on.

The study of elastic wave propagation in anisotropy materials is quite complicated. Fundamental studies on the wave propagation in media possessing general anisotropy were done by Barnett and Lothe (1974) and Chadwick and Smith (1977). Anisotropic materials possessing a plane of isotropy are called transversely isotropic materials (Lekhnitskii, 1963) (Section 2.1). Early studies on the elastostatics and elementary stress analysis of such media were presented by Elliot (1948), Hu (1954), Eubanks and Sternberg (1954), Lekhnitskii (1963) and Green and Zerna (1968). However, the earliest research work concerned with the elastic wave propagation in transversely isotropic media, which is a problem of higher interest to the present study, was done by Stoneley (1924) (Rajapakse and Wang, 1993). State-of-the-art reviews on the wave propagation in anisotropic media are provided by Crampin, Chesnokov and Hipkin (1984) and Payton (1983), and in the references therein. More recently, Barros (1997) presented solutions for the time-harmonic behavior of three-dimensional viscoelastic transversely isotropic full- and half-spaces under time-harmonic loads. Later on, Barros and Mesquita (1999) presented a solution in which the plane of isotropy of the medium does not necessarily correspond to the free-surface of the half-space. A rectangular coordinate system has been used in both cases. Of most interest to the present study is the solution derived by Wang in his PhD thesis (Wang, 1992), which resulted in the paper by Rajapakse and Wang (1993). These authors derived three-dimensional elastodynamic Green's functions for a transversely isotropic full-space and half-space, respectively. A cylindrical coordinate system was used (r, θ, z) . The equation of equilibrium for time-harmonic motions were solved by introducing three potential functions, which were expanded in Fourier series, as introduced by Muki (Muki, 1960; Barros, 2006). Because of the cylindrical coordinate system that was adopted, Hankel transforms were used in the solution. Analytical solutions for Green's functions were derived by considering buried circular ring loads acting on the radial (r) , circumferential (θ) and vertical directions (z) .

Regardless of its anisotropy, any accurate model of unbounded media must take into consideration the Sommerfeld's radiation condition (Sommerfeld, 1949), which establishes that the energy that is radiated from the sources must scatter to infinity, i.e., the model must comply with the physical observation that no energy is radiated back from infinity into the field. Moreover, Christensen's elastic-viscoelastic correspondence principle holds for anisotropic

media (Christensen, 2010). It states that the viscoelasticity of a medium can be introduced by defining its material properties as complex-valued variables involving the damping factor of the medium. An extensive review of attenuation models is presented by Gaul (1999).

Different techniques have been presented over the past decades to model layered media. The most successful ones, the thin-layer method and the exact stiffness method, resemble a finite element analysis. A stiffness matrix of the layered medium is assembled from the stiffness matrices of the layers in the same fashion as the stiffness matrix of a structure is assembled from the elementary stiffness matrices of its components. This method has been used by Wass (1972), Wass (1980), Kausel and Peek (1982), Mesquita and Romanini (1992) and Romanini (1995) to model multilayered isotropic media. Only a few results have been presented regarding the dynamics of multilayered anisotropic media. The most important ones to the present study are by Seale and Kausel (1989), Wang (1992) and Marques de Barros (2001). The first paper presented an extension of the thin-layer method to study the elastodynamics of a multilayered transversely isotropic half-space due to point loads. Wang (1992) and Marques de Barros (2001) used an exact stiffness method to derive solutions for two-dimensional transversely isotropic layered media under time-harmonic loads in cylindrical and rectangular coordinates, respectively.

On a distinct course of study, other researchers have investigated different models for the extensional and flexural deformation of plates. Kirchhoff (1850) improved the equations of equilibrium and free vibrations derived by Poisson and Cauchy (Van der Heijden, 1976) by establishing that two boundary conditions are sufficient for the complete determination of the deflection of the plate. Kirchhoff's model of plate is widely used, and it is based on three hypothesis: (a) there is a surface at the middle of the plate where there is no deformation: this middle surface remains neutral during bending; (b) lines that are initially normal to the middle flat surface of the plate remain normal to the middle bent surface of the plate after bending and (c) on the unstretched middle surface, the normal state of stress can be disregarded. Under these assumptions, Kirchhoff (1850) was able to derive an expression for the potential energy of the deflected plate in terms of the curvature of its middle surface. The principle of virtual work was used to obtain the equations of motion of the plate. A century later, Friedrichs (1950) showed that the Kirchhoff's boundary conditions are rigorously valid for plates. An extensive review on the boundary conditions of models of plate is presented by Van der Heijden (1976). The

corresponding equations of motion of plates are described in details in a book by Timoshenko and Woinowsky-Krieger (1964).

A third branch of study makes use of the theories of plates and the models of elastic media to investigate the behavior of embedded plates. Selvadurai (1980) and Selvadurai and Singh (1984) have derived analytical solutions for the problem of rigid disc inclusions at isotropic full-spaces under the effect of static vertical and transverse point loads, as well as an eccentric point load, the resulting effect of which is that of a moment applied on the transverse axis of the plate. As for the dynamic case, the most relevant developments related to the present research work were done by Bycroft (1956) and Arnold, Bycroft and Warburton (1955), who modeled the behavior of a massless rigid plate by considering that a region of the elastic medium surrounding the plate was rigid. Luco and Westmann (1971) presented solutions for the transverse and rocking vibrations of rigid plates resting on the surface of an isotropic half-space. Lysmer (1965) introduced a significant improvement to the representation of the rigid plate by introducing a discretization to the model of plate. The plate is discretized by a number of concentric annular disc elements and by imposing that the displacement of all of them is the same. Lysmer's method has been used to describe vertical, transverse, torsional and rocking vibrations of rigid plates embedded in a number of different models of surrounding media (Zeng and Rajapakse, 1999; Senjuntichai and Sapsathiarn, 2003, Wu et al., 2006). Zeng and Rajapakse (1999) and Senjuntichai and Sapsathiarn (2003) have derived solutions for the vertical vibrations of rigid plates at arbitrary embedments inside a poroelastic half-space and multilayered poroelastic system, respectively. Wu et al. (2006) presented solutions for the torsional vibration of the rigid plate on a transversely isotropic half-space. A solution for the vertical, twisting, transverse and rocking motion of a rigid cylindrical foundation embedded in transversely isotropic media has been presented by Barros (2006). On the other hand, Pak and Gobert (1991) used a finite difference energy method for the discretization of the rigid plate to describe the vertical vibrations of the plate within a multilayered isotropic system.

The case of elastic plates has been treated by a few different methods. The book by Selvadurai (1979a) contains a detailed review of the various methods which have been used to deal with such problem. According to Rajapakse (1988), the variational method presented by Selvadurai (1979b, 1979c and 1980b) is the most suitable to solve the problem of interaction

between an elastic plate and its surrounding medium. One drawback of the variational method is the difficulty of obtaining an explicit representation of the traction field acting across the surface of the plate in response to the displacement field which is established. The integral equation system corresponding to the mixed boundary value problem only has an explicit solution for the case of the plate resting on the surface of the half-space or buried infinitely deep inside it (Rajapakse, 1988). Rajapakse (1988) derived a solution for the case of the elastic plate embedded at a finite depth inside an isotropic half-space. In Rajapakse's formulation, the deflection profile of the plate is described by a power series together with a term corresponding to a concentrated load derived according to the classical plate theory. The coefficients of the power series are determined through the minimization of a constrained energy functional involving the strain energy of the plate and of the surrounding medium and the potential energy of the external loads. The resulting system of equations from the constrained energy functional is presented in a convenient matrix form, resembling the classical finite element method, and it has some advantages over the direct explicit variational scheme. The results from his paper considered the case of embedment in a three-dimensional isotropic half-space.

Very few research works have dealt with the problem of rigid and flexible plates embedded in non-homogeneous transversely isotropic layered media. Very recently, Eskandari-Ghadi, Mirzapour and Ardeshtir-Behrestaghi (2011), presented the solution of rocking vibrations of a rigid disc at the interface of two transversely isotropic half-spaces. Their solution, however, disregarded the coupled behavior between the rocking and transverse behaviors of such problem.

1.2 Objectives of this work

The literature review presented above indicates that models of the interaction of rigid and flexible circular foundations with the soil represented by a layered transversely isotropic medium are yet to be developed. The aim of this research work is to present such models. The objective is to use bi-material unbounded media and layered transversely isotropic half-spaces to model the media that surrounds the plate. The plate itself is described by either a rigid surface or a thin elastic body. Time-harmonic concentrated and distributed vertical and transverse loads and rocking moments are to be considered as excitations to the plates.

1.3 Organization of the text

The formulations and numerical results in this work are organized as follows.

In Chapter 2, the classical Green's function of transversely isotropic three-dimensional full-spaces presented by Wang (1992) is reviewed. An extension for the bi-material case is provided, as well as simplified particularizations of the main solution for the axisymmetric and antisymmetric cases. The chapter presents a detailed description of distributed and concentrated axisymmetric and antisymmetric ring loads, and it shows how a concentrated moment can be represented by an antisymmetric vertical load.

Next, Chapter 3 reviews the formulation presented by Wang (1992) for the behavior of a two-dimensional multilayered medium, each layer of which consists of a transversely isotropic material. The model presented in that chapter is an extension of the Wang's formulation for the three-dimensional case. The stiffness-matrix approach is used. An example is provided, which emphasizes the resemblance of the method to the finite element approach in structural analysis.

In Chapter 4, the model of rigid plate presented by Lysmer (1965) is reviewed. A rigid massless plate is represented by considering a rigid surface of the surrounding media. The tractions acting across this surface can be accurately computed by discretizing it, on each discretized part of which the traction field is assumed to be uniformly distributed. The chapter presents a comparison of results obtained with the present implementation with results from the literature. It also presents original research results of the vertical, transverse and rocking vibrations of rigid plates in bi-material and multilayered transversely isotropic media. The physical effect that the transverse and rocking responses of inclusions in bi-material interfaces are coupled is carefully incorporated to the present model.

Finally, Chapter 5 presents the model of elastic plate derived by Selvadurai (1979b, 1979c and 1980b) and improved by Rajapakse (1988). A trial solution for the linear partial differential equation that describes the plate is established in terms of a power series. A variational problem is established, in which an energy functional involving the strain energy of the plate and of its surrounding medium is minimized according to the principle of minimum potential energy. The chapter presents a comparison of the present implementation with results from the literature, as

well as original research results of the vertical flexure of plates within bi-material and multilayered transversely isotropic media.

2 GREEN'S FUNCTION FOR TRANSVERSELY ISOTROPIC MEDIA

The dynamic response of transversely isotropic media is presented in this chapter. A brief general introduction on the properties of transversely isotropic materials is presented, along with a few examples. The chapter then describes a classical formulation of Green's Function for three-dimensional transversely isotropic infinite continua, which is conveniently written in cylindrical coordinates. Next, a particular case of this Green's Function is presented, in which two bonded semi-infinite media are considered, each made of a different transversely isotropic material. Finally, the chapter provides an extensive description of concentrated and distributed ring loads.

2.1 Transversely isotropic materials

A transversely isotropic material is one that possesses equivalent elastic material properties in one plane, called "plane of isotropy", and different properties in the direction normal to that plane.

Some soil materials are formed by a sedimentation process. Sedimentation formation pertains to processes by which accumulated sediments are densified, altered in composition, and converted into rock (Mitchell and Soga, 2005). The resulting material presents layered-like property distribution, in which each layer has approximately the same properties length-wise but different properties through the thickness. Because of this process in which sedimentary soil materials are formed, it is reasonable to model them as transversely isotropic materials. These models are especially accurate for problems involving long wavelengths, in which other soil material effects such as plasticity and porosity play a less relevant role (Wood, 1990; Mitchell and Soga, 2005).

Transversely isotropic three dimensional continua are fully described by five independent material properties: Young's modulus E on the plane of isotropy, Young's modulus E_z normal to the plane of isotropy, transverse modulus of elasticity G_{zx} , Poisson's ratio ν between deformations in two orthogonal directions contained in the plane of isotropy and Poisson's ratio ν_{zx} between deformations in the plane of isotropy and in the plane normal to it (Payton, 1983).

Deformations are related to stresses in a transversely isotropic medium according to Hooke's constitutive equation. Consider a transversely isotropic, linear elastic, three-dimensional, unbounded medium. A cylindrical coordinate system $O(r, \theta, z)$ is adopted, the z -axis of which is perpendicular to the material's plane of isotropy (Fig. 2.1). In Fig. 2.1, u_r , u_θ and u_z denote the displacements of the point P of coordinates (r, θ, z) in the r , θ and z directions, respectively.

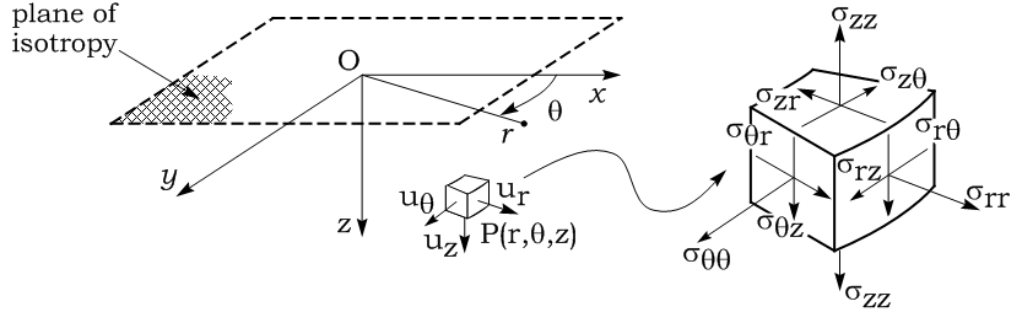


Figure 2.1 Illustration of the coordinate system and the state of stress of a point $P(r, \theta, z)$.

Hooke's constitutive equation is given for this medium, in cylindrical coordinates, by (Lekhnitskii, 1963):

$$\sigma_{rr} = c_{11}\epsilon_{rr} + c_{12}\epsilon_{\theta\theta} + c_{13}\epsilon_{zz} \quad (2.1)$$

$$\sigma_{\theta\theta} = c_{12}\epsilon_{rr} + c_{11}\epsilon_{\theta\theta} + c_{13}\epsilon_{zz} \quad (2.2)$$

$$\sigma_{zz} = c_{13}\epsilon_{rr} + c_{13}\epsilon_{\theta\theta} + c_{33}\epsilon_{zz} \quad (2.3)$$

$$\sigma_{r\theta} = (c_{11} - c_{12})\epsilon_{r\theta} \quad (2.4)$$

$$\sigma_{\theta z} = 2c_{44}\epsilon_{\theta z} \quad (2.5)$$

$$\sigma_{rz} = 2c_{44}\epsilon_{rz} \quad (2.6)$$

In the nomenclature of Hooke's constitutive equation, the five independent material properties are written as (Lekhnitskii, 1963):

$$c_{11} = E \left(1 - n v_{zr}^2 \right) / a \quad (2.7)$$

$$c_{12} = E \left(n v_{zr}^2 + \nu \right) / a \quad (2.8)$$

$$c_{13} = E \nu_{zr} (1 + \nu) / a \quad (2.9)$$

$$c_{33} = E_z \left(1 - \nu^2 \right) / a \quad (2.10)$$

$$c_{44} = G_{zr} \quad (2.11)$$

In Eqs. 2.7 to 2.11,

$$n = E / E_z \quad (2.12)$$

$$a = (1 + \nu) \left(1 - \nu - 2n v_{zr}^2 \right) \quad (2.13)$$

The requirement that the strain energy of a medium be positive definite subjects the material constants to the following constraints (Payton, 1983):

$$c_{11} > |c_{12}|; (c_{11} + c_{12}) c_{33} > 2c_{13}^2; c_{44} > 0 \quad (2.14)$$

A classical set of nondimensional parameters used in the modeling of transversely isotropic media is (Wang, 1992):

$$\alpha = \frac{c_{33}}{c_{44}} \quad (2.15)$$

$$\beta = \frac{c_{11}}{c_{44}} \quad (2.16)$$

$$\kappa = \frac{(c_{13} + c_{44})}{c_{44}} \quad (2.17)$$

$$\gamma = 1 + \alpha\beta - \kappa^2 \quad (2.18)$$

$$\zeta = \frac{(c_{11} - c_{12})}{2c_{44}} \quad (2.19)$$

Other classical set of nondimensional parameters is useful when dealing with transversely isotropic media in order to identify how far their behavior deviates from that of an isotropic material. These parameters are called anisotropy indices and one definition for them was presented by Anderson (1961):

$$n_1 = c_{33}/c_{11} \quad (2.20)$$

$$n_2 = (c_{11} - c_{12})/2c_{44} \quad (2.21)$$

$$n_3 = (c_{11} - 2c_{44})/c_{13} \quad (2.22)$$

Table 2.1 illustrates how the material properties are affected by n_1 , for example. In these results, $c_{44}=1$, $\nu=0.25$ and $n_2=n_3=1$. All materials from this table satisfy the constraints established in Eq. 2.14.

Table 2.1 Effect of the anisotropy index on the properties of transversely isotropic materials.

n_1	n_2	n_3	c_{11}	c_{12}	c_{13}	c_{33}	E	E_z	ν	ν_{zx}
1.0	1.0	1.0	3.0000	1.0000	1.0000	3.0000	2.5	2.5000	0.25	0.2500
1.5	1.0	1.0	2.8284	0.8284	0.8284	4.2426	2.5	3.8673	0.25	0.2265
2.0	1.0	1.0	2.7749	0.7749	0.7749	5.5497	2.5	5.2114	0.25	0.2183
2.5	1.0	1.0	2.7481	0.7481	0.7481	6.8703	2.5	6.5502	0.25	0.2140
3.0	1.0	1.0	2.7321	0.7321	0.7321	8.1962	2.5	7.8868	0.25	0.2113
3.5	1.0	1.0	2.7213	0.7213	0.7213	9.5245	2.5	9.2223	0.25	0.2095
4.0	1.0	1.0	2.7136	0.7136	0.7136	10.8543	2.5	10.5572	0.25	0.2082

Table 2.2 brings a few selected examples of real transversely isotropic soil materials, and one example of an isotropic one with $E=2.5$ and $\nu=0.25$ taken from the work of Wang and Rajapakse (1994). Their corresponding anisotropy indices are also shown. The layered soil in this table is a limestone-sandstone system.

Table 2.2 Examples of transversely isotropic materials. Units of c_{ij} : 10^{10} N/m².

Material	c_{11}	c_{12}	c_{13}	c_{33}	c_{44}	n_1	n_2	n_3
Silty Clay	5.70	1.16	1.27	6.97	2.70	1.22	0.84	0.24
Beryl rock	4.13	1.47	1.01	3.62	1.00	0.88	1.33	2.11
Layered soil	6.24	2.18	1.74	4.56	1.40	0.73	1.45	1.98
Clay	0.047	0.017	0.012	0.033	0.01	0.70	1.50	2.25
Ice (257K)	1.35	0.65	0.52	1.45	0.32	1.07	1.09	1.36
Isotropic	3.0	1.0	1.0	3.0	1.0	1.00	1.00	1.00

2.2 Transversely isotropic three-dimensional full-space

Consider a three-dimensional transversely isotropic full-space, with a cylindrical coordinate system $O(r, \theta, z)$ positioned in such a way that its z axis is orthogonal to the material's plane of isotropy (Fig. 2.1). In the absence of body forces, the equations of motion are expressed by (Slaughter, 2002):

$$\frac{\partial}{\partial r} \sigma_{rr} + \frac{1}{r} \frac{\partial}{\partial \theta} \sigma_{r\theta} + \frac{\partial}{\partial z} \sigma_{rz} + \frac{1}{r} (\sigma_{rr} - \sigma_{\theta\theta}) = \rho \frac{\partial^2}{\partial t^2} u_r \quad (2.23)$$

$$\frac{\partial}{\partial r} \sigma_{r\theta} + \frac{1}{r} \frac{\partial}{\partial \theta} \sigma_{\theta\theta} + \frac{\partial}{\partial z} \sigma_{\theta z} + \frac{2}{r} \sigma_{r\theta} = \rho \frac{\partial^2}{\partial t^2} u_\theta \quad (2.24)$$

$$\frac{\partial}{\partial r} \sigma_{rz} + \frac{1}{r} \frac{\partial}{\partial \theta} \sigma_{\theta z} + \frac{\partial}{\partial z} \sigma_{zz} + \frac{1}{r} \sigma_{rz} = \rho \frac{\partial^2}{\partial t^2} u_z \quad (2.25)$$

On the other hand, the strain-displacement relations in cylindrical coordinates are (Slaughter, 2002):

$$\varepsilon_{rr} = \frac{\partial}{\partial r} u_r \quad (2.26)$$

$$\varepsilon_{\theta\theta} = \frac{1}{r} \left(\frac{\partial}{\partial \theta} u_\theta + u_r \right) \quad (2.27)$$

$$\varepsilon_{zz} = \frac{\partial}{\partial z} u_z \quad (2.28)$$

$$\varepsilon_{r\theta} = \frac{1}{2} \left(\frac{1}{r} \frac{\partial}{\partial \theta} u_r + \frac{\partial}{\partial \theta} u_\theta - \frac{1}{r} u_\theta \right) \quad (2.29)$$

$$\varepsilon_{\theta z} = \frac{1}{2} \left(\frac{\partial}{\partial z} u_\theta + \frac{1}{r} \frac{\partial}{\partial \theta} u_z \right) \quad (2.30)$$

$$\varepsilon_{rz} = \frac{1}{2} \left(\frac{\partial}{\partial z} u_r + \frac{\partial}{\partial r} u_z \right) \quad (2.31)$$

The substitution of Eqs. 2.1 to 2.6 into Eqs. 2.23 to 2.25, in view of Eqs. 2.26 to 2.31, yields the equations of motion for the transversely isotropic full-space in terms of the displacement components:

$$\begin{aligned} c_{11} \left(\frac{\partial^2}{\partial r^2} u_r + \frac{1}{r} \frac{\partial}{\partial r} u_r - \frac{u_r}{r^2} \right) + \frac{c_{11} - c_{12}}{2} \frac{1}{r^2} \frac{\partial^2}{\partial \theta^2} u_r + c_{44} \frac{\partial^2}{\partial z^2} u_r \\ + \frac{c_{11} + c_{12}}{2} \left(\frac{1}{r} \frac{\partial^2}{\partial r \partial \theta} u_\theta + \frac{1}{r^2} \frac{\partial}{\partial \theta} u_\theta \right) - 2c_{11} \frac{1}{r^2} \frac{\partial}{\partial \theta} u_\theta + (c_{13} + c_{44}) \frac{\partial^2}{\partial r \partial z} u_z = \rho \frac{\partial^2}{\partial t^2} u_r \end{aligned} \quad (2.32)$$

$$\begin{aligned} \frac{c_{11} - c_{12}}{2} \left(\frac{\partial^2}{\partial r^2} u_\theta + \frac{1}{r} \frac{\partial}{\partial r} u_\theta - \frac{u_\theta}{r^2} \right) + c_{11} \frac{1}{r^2} \frac{\partial^2}{\partial \theta^2} u_\theta + c_{44} \frac{\partial^2}{\partial z^2} u_\theta \\ + \frac{c_{11} + c_{12}}{2} \left(\frac{1}{r} \frac{\partial^2}{\partial r \partial \theta} u_r - \frac{1}{r^2} \frac{\partial}{\partial \theta} u_r \right) + 2c_{11} \frac{1}{r^2} \frac{\partial}{\partial \theta} u_r + (c_{13} + c_{44}) \frac{1}{r} \frac{\partial^2}{\partial \theta \partial z} u_z = \rho \frac{\partial^2}{\partial t^2} u_\theta \end{aligned} \quad (2.33)$$

$$\begin{aligned} c_{44} \left(\frac{\partial^2}{\partial r^2} u_z + \frac{1}{r} \frac{\partial}{\partial r} u_z + \frac{1}{r^2} \frac{\partial^2}{\partial \theta^2} u_z \right) + c_{33} \frac{\partial^2}{\partial z^2} u_z \\ + (c_{13} + c_{44}) \left(\frac{\partial^2}{\partial r \partial z} u_r + \frac{1}{r} \frac{\partial}{\partial z} u_z + \frac{1}{r} \frac{\partial^2}{\partial \theta \partial z} u_\theta \right) = \rho \frac{\partial^2}{\partial t^2} u_z \end{aligned} \quad (2.34)$$

In Eqs. 2.32 to 2.34, ρ is the density of the medium and c_{ij} are elastic constants of the transversely isotropic material, while u_r , u_θ and u_z denote the displacements of the full-space in

the r , θ and z directions, respectively (Fig. 2.1).

Wang (1992) derived a solution for this coupled equation system. His solution is based on the definition of three potential functions ψ , ϕ and χ such that:

$$u_r = \frac{\partial}{\partial r} \phi + \frac{1}{r} \frac{\partial}{\partial \theta} \psi \quad (2.35)$$

$$u_\theta = \frac{1}{r} \frac{\partial}{\partial \theta} \phi - \frac{\partial}{\partial r} \psi \quad (2.36)$$

$$u_z = \frac{\partial}{\partial z} \chi \quad (2.37)$$

Substitution of Eqs. 2.35 to 2.37 into Eqs. 2.32 to 2.34 yields:

$$\kappa \nabla^2 \frac{\partial^2}{\partial z^2} \chi + \left(\beta \nabla^2 + \frac{\partial^2}{\partial z^2} + \delta^2 \right) \nabla^2 \phi = 0 \quad (2.38)$$

$$\kappa \nabla^2 \frac{\partial^2}{\partial z^2} \phi + \left(\nabla^2 + \alpha \frac{\partial^2}{\partial z^2} + \delta^2 \right) \frac{\partial^2}{\partial z^2} \chi = 0 \quad (2.39)$$

$$\left(\varsigma \nabla^2 + \frac{\partial^2}{\partial z^2} + \delta^2 \right) \nabla^2 \psi = 0 \quad (2.40)$$

Equations 2.38 and 2.39 form a set of equations with coupled potential functions ϕ and χ . Equation 2.40 describes the uncoupled behavior of the potential function ψ . The nondimensional material parameters shown in Eqs. 2.38 to 2.40 have been defined in Eqs. 2.15 to 2.19. The Laplace differential operator ∇^2 and the parameter δ are defined as:

$$\nabla^2 = \frac{\partial^2}{\partial r^2} + \frac{1}{r} \frac{\partial}{\partial r} + \frac{1}{r^2} \frac{\partial^2}{\partial \theta^2} \quad (2.41)$$

$$\delta^2 = \rho \omega^2 / c_{44} \quad (2.42)$$

The solution presented by Wang (1992) involves a Fourier series expansion of the potential functions ψ , ϕ and χ . This Fourier expansion, with respect to θ , was proposed by Muki (1960):

$$\chi(r, \theta, z) = \sum_{m=0}^{\infty} \left[\chi_m(r, z) \cos(m\theta) + \chi_m^*(r, z) \sin(m\theta) \right] \quad (2.43)$$

$$\phi(r, \theta, z) = \sum_{m=0}^{\infty} \left[\phi_m(r, z) \cos(m\theta) + \phi_m^*(r, z) \sin(m\theta) \right] \quad (2.44)$$

$$\psi(r, \theta, z) = \sum_{m=0}^{\infty} \left[\psi_m(r, z) \sin(m\theta) - \psi_m^*(r, z) \cos(m\theta) \right] \quad (2.45)$$

In Eqs. 2.43 to 2.45, ψ_m , ϕ_m and χ_m correspond to deformations that are symmetric with respect to $\theta=0$ for the m^{th} harmonic, while their counterparts ψ_m^* , ϕ_m^* and χ_m^* correspond to antisymmetric deformations (Muki, 1960). In this work, only the symmetric components ψ_m , ϕ_m and χ_m are considered, without loss of generality (Muki, 1960; Wang, 1992).

The potential functions ψ , ϕ and χ undergo a transformation of space so that they can be dealt with algebraically. A natural choice of transform for these equations, which are in cylindrical coordinates, is the Hankel transform in the radial coordinate:

$$\tilde{\chi}_m(\lambda, z) = \mathcal{H}_m \{ \chi_m(r, z) \} = \int_0^{\infty} \chi_m(r, z) J_m(\lambda r) r dr \quad (2.46)$$

$$\chi_m(r, z) = \mathcal{H}_m^{-1} \{ \tilde{\chi}_m(\lambda, z) \} = \int_0^{\infty} \tilde{\chi}_m(\lambda, z) J_m(\lambda r) \lambda d\lambda \quad (2.47)$$

In Eqs. 2.46 and 2.47, \mathcal{H}_m and \mathcal{H}_m^{-1} represent, respectively, the Hankel transform of order m and its inverse, J_m represents Bessel functions of the first kind and order m (Abramowitz and Stegun, 1965) and λ is the Hankel space variable. Analogous definitions hold for ψ and ϕ .

Hankel transform is applied to Eqs. 2.38 to 2.40, which yields:

$$\kappa \frac{d^2}{dz^2} \check{\chi}_m + \frac{d^2}{dz^2} \check{\phi}_m - (\beta\lambda^2 - \delta^2) \check{\phi}_m = 0 \quad (2.48)$$

$$-\kappa\lambda^2 \check{\phi}_m + \alpha \frac{d^2}{dz^2} \check{\chi}_m - (\lambda^2 - \delta^2) \check{\chi}_m = 0 \quad (2.49)$$

$$\frac{d^2}{dz^2} \check{\psi}_m - (\zeta\lambda^2 - \delta^2) \check{\psi}_m = 0 \quad (2.50)$$

In Eqs. 2.48 to 2.50, $\check{\chi}_m$, $\check{\phi}_m$ and $\check{\psi}_m$ are the m^{th} symmetric components of the Fourier series expansion (Eqs. 2.43 to 2.45), in the transformed domain.

The coupled behavior between the functions ϕ and χ , which was observed in Eqs. 2.38 and 2.39, remains in Eqs. 2.48 and 2.49 after the application of the Hankel transform. Equation 2.50 describes the uncoupled behavior of the potential function ψ in the transformed domain. One solution to the coupled equations 2.48 and 2.49 is obtained by assuming that:

$$\check{\phi}_m = P e^{\delta \xi z} \quad \text{and} \quad \check{\chi}_m = Q e^{\delta \xi z} \quad (2.51)$$

Substitution of Eq. 2.51 into 2.48 and 2.49 yields:

$$(\xi^2 - \beta\zeta^2 + 1)P + \kappa\xi^2 Q = 0 \quad (2.52)$$

$$(\alpha\xi^2 - \zeta^2 + 1)Q - \kappa\zeta^2 P = 0 \quad (2.53)$$

in which $\zeta = \lambda/\delta$. For a non-trivial solution of Eqs. 2.52 and 2.53, the parameter ξ must satisfy:

$$\xi_{1,2}(\zeta) = \frac{1}{\sqrt{2\alpha}} \left(\gamma\zeta^2 - 1 - \alpha \pm \sqrt{\Phi} \right)^{\frac{1}{2}} \quad (2.54)$$

and

$$\Phi(\zeta) = (\gamma\zeta^2 - 1 - \alpha)^2 - 4\alpha(\beta\zeta^4 - \beta\zeta^2 - \zeta^2 + 1) \quad (2.55)$$

Finally, a solution for the third and uncoupled Eq. 2.50 is obtained by assuming that:

$$\check{\Psi}_m = C e^{\delta\xi_3 z} \quad (2.56)$$

Substitution of Eq. 2.56 into 2.50 yields:

$$\xi^2 - (\zeta\zeta^2 - 1) = 0 \quad (2.57)$$

from which it comes:

$$\xi_3 = \pm\sqrt{\zeta\zeta^2 - 1} \quad (2.58)$$

From the solutions of ξ_i ($i=1,2,3$) from Eqs. 2.54 and 2.58, and in view of the assumed forms of the potential functions established in Eqs. 2.51 and 2.56, general solutions for the m^{th} symmetric component of these potential functions in the Hankel transformed domain are obtained:

$$\check{\Phi}_m = \vartheta_1 A_m e^{-\delta\xi_1 z} + \vartheta_1 B_m e^{\delta\xi_1 z} + \vartheta_2 C_m e^{-\delta\xi_2 z} + \vartheta_2 D_m e^{\delta\xi_2 z} \quad (2.59)$$

$$\check{\Psi}_m = E_m e^{-\delta\xi_3 z} + F_m e^{\delta\xi_3 z} \quad (2.60)$$

$$\check{\chi}_m = A_m e^{-\delta\xi_1 z} + B_m e^{\delta\xi_1 z} + C_m e^{-\delta\xi_2 z} + D_m e^{\delta\xi_2 z} \quad (2.61)$$

in which,

$$\vartheta_{1,2} = \frac{\alpha\xi_{1,2}^2 - \zeta^2 + 1}{\kappa\zeta^2} \quad (2.62)$$

In Eqs. 2.59 to 2.61, A_m , B_m , C_m , D_m , E_m and F_m are arbitrary functions to be determined according to the boundary conditions of a given problem.

The corresponding solutions to ψ , ϕ and χ in the physical domain are achieved upon integration of Eqs. 2.59 to 2.61 according to Eq. 2.47. Substitution of these potential functions into Eqs. 2.35 to 2.37 results in the m^{th} symmetric Fourier component of displacement of the three-dimensional transversely isotropic full-space (Wang, 1992) in the physical domain:

$$u_{im} = \int_0^{\infty} u_{im}^* \lambda d\lambda, \quad i = r, \theta, z \quad (2.63)$$

in which

$$\lambda = \delta \cdot \zeta \quad (2.64)$$

and

$$u_{rm}^* = a_1 \bar{A}_m + a_1 \bar{B}_m + a_2 \bar{C}_m + a_2 \bar{D}_m + a_3 \bar{E}_m + a_3 \bar{F}_m \quad (2.65)$$

$$u_{\theta m}^* = -(a_4 \bar{A}_m + a_4 \bar{B}_m + a_5 \bar{C}_m + a_5 \bar{D}_m + a_6 \bar{E}_m + a_6 \bar{F}_m) \quad (2.66)$$

$$u_{zm}^* = -(a_7 \bar{A}_m - a_7 \bar{B}_m + a_8 \bar{C}_m - a_8 \bar{D}_m) \quad (2.67)$$

The corresponding stress solutions are given by:

$$\sigma_{ijm} = \int_0^{\infty} \sigma_{ijm}^* \lambda d\lambda, \quad i, j = r, \theta, z \quad (2.68)$$

in which:

$$\sigma_{rrm}^* = c_{44} (b_{11} \bar{A}_m + b_{11} \bar{B}_m + b_{12} \bar{C}_m + b_{12} \bar{D}_m + b_{13} \bar{E}_m + b_{13} \bar{F}_m) \quad (2.69)$$

$$\sigma_{\theta\theta m}^* = c_{44} (b_{61} \bar{A}_m + b_{61} \bar{B}_m + b_{62} \bar{C}_m + b_{62} \bar{D}_m - b_{13} \bar{E}_m - b_{13} \bar{F}_m) \quad (2.70)$$

$$\sigma_{zzm}^* = c_{44} (b_{21} \bar{A}_m + b_{21} \bar{B}_m + b_{22} \bar{C}_m + b_{22} \bar{D}_m) \quad (2.71)$$

$$\sigma_{r\theta m}^* = c_{44} (b_{31} \bar{A}_m + b_{31} \bar{B}_m + b_{32} \bar{C}_m + b_{32} \bar{D}_m + b_{33} \bar{E}_m + b_{33} \bar{F}_m) \quad (2.72)$$

$$\sigma_{\theta zm}^* = c_{44} (b_{41} \bar{A}_m - b_{41} \bar{B}_m + b_{42} \bar{C}_m - b_{42} \bar{D}_m + b_{43} \bar{E}_m - b_{43} \bar{F}_m) \quad (2.73)$$

$$\sigma_{rzm}^* = -c_{44} (b_{51} \bar{A}_m - b_{51} \bar{B}_m + b_{52} \bar{C}_m - b_{52} \bar{D}_m + b_{53} \bar{E}_m - b_{53} \bar{F}_m) \quad (2.74)$$

In Eqs. 2.65 to 2.67 and 2.69 to 2.74,

$$\bar{A}_m = A_m e^{-\delta \xi_1 z}, \bar{B}_m = B_m e^{+\delta \xi_1 z}, \bar{C}_m = C_m e^{-\delta \xi_2 z} \quad (2.75)$$

$$\bar{D}_m = D_m e^{+\delta \xi_2 z}, \bar{E}_m = E_m e^{-\delta \xi_3 z} \text{ and } \bar{F}_m = F_m e^{+\delta \xi_3 z} \quad (2.76)$$

and

$$b_{li} = \frac{\varsigma \vartheta_i \delta \zeta}{2r} [(m-1) J_{m-1}(\delta \zeta r) - (m+1) J_{m+1}(\delta \zeta r)] \quad (2.77)$$

$$- [\delta^2 \zeta^2 \beta \vartheta_i - (\kappa - 1) \delta^2 \xi_i^2] J_m(\delta \zeta r), \quad i=1,2$$

$$\frac{b_{13}}{\varsigma} = \frac{2b_{3i}}{\varsigma \vartheta_i \delta \zeta} = \frac{2b_{33}}{[1 + (\delta^2 \zeta^2 r^2 / 2m)] \varsigma \delta \zeta} = [(m-1) J_{m-1}(\delta \zeta r) - (m+1) J_{m+1}(\delta \zeta r)]; \quad i=1,2 \quad (2.78)$$

$$b_{6i} = -\frac{\varsigma \vartheta_i \delta \zeta}{2r} [(m-1) J_{m-1}(\delta \zeta r) - (m+1) J_{m+1}(\delta \zeta r)] \quad (2.79)$$

$$- [\delta^2 \zeta^2 \beta \vartheta_i - (\kappa - 1) \delta^2 \xi_i^2] J_m(\delta \zeta r), \quad i=1,2$$

$$b_{2i} = [\alpha \delta^2 \xi_i^2 - (\kappa - 1) \delta^2 \zeta^2 \vartheta_i] J_m(\delta \zeta r), \quad i=1,2 \quad (2.80)$$

$$\frac{a_7}{\delta \xi_1} = \frac{a_8}{\delta \xi_2} = J_m(\delta \zeta r) \quad (2.81)$$

$$a_3 = \frac{a_4}{\vartheta_1} = \frac{a_5}{\vartheta_2} = \frac{b_{4i}}{(1 + \vartheta_i) \delta \xi_i} = \frac{b_{53}}{\delta \xi_3} = \frac{\delta \zeta}{2} [J_{m-1}(\delta \zeta r) + J_{m+1}(\delta \zeta r)], \quad i=1,2 \quad (2.82)$$

$$a_6 = \frac{a_1}{\vartheta_1} = \frac{a_2}{\vartheta_2} = \frac{b_{5i}}{(1 + \vartheta_i) \delta \xi_i} = \frac{b_{43}}{\delta \xi_3} = \frac{\delta \zeta}{2} [J_{m-1}(\delta \zeta r) - J_{m+1}(\delta \zeta r)], \quad i=1,2 \quad (2.83)$$

In this section general solutions for the behavior of three-dimensional transversely isotropic full-spaces have been presented. Expressions for the m^{th} symmetric Fourier component of the displacement (Eq. 2.63) and stress field (Eq. 2.68) in the physical domain were also obtained. These solutions are written in terms of arbitrary functions A_m, \dots, F_m that depend on the boundary conditions of a problem. The next two sections will present two different boundary-value problems from which specific values of these functions are obtained.

2.3 Elastodynamic three-dimensional bi-material interface

Consider two transversely isotropic elastic half-spaces perfectly bonded along their plane of isotropy. A cylindrical coordinate system $O(r, \theta, z)$ is adopted, the z -axis of which is orthogonal to their material plane of isotropy (Fig. 2.2). The origin of the coordinate system is placed at the interface of the two media. In this section, boundary-value problems corresponding to distributed annular loads acting at that bi-material interface ($z=0$) are considered.

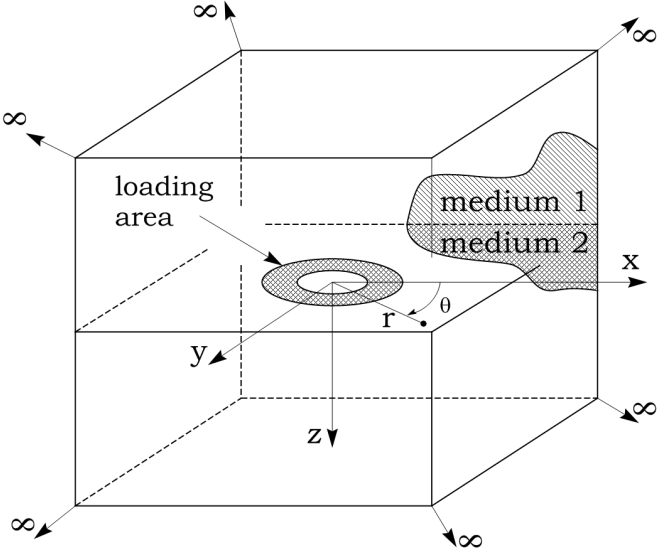


Figure 2.2 Definition of coordinate system, domains and loading area.

The first two loading cases treated in this work represent vertical and transverse loads uniformly distributed over an annular area of inner and outer radii s_1 and s_2 (Figs. 2.3a and 2.3b). The third case represents a vertical load whose intensity varies linearly along the x -axis (Fig. 2.3c). In the third case, the configuration of the loading is such that it represents a net moment about the y -axis. The subsequent formulation assumes that both concentrated and distributed

loads can be applied in all three cases. Section 2.4 brings a detailed description of these three types of loading configuration. Figures 2.3a and 2.3b illustrate the case of uniformly distributed vertical and transverse loads, respectively. Figure 2.3c illustrates the case in which an antisymmetric vertical load is applied to a ring of radius r , resulting in a net moment about the y -axis. In the case shown in Fig. 2.3c, the load is considered to be applied in a concentrated way to a ring of radius r . Notice how the intensity of the load presents a cosine variation about the angle θ .

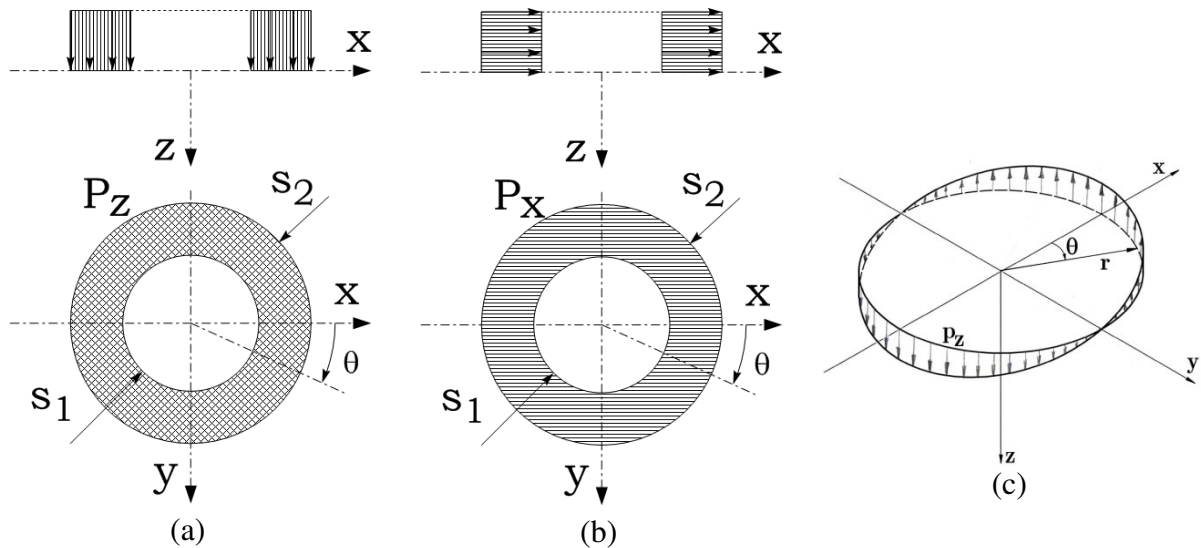


Figure 2.3 Internal loading configurations considering (a) vertical loads, (b) transverse loads along x and (c) varying vertical load representing a concentrated moment about the y -axis.

Each of the two media $d=1$ ($-\infty < z \leq 0$) or $d=2$ ($0 \leq z < +\infty$) has its own particular expressions for displacements and stresses $u_{im}^{(d)}(r,z)$ and $\sigma_{ijm}^{(d)}(r,z)$ ($i,j=r,\theta,z$), which are distinguished by the upper index d .

Consider for example the component $u_{\theta m}(r,z)$ (Eqs. 2.63 and 2.66). The arbitrary constants A_m, B_m, C_m, D_m, E_m and F_m must be selected so that Sommerfeld's radiation condition is satisfied (Sommerfeld, 1949). Since the domains $d=1$ and $d=2$ are respectively $-\infty < z \leq 0$ (z is always negative) and $0 \leq z < +\infty$ (z is always positive), the expressions of $u_{\theta m}^{(d)}(r,z)$, $d=1,2$ for each domain are:

$$u_{\theta m}^{(1)}(r, z) = -\int_0^\infty \left(a_4^{(1)} B_m^{(1)} e^{\delta^{(1)} \xi_1^{(1)} z} + a_5^{(1)} D_m^{(1)} e^{\delta^{(1)} \xi_2^{(1)} z} + a_6^{(1)} F_m^{(1)} e^{\delta^{(1)} \xi_3^{(1)} z} \right) \lambda d\lambda \quad (2.84)$$

$$u_{\theta m}^{(2)}(r, z) = -\int_0^\infty \left(a_4^{(2)} A_m^{(2)} e^{-\delta^{(2)} \xi_1^{(2)} z} + a_5^{(2)} C_m^{(2)} e^{-\delta^{(2)} \xi_2^{(2)} z} + a_6^{(2)} E_m^{(2)} e^{-\delta^{(2)} \xi_3^{(2)} z} \right) \lambda d\lambda \quad (2.85)$$

Notice that the material constants and other parameters also depend on the respective medium and are identified by an appropriate superscript (for example, $a^{(d)}_4$ and $\xi^{(d)}_1$). The same particularization holds for the stress components.

2.3.1 Displacement boundary conditions

Under the hypothesis that the two half-spaces are perfectly bonded together along their interface ($z=0$), the kinematic continuity condition for all loading cases is that

$$u_{im}^{(1)}(r, 0) = u_{im}^{(2)}(r, 0); \quad i=r, \theta, z \quad (2.86)$$

The stress boundary conditions, on the other hand, vary according to each load configuration.

2.3.2 Stress boundary conditions

In this section, the stress boundary conditions are derived for the three loading configurations presented in Fig. 2.3. For each of the three cases, depending on whether the problem presents axisymmetry or not, particularized expressions for the displacement and stress components are derived, i.e., particular expressions for Eqs. 2.65 to 2.67 (displacement components) and Eqs. 2.69 to 2.74 (stress components). Then the stress boundary conditions are introduced, using these particularized expressions.

For the axisymmetric case of vertical load shown in Fig. 2.3a, in view of axial symmetry, $m=0$. In this work, only symmetric components are used in the Fourier series expansion (Eqs. 2.43 to 2.45). Therefore, in the case of axisymmetric vertical loads, the solutions do not depend on the parameter θ . Subsection 2.3.2.1 begins with the particularization of the expressions of displacement and stress (Eqs. 2.65 to 2.74) for the case of $m=0$ and no θ dependence, then introduces the respective boundary conditions using these particularized expressions.

Conversely, in the case of antisymmetric loads presented in Figs. 2.3b and 2.3c, it is necessary to account for the antisymmetric behavior of the displacement and stress components as well. To comply with this, a θ -dependence is introduced in the Fourier expansion of the displacement and stress components according to Eqs. 2.43 to 2.45 ($m=1$). Subsection 2.3.2.2 begins with the particularization of the expressions of displacement and stress (Eqs. 2.65 to 2.74) for the case of $m=1$ and with θ -dependence, then introduces the boundary conditions corresponding to the transverse load shown in Fig. 2.3b. In Subsection 2.3.2.3, these same particularized expressions for $m=1$ are used for the case of the antisymmetric vertical load shown in Fig. 2.3c.

2.3.2.1 Vertical load

Consider the problem of a dynamic vertical load uniformly distributed on an annular area, such as depicted in Fig. 2.3a. In view of axial symmetry, $m=0$. Consider also the following property of the Bessel function (Abramowitz and Stegun, 1965):

$$J_{-v}(r) = (-1)^v J_v(r) \quad (2.87)$$

For the case in which $m=0$, considering Eq. 2.87, the parameters defined in Eqs. 2.77 to 2.83 become, for $i=1,2$:

$$b_{1i} = -\frac{\varsigma \vartheta_i \delta \zeta}{r} J_1(\delta \zeta r) - \left[\delta^2 \zeta^2 \beta \vartheta_i - (\kappa - 1) \delta^2 \xi_i^2 \right] J_0(\delta \zeta r) \quad (2.88)$$

$$\frac{b_{13}}{\varsigma} = \frac{2b_{3i}}{\varsigma \vartheta_i \delta \zeta} = \frac{2b_{33}}{\left[1 + \left(\delta^2 \zeta^2 r^2 / 2m \right) \right] \varsigma \delta \zeta} = \left[-J_{-1}(\delta \zeta r) - J_1(\delta \zeta r) \right] = 0 \quad (2.89)$$

$$b_{6i} = -\left[\delta^2 \zeta^2 \beta \vartheta_i - (\kappa - 1) \delta^2 \xi_i^2 \right] J_0(\delta \zeta r) \quad (2.90)$$

$$b_{2i} = \left[\alpha \delta^2 \xi_i^2 - (\kappa - 1) \delta^2 \zeta^2 \vartheta_i \right] J_0(\delta \zeta r) \quad (2.91)$$

$$\frac{a_7}{\delta \xi_1} = \frac{a_8}{\delta \xi_2} = J_0(\delta \zeta r) \quad (2.92)$$

$$a_3 = \frac{a_4}{\vartheta_1} = \frac{a_5}{\vartheta_2} = \frac{b_{4i}}{(1+\vartheta_i)\delta\xi_i} = \frac{b_{53}}{\delta\xi_3} = \frac{\delta\zeta}{2} [J_{-1}(\delta\zeta_r) + J_1(\delta\zeta_r)] = 0 \quad (2.93)$$

$$a_6 = \frac{a_1}{\vartheta_1} = \frac{a_2}{\vartheta_2} = \frac{b_{5i}}{(1+\vartheta_i)\delta\xi_i} = \frac{b_{43}}{\delta\xi_3} = \frac{\delta\zeta}{2} [J_{-1}(\delta\zeta_r) - J_1(\delta\zeta_r)] = -\delta\zeta J_1(\delta\zeta_r) \quad (2.94)$$

In Eqs. 2.88 to 2.94, the upper index d indicating the medium d=1,2 was omitted for conciseness.

Based on these results, the expression of displacements and stresses for the case of m=0 are:

$$u_{i0}^{(d)} = \int_0^\infty u_{i0}^{*(d)} \lambda d\lambda ; i=r,z; d=1,2 \quad (2.95)$$

$$\sigma_{ij0}^{(d)} = \int_0^\infty \sigma_{ij0}^{*(d)} \lambda d\lambda ; i=r,z; d=1,2 \quad (2.96)$$

in which,

$$\lambda = \delta^{(d)} \cdot \zeta \quad (2.97)$$

For medium d=1,

$$u_{r0}^{*(1)} = a_1^{(1)} B_0^{(1)} e^{\delta^{(1)} \xi_1^{(1)} z} + a_2^{(1)} D_0^{(1)} e^{\delta^{(1)} \xi_2^{(1)} z} \quad (2.98)$$

$$u_{z0}^{*(1)} = -\left(-a_7^{(1)} B_0^{(1)} e^{\delta^{(1)} \xi_1^{(1)} z} - a_8^{(1)} D_0^{(1)} e^{\delta^{(1)} \xi_2^{(1)} z} \right) \quad (2.99)$$

$$\sigma_{rr0}^{*(1)} = c_{44}^{(1)} \left(+b_{11}^{(1)} B_0^{(1)} e^{\delta^{(1)} \xi_1^{(1)} z} + b_{12}^{(1)} D_0^{(1)} e^{\delta^{(1)} \xi_2^{(1)} z} \right) \quad (2.100)$$

$$\sigma_{zz0}^{*(1)} = c_{44}^{(1)} \left(+b_{21}^{(1)} B_0^{(1)} e^{\delta^{(1)} \xi_1^{(1)} z} + b_{22}^{(1)} D_0^{(1)} e^{\delta^{(1)} \xi_2^{(1)} z} \right) \quad (2.101)$$

$$\sigma_{rz0}^{*(1)} = -c_{44}^{(1)} \left(-b_{51}^{(1)} B_0^{(1)} e^{\delta^{(1)} \xi_1^{(1)} z} - b_{52}^{(1)} D_0^{(1)} e^{\delta^{(1)} \xi_2^{(1)} z} \right) \quad (2.102)$$

For medium d=2,

$$u_{r0}^{*(2)} = a_1^{(2)} A_0^{(2)} e^{-\delta^{(1)} \xi_1^{(1)} z} + a_2^{(2)} C_0^{(2)} e^{-\delta^{(1)} \xi_2^{(1)} z} \quad (2.103)$$

$$u_{z0}^{*(2)} = -\left(a_7^{(2)} A_0^{(2)} e^{-\delta^{(1)} \xi_1^{(1)} z} + a_8^{(2)} C_0^{(2)} e^{-\delta^{(1)} \xi_2^{(1)} z} \right) \quad (2.104)$$

$$\sigma_{rr0}^{*(2)} = c_{44}^{(2)} \left(b_{11}^{(2)} A_0^{(2)} e^{-\delta^{(1)} \xi_1^{(1)} z} + b_{12}^{(2)} C_0^{(2)} e^{-\delta^{(1)} \xi_2^{(1)} z} \right) \quad (2.105)$$

$$\sigma_{zz0}^{*(2)} = c_{44}^{(2)} \left(b_{21}^{(2)} A_0^{(2)} e^{-\delta^{(1)} \xi_1^{(1)} z} + b_{22}^{(2)} C_0^{(2)} e^{-\delta^{(1)} \xi_2^{(1)} z} \right) \quad (2.106)$$

$$\sigma_{rz0}^{*(2)} = -c_{44}^{(2)} \left(b_{51}^{(2)} A_0^{(2)} e^{-\delta^{(1)} \xi_1^{(1)} z} + b_{52}^{(2)} C_0^{(2)} e^{-\delta^{(1)} \xi_2^{(1)} z} \right) \quad (2.107)$$

Notice that, since the terms b_{13} , b_{31} , b_{32} , b_{33} , b_{41} , b_{42} and b_{53} , and a_3 , a_4 and a_5 are all zero for $m=0$, the antisymmetric components of displacement and stress u_θ , $\sigma_{\theta\theta}$, $\sigma_{r\theta}$ and $\sigma_{\theta z}$ are all zero. The arbitrary functions E_0 and F_0 , which come from the antisymmetric potential function ψ (Eq. 2.60), also vanish.

The continuity at the interface ($z=0$) established in Eq. 2.86 results in:

$$u_{r0}^{(1)} = \int_0^\infty \left[a_1^{(1)} B_0^{(1)} + a_2^{(1)} D_0^{(1)} \right] \lambda d\lambda = u_{r0}^{(2)} = \int_0^\infty \left[a_1^{(2)} A_0^{(2)} + a_2^{(2)} C_0^{(2)} \right] \lambda d\lambda \quad (2.108)$$

$$a_1^{(2)} A_0^{(2)} - a_1^{(1)} B_0^{(1)} + a_2^{(2)} C_0^{(2)} - a_2^{(1)} D_0^{(1)} = 0 \quad (2.109)$$

$$u_{z0}^{(1)} = \int_0^\infty \left[-\left(-a_7^{(1)} B_0^{(1)} - a_8^{(1)} D_0^{(1)} \right) \right] \lambda d\lambda = u_{z0}^{(2)} = \int_0^\infty \left[-\left(a_7^{(2)} A_0^{(2)} + a_8^{(2)} C_0^{(2)} \right) \right] \lambda d\lambda \quad (2.110)$$

$$a_7^{(2)} A_m^{(2)} + a_7^{(1)} B_m^{(1)} + a_8^{(2)} C_m^{(2)} + a_8^{(1)} D_m^{(1)} = 0 \quad (2.111)$$

On the other hand, the traction discontinuity at the interface ($z=0$) due to the axisymmetric vertical load shown in Fig. 2.3a is, for this case of $m=0$, in the physical domain:

$$p_{z0}^{(1)} + p_{z0}^{(2)} = \tilde{\wp}_0 \quad (2.112)$$

$$p_{r0}^{(1)} + p_{r0}^{(2)} = 0 \quad (2.113)$$

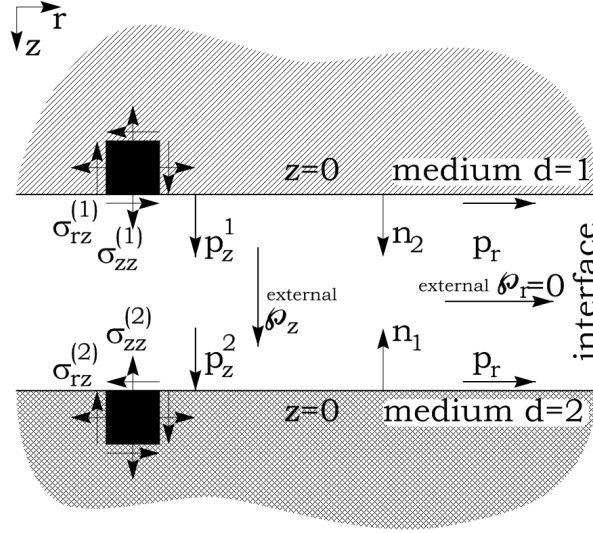


Figure 2.4 Definitions and sign conventions for tractions, stresses and external loads, considering the normal vectors at the free surfaces of each medium. The subscript m is omitted for conciseness.

In Eqs. 2.112 and 2.113, p_{z0} and p_{r0} indicate axisymmetric tractions acting at the interface ($z=0$) in the vertical and radial directions, respectively. In this work, the term \wp_m with a tilde is used to represent axisymmetric ($m=0$) or antisymmetric ($m=1$) distributed loads in the physical domain. A further discussion on the mathematical description of the diverse loading configurations is given in Section 2.4.

Notice that the stress components at the surface of medium 2 have opposite directions to the traction vectors acting on that surface (Fig. 2.4). Taking that into consideration, then Eqs. 2.112 and 2.113 can be written in terms of stresses, in the physical domain:

$$\sigma_{zz0}^{(1)}(r,0) - \sigma_{zz0}^{(2)}(r,0) = \tilde{\wp}_0 \quad (2.114)$$

$$\sigma_{rz0}^{(1)}(r,0) - \sigma_{rz0}^{(2)}(r,0) = 0 \quad (2.115)$$

Substitution of Eqs. 2.100 to 2.107 into Eqs. 2.114 yields:

$$\begin{aligned}
& \sigma_{zz0}^{(1)} - \sigma_{zz0}^{(2)} \\
&= \int_0^\infty \left[c_{44}^{(1)} \left(b_{21}^{(1)} B_0^{(1)} + b_{22}^{(1)} D_0^{(1)} \right) \right] \lambda d\lambda - \int_0^\infty \left[c_{44}^{(2)} \left(b_{21}^{(2)} A_0^{(2)} + b_{22}^{(2)} C_0^{(2)} \right) \right] \lambda d\lambda \\
&= \tilde{\rho}_0 = \mathcal{H}_0^{-1} \{ \mathcal{H}_0 \{ \tilde{\rho}_0 \} \} = \int_0^\infty \mathcal{H}_0 \{ \tilde{\rho}_0 \} J_0(\lambda r) \lambda d\lambda
\end{aligned} \tag{2.116}$$

$$-c_{44}^{(2)} b_{21}^{(2)} A_0^{(2)} + c_{44}^{(1)} b_{21}^{(1)} B_0^{(1)} - c_{44}^{(2)} b_{22}^{(2)} C_0^{(2)} + c_{44}^{(1)} b_{22}^{(1)} D_0^{(1)} = \mathcal{H}_0 \{ \tilde{\rho}_0 \} J_0(\lambda r) \tag{2.117}$$

in which \mathcal{H}_m and \mathcal{H}_m^{-1} represent respectively the Hankel transform of order m and its inverse, and J_m represents Bessel functions of order m (Abramowitz and Stegun, 1965). This is explained in detail in Section 2.4.

Substitution of Eqs. 2.100 to 2.107 into Eqs. 2.115 yields:

$$\begin{aligned}
& \sigma_{rz0}^{(1)} - \sigma_{rz0}^{(2)} \\
&= \int_0^\infty \left[-c_{44}^{(1)} \left(-b_{51}^{(1)} B_0^{(1)} - b_{52}^{(1)} D_0^{(1)} \right) \right] \lambda d\lambda - \int_0^\infty \left[-c_{44}^{(2)} \left(b_{51}^{(2)} A_0^{(2)} + b_{52}^{(2)} C_0^{(2)} \right) \right] \lambda d\lambda = 0
\end{aligned} \tag{2.118}$$

$$c_{44}^{(2)} b_{51}^{(2)} A_0^{(2)} + c_{44}^{(1)} b_{51}^{(1)} B_0^{(1)} + c_{44}^{(2)} b_{52}^{(2)} C_0^{(2)} + c_{44}^{(1)} b_{52}^{(1)} D_0^{(1)} = 0 \tag{2.119}$$

Equations 2.109, 2.111, 2.117 and 2.119 result in the following set of four linear equations, from which the values of A_0 , B_0 , C_0 and D_0 are obtained:

$$\begin{bmatrix} a_1^{(2)} & -a_1^{(1)} & a_2^{(2)} & -a_2^{(1)} \\ a_7^{(2)} & a_7^{(1)} & a_8^{(2)} & a_8^{(1)} \\ -c_{44}^{(2)} b_{21}^{(2)} & c_{44}^{(1)} b_{21}^{(1)} & -c_{44}^{(2)} b_{22}^{(2)} & c_{44}^{(1)} b_{22}^{(1)} \\ c_{44}^{(2)} b_{51}^{(2)} & c_{44}^{(1)} b_{51}^{(1)} & c_{44}^{(2)} b_{52}^{(2)} & c_{44}^{(1)} b_{52}^{(1)} \end{bmatrix} \begin{bmatrix} A_0^{(2)} \\ B_0^{(1)} \\ C_0^{(2)} \\ D_0^{(1)} \end{bmatrix} = \begin{Bmatrix} 0 \\ 0 \\ \mathcal{H}_0 \{ \tilde{\rho}_0 \} J_0(\lambda r) \\ 0 \end{Bmatrix} \tag{2.120}$$

The solution of Eq. 2.120 results in the specific values of A_0 , B_0 , C_0 and D_0 corresponding to the case of an axisymmetric vertical load at the interface of the two media. A closed-form solution of 2.120 is too long to be shown here, but it is achievable with the help of some

mathematical software. This equation can also be solved numerically. The functions A_0 , B_0 , C_0 and D_0 involved in Eq. 2.120 are functions of the Hankel space variable λ ; so are the displacement and stress components resulting from them. The substitution of these values of A_0 , B_0 , C_0 and D_0 into Eqs. 2.98 to 2.107 results in the expressions of displacements and stresses at points of media $d=1,2$ due to axisymmetric vertical loads. Their counterparts in the physical domain are achieved upon their integration according to Eq. 2.95 and 2.96.

For convenience, an extra index is added to the displacement and stress components to indicate the direction of load they refer to. In this work, u_{iz} denotes the displacements in the i -direction ($i=r,z$) due to vertical loads, while σ_{ijz} denotes the ij component of stress ($i,j=r,z$) due to vertical loads.

2.3.2.2 Transverse load

Consider the problem of a transverse load in the x -direction, ϕ_x , uniformly distributed on an annular area, such as depicted in Fig. 2.3b. This load can be decomposed into an axisymmetric component ϕ_0 acting on the radial direction and an antisymmetric component ϕ_1 acting on the θ -direction. The component loads ϕ_0 and ϕ_1 , as well as the resulting horizontal load ϕ_x are illustrated in Fig. 2.5.

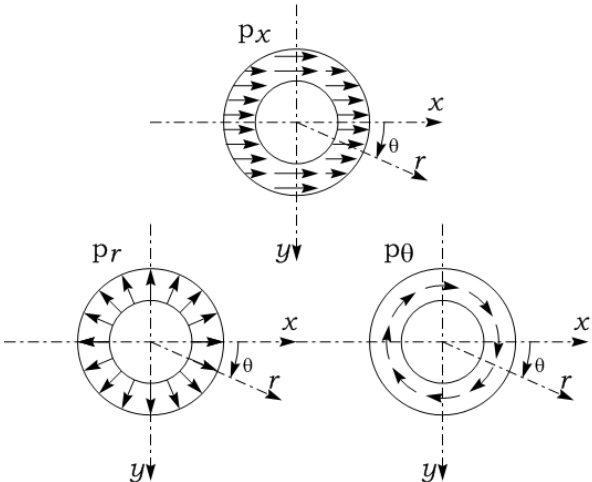


Figure 2.5 Decomposition of the transverse load ϕ_x into an axisymmetric term ϕ_0 in the radial direction and an antisymmetric term ϕ_1 in the θ -direction.

This decomposition is stated mathematically as:

$$\wp_0 = \wp_x \cos(\theta) \text{ and } \wp_1 = -\wp_x \sin(\theta) \quad (2.121)$$

Figure 2.6 illustrates this decomposition for a sample part of \wp_x acting on a point of coordinates (r, θ) .

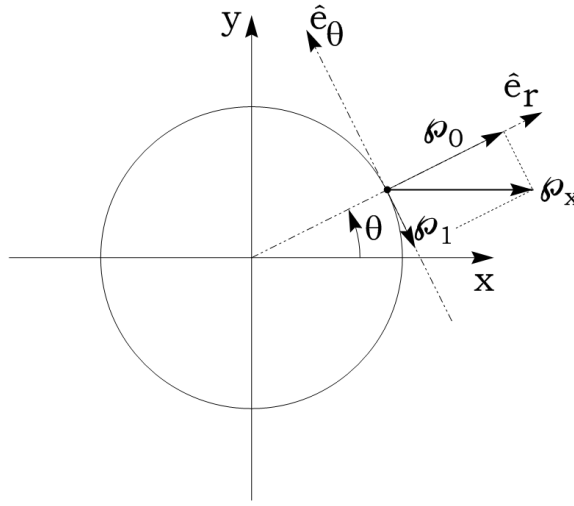


Figure 2.6 Decomposition of the transverse load \wp_x into an axisymmetric term \wp_0 in the radial direction and an antisymmetric term \wp_1 in the θ -direction.

It is worth mentioning that the decomposition stated in Eq. 2.121 is not the only way in which the components \wp_0 and \wp_1 can be combined. Barros (2006), proposed another combination which results in a distorting load \wp_d (Fig. 2.7). Distorting loads, however, are disregarded in the present work.

The traction discontinuities at the interface ($z=0$) due to the transverse load, in the absence of vertical loads, is:

$$p_{r1}^{(1)} + p_{r1}^{(2)} = \tilde{\wp}_0 = \tilde{\wp}_x \cos(\theta) \quad (2.122)$$

$$p_{\theta 1}^{(1)} + p_{\theta 1}^{(2)} = \tilde{\wp}_1 = -\tilde{\wp}_x \sin(\theta) \quad (2.123)$$

$$p_{z1}^{(1)} + p_{z2}^{(2)} = 0 \quad (2.124)$$

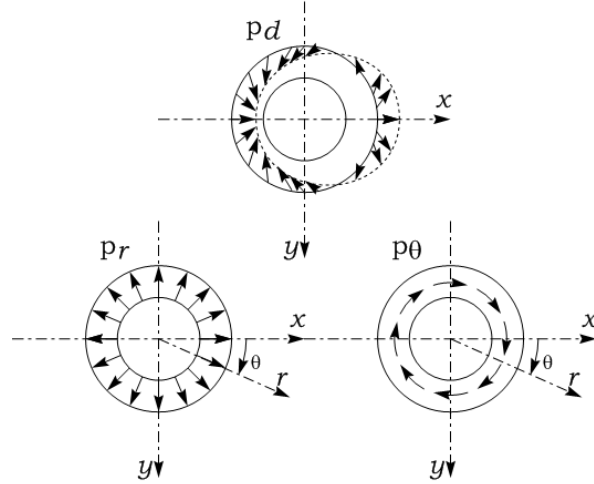


Figure 2.7 Decomposition of the distorting load \wp_d into an axisymmetric term \wp_0 in the radial direction and an antisymmetric term \wp_1 in the θ -direction.

In Eqs. 2.122, 2.123 and 2.124, p_{r1} , $p_{\theta 1}$ and p_{z1} indicate tractions acting at the interface ($z=0$) in the r -, θ - and vertical directions, respectively.

In terms of the stress components, in view of the sign conventions established in Fig. 2.4, these traction discontinuities are written as:

$$\frac{\sigma_{rz1}^{(1)}(r,0)}{\cos(\theta)} - \frac{\sigma_{rz1}^{(2)}(r,0)}{\cos(\theta)} = \tilde{\wp}_x \quad (2.125)$$

$$\frac{\sigma_{\theta z1}^{(1)}(r,0)}{\sin(\theta)} - \frac{\sigma_{\theta z1}^{(2)}(r,0)}{\sin(\theta)} = -\tilde{\wp}_x \quad (2.126)$$

$$\sigma_{zz1}^{(1)}(r,0) - \sigma_{zz1}^{(2)}(r,0) = 0 \quad (2.127)$$

Summation of Eqs. 2.125 and 2.126 yields:

$$\left(\frac{\sigma_{rz1}^{(1)}(r,0)}{\cos(\theta)} - \frac{\sigma_{rz1}^{(2)}(r,0)}{\cos(\theta)} \right) + \left(\frac{\sigma_{\theta z1}^{(1)}(r,0)}{\sin(\theta)} - \frac{\sigma_{\theta z1}^{(2)}(r,0)}{\sin(\theta)} \right) = \tilde{\wp}_x + (-\tilde{\wp}_x) = 0 \quad (2.128)$$

Subtraction of Eq. 2.126 from 2.125 yields:

$$\left(\frac{\sigma_{rz1}^{(1)}(r,0)}{\cos(\theta)} - \frac{\sigma_{rz1}^{(2)}(r,0)}{\cos(\theta)} \right) - \left(\frac{\sigma_{\theta z1}^{(1)}(r,0)}{\sin(\theta)} - \frac{\sigma_{\theta z1}^{(2)}(r,0)}{\sin(\theta)} \right) = \tilde{\rho}_x - (-\tilde{\rho}_x) = 2\tilde{\rho}_x = 2\frac{\tilde{\rho}_0}{\cos(\theta)} \quad (2.129)$$

The continuity boundary conditions are given by:

$$u_{r1}^{(1)}(r,0) - u_{r1}^{(2)}(r,0) = 0 \quad (2.130)$$

$$u_{\theta 1}^{(1)}(r,0) - u_{\theta 1}^{(2)}(r,0) = 0 \quad (2.131)$$

$$u_{z1}^{(1)}(r,0) - u_{z1}^{(2)}(r,0) = 0 \quad (2.132)$$

Antisymmetric terms of displacement and stress are involved in this boundary value problem. To comply with this antisymmetry, the θ -dependence is introduced in the Fourier expansion of the displacement and stress components by making $m=1$ in Eqs. 2.43 to 2.45. A particularization of the displacement and stress fields for the case of antisymmetric loads ($m=1$) is derived, so that the boundary conditions expressed in the previous equations can be applied. Equations 2.43 to 2.45 become, for $m=1$:

$$\chi(r, \theta, z) = \chi_m(r, z) \cos(m\theta) = \chi_1(r, z) \cos(\theta) \quad (2.133)$$

$$\phi(r, \theta, z) = \phi_m(r, z) \cos(m\theta) = \phi_1(r, z) \cos(\theta) \quad (2.134)$$

$$\psi(r, \theta, z) = \psi_m(r, z) \sin(m\theta) = \psi_1(r, z) \sin(\theta) \quad (2.135)$$

From Eqs. 2.35 to 2.37, it comes:

$$u_{r1} = \frac{\partial}{\partial r} \phi_1(r, z) \cos(\theta) + \frac{1}{r} \frac{\partial}{\partial \theta} \psi_1(r, z) \sin(\theta) = \frac{\partial}{\partial r} \phi_1(r, z) \cos(\theta) + \frac{1}{r} \psi_1(r, z) \cos(\theta) \quad (2.136)$$

$$u_{\theta 1} = \frac{1}{r} \frac{\partial}{\partial \theta} \phi_1(r, z) \cos(\theta) - \frac{\partial}{\partial r} \psi_1(r, z) \sin(\theta) = -\frac{1}{r} \phi_1(r, z) \sin(\theta) - \frac{\partial}{\partial r} \psi_1(r, z) \sin(\theta) \quad (2.137)$$

$$u_{z1} = \frac{\partial}{\partial z} \chi_1(r, z) \cos(\theta) \quad (2.138)$$

$$\frac{u_{r1}}{\cos(\theta)} = \frac{\partial}{\partial r} \phi_1(r, z) + \frac{1}{r} \psi_1(r, z) \quad (2.139)$$

$$\frac{u_{\theta 1}}{\sin(\theta)} = -\frac{1}{r} \phi_1(r, z) - \frac{\partial}{\partial r} \psi_1(r, z) \quad (2.140)$$

$$\frac{u_{z1}}{\cos(\theta)} = \frac{\partial}{\partial z} \chi_1(r, z) \quad (2.141)$$

A particular solution for the potential functions ϕ_1 , ψ_1 and χ_1 for the case of antisymmetric loads ($m=1$) is obtained following the development from Eqs. 2.46 to 2.62. Substitution of those solutions into Eqs. 2.139 to 2.141 results in the particularized expressions of displacement and stress components for this antisymmetric case. The resulting expressions for displacement and stresses in the physical domain in this case are:

$$u_{ijl}^{(d)} = \int_0^\infty u_{ijl}^{*(d)} \lambda d\lambda ; i=r,\theta,z; d=1,2 \quad (2.142)$$

$$\sigma_{ijl}^{(d)} = \int_0^\infty \sigma_{ijl}^{*(d)} \lambda d\lambda ; i=r,\theta,z; d=1,2 \quad (2.143)$$

in which,

$$\lambda = \delta^{(d)} \cdot \zeta \quad (2.144)$$

For medium $d=1$,

$$u_{r1}^{*(1)} = \left(a_1^{(1)} B_1^{(1)} e^{\delta^{(1)} \xi_1^{(1)} z} + a_2^{(1)} D_1^{(1)} e^{\delta^{(1)} \xi_2^{(1)} z} + a_3^{(1)} F_1^{(1)} e^{\delta^{(1)} \xi_3^{(1)} z} \right) \cos(\theta) \quad (2.145)$$

$$u_{\theta 1}^{*(1)} = - \left(a_4^{(1)} B_1^{(1)} e^{\delta^{(1)} \xi_1^{(1)} z} + a_5^{(1)} D_1^{(1)} e^{\delta^{(1)} \xi_2^{(1)} z} + a_6^{(1)} F_1^{(1)} e^{\delta^{(1)} \xi_3^{(1)} z} \right) \sin(\theta) \quad (2.146)$$

$$u_{z1}^{*(1)} = -\left(-a_7^{(1)}B_1^{(1)}e^{\delta^{(1)}\xi_1^{(1)}z} - a_8^{(1)}D_1^{(1)}e^{\delta^{(1)}\xi_2^{(1)}z}\right)\cos(\theta) \quad (2.147)$$

$$\sigma_{rr1}^{*(1)} = c_{44}^{(1)}\left(+b_{11}^{(1)}B_1^{(1)}e^{\delta^{(1)}\xi_1^{(1)}z} + b_{12}^{(1)}D_1^{(1)}e^{\delta^{(1)}\xi_2^{(1)}z} + b_{13}^{(1)}F_1^{(1)}e^{\delta^{(1)}\xi_3^{(1)}z}\right)\cos(\theta) \quad (2.148)$$

$$\sigma_{\theta\theta 1}^{*(1)} = c_{44}^{(1)}\left(b_{61}^{(1)}B_1^{(1)}e^{\delta^{(1)}\xi_1^{(1)}z} + b_{62}^{(1)}D_1^{(1)}e^{\delta^{(1)}\xi_2^{(1)}z} - b_{13}^{(1)}F_1^{(1)}e^{\delta^{(1)}\xi_3^{(1)}z}\right)\cos(\theta) \quad (2.149)$$

$$\sigma_{zz1}^{*(1)} = c_{44}^{(1)}\left(+b_{21}^{(1)}B_1^{(1)}e^{\delta^{(1)}\xi_1^{(1)}z} + b_{22}^{(1)}D_1^{(1)}e^{\delta^{(1)}\xi_2^{(1)}z}\right)\cos(\theta) \quad (2.150)$$

$$\sigma_{r\theta 1}^{*(1)} = c_{44}^{(1)}\left(b_{31}^{(1)}B_1^{(1)}e^{\delta^{(1)}\xi_1^{(1)}z} + b_{32}^{(1)}D_1^{(1)}e^{\delta^{(1)}\xi_2^{(1)}z} + b_{33}^{(1)}F_1^{(1)}e^{\delta^{(1)}\xi_3^{(1)}z}\right)\sin(\theta) \quad (2.151)$$

$$\sigma_{\theta z 1}^{*(1)} = c_{44}^{(1)}\left(-b_{41}^{(1)}B_1^{(1)}e^{\delta^{(1)}\xi_1^{(1)}z} - b_{42}^{(1)}D_1^{(1)}e^{\delta^{(1)}\xi_2^{(1)}z} - b_{43}^{(1)}F_1^{(1)}e^{\delta^{(1)}\xi_3^{(1)}z}\right)\sin(\theta) \quad (2.152)$$

$$\sigma_{rz1}^{*(1)} = -c_{44}^{(1)}\left(-b_{51}^{(1)}B_1^{(1)}e^{\delta^{(1)}\xi_1^{(1)}z} - b_{52}^{(1)}D_1^{(1)}e^{\delta^{(1)}\xi_2^{(1)}z} - b_{53}^{(1)}F_1^{(1)}e^{\delta^{(1)}\xi_3^{(1)}z}\right)\cos(\theta) \quad (2.153)$$

For medium d=2,

$$u_{r1}^{*(2)} = \left(a_1^{(2)}A_1^{(2)}e^{-\delta^{(2)}\xi_1^{(2)}z} + a_2^{(2)}C_1^{(2)}e^{-\delta^{(2)}\xi_2^{(2)}z} + a_3^{(2)}E_1^{(2)}e^{-\delta^{(2)}\xi_3^{(2)}z}\right)\cos(\theta) \quad (2.154)$$

$$u_{\theta 1}^{*(2)} = -\left(a_4^{(2)}A_1^{(2)}e^{-\delta^{(2)}\xi_1^{(2)}z} + a_5^{(2)}C_1^{(2)}e^{-\delta^{(2)}\xi_2^{(2)}z} + a_6^{(2)}E_1^{(2)}e^{-\delta^{(2)}\xi_3^{(2)}z}\right)\sin(\theta) \quad (2.155)$$

$$u_{z1}^{*(2)} = -\left(a_7^{(2)}A_1^{(2)}e^{-\delta^{(2)}\xi_1^{(2)}z} + a_8^{(2)}C_1^{(2)}e^{-\delta^{(2)}\xi_2^{(2)}z}\right)\cos(\theta) \quad (2.156)$$

$$\sigma_{rr1}^{*(2)} = c_{44}^{(2)}\left(b_{11}^{(2)}A_1^{(2)}e^{-\delta^{(2)}\xi_1^{(2)}z} + b_{12}^{(2)}C_1^{(2)}e^{-\delta^{(2)}\xi_2^{(2)}z} + b_{13}^{(2)}E_1^{(2)}e^{-\delta^{(2)}\xi_3^{(2)}z}\right)\cos(\theta) \quad (2.157)$$

$$\sigma_{\theta\theta 1}^{*(2)} = c_{44}^{(2)}\left(b_{61}^{(2)}A_1^{(2)}e^{-\delta^{(2)}\xi_1^{(2)}z} + b_{62}^{(2)}C_1^{(2)}e^{-\delta^{(2)}\xi_2^{(2)}z} - b_{13}^{(2)}E_1^{(2)}e^{-\delta^{(2)}\xi_3^{(2)}z}\right)\cos(\theta) \quad (2.158)$$

$$\sigma_{zz1}^{*(2)} = c_{44}^{(2)}\left(b_{21}^{(2)}A_1^{(2)}e^{-\delta^{(2)}\xi_1^{(2)}z} + b_{22}^{(2)}C_1^{(2)}e^{-\delta^{(2)}\xi_2^{(2)}z}\right)\cos(\theta) \quad (2.159)$$

$$\sigma_{r\theta 1}^{*(2)} = c_{44}^{(2)} \left(b_{31}^{(2)} A_1^{(2)} e^{-\delta^{(2)} \xi_1^{(2)} z} + b_{32}^{(2)} C_1^{(2)} e^{-\delta^{(2)} \xi_2^{(2)} z} + b_{33}^{(2)} E_1^{(2)} e^{-\delta^{(2)} \xi_3^{(2)} z} \right) \sin(\theta) \quad (2.160)$$

$$\sigma_{\theta z 1}^{*(2)} = c_{44}^{(2)} \left(b_{41}^{(2)} A_1^{(2)} e^{\delta^{(2)} \xi_1^{(2)} z} + b_{42}^{(2)} C_1^{(2)} e^{\delta^{(2)} \xi_2^{(2)} z} + b_{43}^{(2)} E_1^{(2)} e^{\delta^{(2)} \xi_3^{(2)} z} \right) \sin(\theta) \quad (2.161)$$

$$\sigma_{rz 1}^{*(2)} = -c_{44}^{(2)} \left(b_{51}^{(2)} A_1^{(2)} e^{-\delta^{(2)} \xi_1^{(2)} z} + b_{52}^{(2)} C_1^{(2)} e^{-\delta^{(2)} \xi_2^{(2)} z} + b_{53}^{(2)} E_1^{(2)} e^{-\delta^{(2)} \xi_3^{(2)} z} \right) \cos(\theta) \quad (2.162)$$

Consider the following properties of the Bessel functions (Debnath and Bhatta, 2006):

$$J_{v+1}(\lambda r) = \frac{2v}{\lambda r} J_v(\lambda r) - J_{v-1}(\lambda r) \quad (2.163)$$

$$\therefore J_2(\delta \zeta r) = \frac{2}{\delta \zeta r} J_1(\delta \zeta r) - J_0(\delta \zeta r) \quad (2.164)$$

In view of these properties, the parameters defined in Eqs. 2.77 to 2.83 become as shown in Eqs. 2.165 to 2.171. In Eqs. 2.165 to 2.171, the upper index d indicating the medium d=1,2 is omitted for conciseness.

$$b_{1i} = -\frac{\zeta \vartheta_i \delta \zeta}{r} J_2(\delta \zeta r) - \left[\delta^2 \zeta^2 \beta \vartheta_i - (\kappa - 1) \delta^2 \xi_i^2 \right] J_1(\delta \zeta r), \quad i=1,2 \quad (2.165)$$

$$\frac{b_{13}}{2\zeta} = \frac{b_{3i}}{\zeta \vartheta_i \delta \zeta} = \frac{b_{33}}{\left[1 + \left(\delta^2 \zeta^2 r^2 / 2 \right) \right] \zeta \delta \zeta} = -J_2(\delta \zeta r), \quad i=1,2 \quad (2.166)$$

$$b_{6i} = +\frac{\zeta \vartheta_i \delta \zeta}{r} J_2(\delta \zeta r) - \left[\delta^2 \zeta^2 \beta \vartheta_i - (\kappa - 1) \delta^2 \xi_i^2 \right] J_1(\delta \zeta r), \quad i=1,2 \quad (2.167)$$

$$b_{2i} = \left[\alpha \delta^2 \xi_i^2 - (\kappa - 1) \delta^2 \zeta^2 \vartheta_i \right] J_1(\delta \zeta r), \quad i=1,2 \quad (2.168)$$

$$\frac{a_7}{\delta \xi_1} = \frac{a_8}{\delta \xi_2} = J_1(\delta \zeta r) \quad (2.169)$$

$$a_3 = \frac{a_4}{\vartheta_1} = \frac{a_5}{\vartheta_2} = \frac{b_{4i}}{(1 + \vartheta_i) \delta \xi_i} = \frac{b_{53}}{\delta \xi_3} = \frac{1}{r} J_1(\delta \zeta r), \quad i=1,2 \quad (2.170)$$

$$a_6 = \frac{a_1}{\vartheta_1} = \frac{a_2}{\vartheta_2} = \frac{b_{5i}}{(1+\vartheta_i)\delta\xi_i} = \frac{b_{43}}{\delta\xi_3} = \delta\zeta J_0(\delta\zeta r) - \frac{1}{r} J_1(\delta\zeta r), \quad i=1,2 \quad (2.171)$$

Substitution of Eqs. 2.142 and 2.143 into the continuity conditions in Eqs. 2.130 to 2.132 yields:

$$\begin{aligned} u_{r1}^{(1)}(r,0) &= \int_0^\infty \left[a_1^{(1)} B_1^{(1)} + a_2^{(1)} D_1^{(1)} + a_3^{(1)} F_1^{(1)} \right] \cos(\theta) \lambda d\lambda \\ &= u_{r1}^{(2)}(r,0) = \int_0^\infty \left[a_1^{(2)} A_1^{(2)} + a_2^{(2)} C_1^{(2)} + a_3^{(2)} E_1^{(2)} \right] \cos(\theta) \lambda d\lambda \end{aligned} \quad (2.172)$$

$$a_1^{(2)} A_1^{(2)} - a_1^{(1)} B_1^{(1)} + a_2^{(2)} C_1^{(2)} - a_2^{(1)} D_1^{(1)} + a_3^{(2)} E_1^{(2)} - a_3^{(1)} F_1^{(1)} = 0 \quad (2.173)$$

$$\begin{aligned} u_{\theta 1}^{(1)}(r,0) &= \int_0^\infty \left[-\left(a_4^{(1)} B_1^{(1)} + a_5^{(1)} D_1^{(1)} + a_6^{(1)} F_1^{(1)} \right) \right] \sin(\theta) \lambda d\lambda \\ &= u_{\theta 1}^{(2)}(r,0) = \int_0^\infty \left[-\left(a_4^{(2)} A_1^{(2)} + a_5^{(2)} C_1^{(2)} + a_6^{(2)} E_1^{(2)} \right) \right] \sin(\theta) \lambda d\lambda \end{aligned} \quad (2.174)$$

$$a_4^{(2)} A_1^{(2)} - a_4^{(1)} B_1^{(1)} + a_5^{(2)} C_1^{(2)} - a_5^{(1)} D_1^{(1)} + a_6^{(2)} E_1^{(2)} - a_6^{(1)} F_1^{(1)} = 0 \quad (2.175)$$

$$\begin{aligned} u_{z1}^{(1)}(r,0) &= \int_0^\infty \left[-\left(-a_7^{(1)} B_1^{(1)} - a_8^{(1)} D_1^{(1)} \right) \right] \cos(\theta) \lambda d\lambda \\ &= u_{z1}^{(2)}(r,0) = \int_0^\infty \left[-\left(a_7^{(2)} A_1^{(2)} + a_8^{(2)} C_1^{(2)} \right) \right] \cos(\theta) \lambda d\lambda \end{aligned} \quad (2.176)$$

$$a_7^{(2)} A_1^{(2)} + a_7^{(1)} B_1^{(1)} + a_8^{(2)} C_1^{(2)} + a_8^{(1)} D_1^{(1)} = 0 \quad (2.177)$$

Substitution of Eqs. 2.142 and 2.143 into the stress boundary conditions in Eqs. 2.127 to 2.129 yields:

$$\begin{aligned} \sigma_{zz1}^{(1)}(r,0) - \sigma_{zz1}^{(2)}(r,0) &= \int_0^\infty \left[c_{44}^{(1)} \left(+b_{21}^{(1)} B_1^{(1)} + b_{22}^{(1)} D_1^{(1)} \right) \cos(\theta) \right] \lambda d\lambda \\ - \int_0^\infty \left[c_{44}^{(2)} \left(b_{21}^{(2)} A_1^{(2)} + b_{22}^{(2)} C_1^{(2)} \right) \cos(\theta) \right] \lambda d\lambda &= 0 \end{aligned} \quad (2.178)$$

$$c_{44}^{(2)}b_{21}^{(2)}A_1^{(2)} - c_{44}^{(1)}b_{21}^{(1)}B_1^{(1)} + c_{44}^{(2)}b_{22}^{(2)}C_1^{(2)} - c_{44}^{(1)}b_{22}^{(1)}D_1^{(1)} = 0 \quad (2.179)$$

$$\begin{aligned} & \left(\frac{\sigma_{rz1}^{(1)}(r,0)}{\cos(\theta)} - \frac{\sigma_{rz1}^{(2)}(r,0)}{\cos(\theta)} \right) + \left(\frac{\sigma_{\theta z1}^{(1)}(r,0)}{\sin(\theta)} - \frac{\sigma_{\theta z1}^{(2)}(r,0)}{\sin(\theta)} \right) \\ &= \int_0^\infty \left[-c_{44}^{(1)} \left(-b_{51}^{(1)}B_1^{(1)} - b_{52}^{(1)}D_1^{(1)} - b_{53}^{(1)}F_1^{(1)} \right) \right] \lambda d\lambda \\ & - \int_0^\infty \left[-c_{44}^{(2)} \left(b_{51}^{(2)}A_1^{(2)} + b_{52}^{(2)}C_1^{(2)} + b_{53}^{(2)}E_1^{(2)} \right) \right] \lambda d\lambda \\ & + \int_0^\infty \left[c_{44}^{(1)} \left(-b_{41}^{(1)}B_1^{(1)} - b_{42}^{(1)}D_1^{(1)} - b_{43}^{(1)}F_1^{(1)} \right) \right] d\lambda \\ & - \int_0^\infty \left[c_{44}^{(2)} \left(b_{41}^{(2)}A_1^{(2)} + b_{42}^{(2)}C_1^{(2)} + b_{43}^{(2)}E_1^{(2)} \right) \right] d\lambda = 0 \end{aligned} \quad (2.180)$$

$$\begin{aligned} & c_{44}^{(2)} \left(b_{51}^{(2)} - b_{41}^{(2)} \right) A_1^{(2)} + c_{44}^{(1)} \left(b_{51}^{(1)} - b_{41}^{(1)} \right) B_1^{(1)} + c_{44}^{(2)} \left(b_{52}^{(2)} - b_{42}^{(2)} \right) C_1^{(2)} \\ & + c_{44}^{(1)} \left(b_{52}^{(1)} - b_{42}^{(1)} \right) D_1^{(1)} + c_{44}^{(2)} \left(b_{53}^{(2)} - b_{43}^{(2)} \right) E_1^{(2)} + c_{44}^{(1)} \left(b_{53}^{(1)} - b_{43}^{(1)} \right) F_1^{(1)} = 0 \end{aligned} \quad (2.181)$$

$$\begin{aligned} & \left(\frac{\sigma_{rz1}^{(1)}(r,0)}{\cos(\theta)} - \frac{\sigma_{rz1}^{(2)}(r,0)}{\cos(\theta)} \right) - \left(\frac{\sigma_{\theta z1}^{(1)}(r,0)}{\sin(\theta)} - \frac{\sigma_{\theta z1}^{(2)}(r,0)}{\sin(\theta)} \right) = 2 \frac{\tilde{\rho}_0}{\cos(\theta)} \\ &= \int_0^\infty \left[-c_{44}^{(1)} \left(-b_{51}^{(1)}B_1^{(1)} - b_{52}^{(1)}D_1^{(1)} - b_{53}^{(1)}F_1^{(1)} \right) \right] \lambda d\lambda \\ & - \int_0^\infty \left[-c_{44}^{(2)} \left(b_{51}^{(2)}A_1^{(2)} + b_{52}^{(2)}C_1^{(2)} + b_{53}^{(2)}E_1^{(2)} \right) \right] \lambda d\lambda \\ & - \int_0^\infty \left[c_{44}^{(1)} \left(-b_{41}^{(1)}B_1^{(1)} - b_{42}^{(1)}D_1^{(1)} - b_{43}^{(1)}F_1^{(1)} \right) \right] d\lambda \\ & + \int_0^\infty \left[c_{44}^{(2)} \left(b_{41}^{(2)}A_1^{(2)} + b_{42}^{(2)}C_1^{(2)} + b_{43}^{(2)}E_1^{(2)} \right) \right] d\lambda \end{aligned} \quad (2.182)$$

$$\begin{aligned} & c_{44}^{(2)} \left(b_{51}^{(2)} + b_{41}^{(2)} \right) A_1^{(2)} + c_{44}^{(1)} \left(b_{51}^{(1)} + b_{41}^{(1)} \right) B_1^{(1)} + c_{44}^{(2)} \left(b_{52}^{(2)} + b_{42}^{(2)} \right) C_1^{(2)} \\ & + c_{44}^{(1)} \left(b_{52}^{(1)} + b_{42}^{(1)} \right) D_1^{(1)} + c_{44}^{(2)} \left(b_{53}^{(2)} + b_{43}^{(2)} \right) E_1^{(2)} + c_{44}^{(1)} \left(b_{53}^{(1)} + b_{43}^{(1)} \right) F_1^{(1)} \\ &= \frac{2}{\cos(\theta)} \mathcal{H}_0 \{ \tilde{\rho}_0 \} J_0(\lambda r) \end{aligned} \quad (2.183)$$

Equations 2.173, 2.175, 2.177 and 2.179, 2.181 and 2.183 form a set of six linear equations,

from which the values of A_1 , B_1 , C_1 , D_1 , E_1 and F_1 are obtained:

$$a_1^{(2)}A_1^{(2)} - a_1^{(1)}B_1^{(1)} + a_2^{(2)}C_1^{(2)} - a_2^{(1)}D_1^{(1)} + a_3^{(2)}E_1^{(2)} - a_3^{(1)}F_1^{(1)} = 0 \quad (2.173)$$

$$a_4^{(2)}A_1^{(2)} - a_4^{(1)}B_1^{(1)} + a_5^{(2)}C_1^{(2)} - a_5^{(1)}D_1^{(1)} + a_6^{(2)}E_1^{(2)} - a_6^{(1)}F_1^{(1)} = 0 \quad (2.175)$$

$$a_7^{(2)}A_1^{(2)} + a_7^{(1)}B_1^{(1)} + a_8^{(2)}C_1^{(2)} + a_8^{(1)}D_1^{(1)} = 0 \quad (2.177)$$

$$c_{44}^{(2)}b_{21}^{(2)}A_1^{(2)} - c_{44}^{(1)}b_{21}^{(1)}B_1^{(1)} + c_{44}^{(2)}b_{22}^{(2)}C_1^{(2)} - c_{44}^{(1)}b_{22}^{(1)}D_1^{(1)} = 0 \quad (2.179)$$

$$\begin{aligned} & c_{44}^{(2)} \left(b_{51}^{(2)} - b_{41}^{(2)} \right) A_1^{(2)} + c_{44}^{(1)} \left(b_{51}^{(1)} - b_{41}^{(1)} \right) B_1^{(1)} + c_{44}^{(2)} \left(b_{52}^{(2)} - b_{42}^{(2)} \right) C_1^{(2)} \\ & + c_{44}^{(1)} \left(b_{52}^{(1)} - b_{42}^{(1)} \right) D_1^{(1)} + c_{44}^{(2)} \left(b_{53}^{(2)} - b_{43}^{(2)} \right) E_1^{(2)} + c_{44}^{(1)} \left(b_{53}^{(1)} - b_{43}^{(1)} \right) F_1^{(1)} = 0 \end{aligned} \quad (2.181)$$

$$\begin{aligned} & c_{44}^{(2)} \left(b_{51}^{(2)} + b_{41}^{(2)} \right) A_1^{(2)} + c_{44}^{(1)} \left(b_{51}^{(1)} + b_{41}^{(1)} \right) B_1^{(1)} + c_{44}^{(2)} \left(b_{52}^{(2)} + b_{42}^{(2)} \right) C_1^{(2)} \\ & + c_{44}^{(1)} \left(b_{52}^{(1)} + b_{42}^{(1)} \right) D_1^{(1)} + c_{44}^{(2)} \left(b_{53}^{(2)} + b_{43}^{(2)} \right) E_1^{(2)} + c_{44}^{(1)} \left(b_{53}^{(1)} + b_{43}^{(1)} \right) F_1^{(1)} \\ & = \frac{2}{\cos(\theta)} \mathcal{H}_6 \{ \tilde{\rho}_0 \} J_0(\lambda r) \end{aligned} \quad (2.183)$$

This system of equations is too long to be shown here in the form of a matrix equation such as Eq. 2.120, but it nevertheless comprises an analogous result: the solution of this system results in the specific values of A_1 , B_1 , C_1 , D_1 , E_1 and F_1 corresponding to the case of a transverse load at the interface of the two media. A closed-form solution of these equations is too long to be shown here, but it is achievable with the help of some mathematical software. These equations can also be solved numerically. The functions A_1 , B_1 , C_1 , D_1 , E_1 and F_1 involved in these equations are functions of the Hankel space variable λ ; so are the displacement and stress components resulting from them. The substitution of these values of A_1 , B_1 , C_1 , D_1 , E_1 and F_1 into Eqs. 2.145 to 2.162 results in the expressions of displacements and stresses at points of media $d=1,2$ due to antisymmetric transverse loads. Their counterparts in the physical domain are achieved upon their integration according to Eq. 2.142 and 2.143.

For convenience, an extra index is added to the displacement and stress components to indicate the direction of load they refer to. In this work, u_{ix} denotes the displacements in the i -direction ($i=r,\theta,z$) due to transverse loads, while σ_{ijx} denotes the ij component of stress ($i,j=r,\theta,z$) due to transverse loads.

2.3.2.3 Pure moment loading

Consider the problem of an antisymmetric vertical load distributed on an annular area, the intensity of which varies with θ , as illustrated in Fig. 2.3c. The traction discontinuities at the interface ($z=0$) due to this vertical load, in the absence of transverse loads, in the physical domain, is

$$p_{r1}^{(1)} + p_{r1}^{(2)} = 0 \quad (2.184)$$

$$p_{\theta 1}^{(1)} + p_{\theta 1}^{(2)} = 0 \quad (2.185)$$

$$p_{z1}^{(1)} + p_{z2}^{(2)} = \tilde{\varphi}_1 \quad (2.186)$$

In Eqs. 2.184 to 2.186, p_{r1} , $p_{\theta 1}$ and p_{z1} indicate tractions acting at the interface ($z=0$) in the r -, θ - and vertical directions, respectively. The tilde on top of φ_1 in Eq. 2.186 indicates distributed loads.

In terms of the stress components, in view of the sign conventions established in Fig. 2.4, these traction discontinuities are written as:

$$\sigma_{rz1}^{(1)}(r,0) - \sigma_{rz1}^{(2)}(r,0) = 0 \quad (2.187)$$

$$\sigma_{\theta z1}^{(1)}(r,0) - \sigma_{\theta z1}^{(2)}(r,0) = 0 \quad (2.188)$$

$$\sigma_{zz1}^{(1)}(r,0) - \sigma_{zz1}^{(2)}(r,0) = \tilde{\varphi}_1 \quad (2.189)$$

Substitution of Eqs. 2.142 and 2.143 into Eqs. 2.187 to 2.189 yields:

$$\begin{aligned}\sigma_{rz1}^{(1)}(r,0) - \sigma_{rz1}^{(2)}(r,0) &= \int_0^\infty \left[-c_{44}^{(1)} \left(-b_{51}^{(1)} B_1^{(1)} - b_{52}^{(1)} D_1^{(1)} - b_{53}^{(1)} F_1^{(1)} \right) \cos(\theta) \right] \lambda d\lambda \\ &- \int_0^\infty \left[-c_{44}^{(2)} \left(b_{51}^{(2)} A_1^{(2)} + b_{52}^{(2)} C_1^{(2)} + b_{53}^{(2)} E_1^{(2)} \right) \cos(\theta) \right] \lambda d\lambda = 0\end{aligned}\quad (2.190)$$

$$c_{44}^{(2)} b_{51}^{(2)} A_1^{(2)} + c_{44}^{(1)} b_{51}^{(1)} B_1^{(1)} + c_{44}^{(2)} b_{52}^{(2)} C_1^{(2)} + c_{44}^{(1)} b_{52}^{(1)} D_1^{(1)} + c_{44}^{(2)} b_{53}^{(2)} E_1^{(2)} + c_{44}^{(1)} b_{53}^{(1)} F_1^{(1)} = 0 \quad (2.191)$$

$$\begin{aligned}\sigma_{\theta z1}^{(1)}(r,0) - \sigma_{\theta z1}^{(2)}(r,0) &= \int_0^\infty \left[c_{44}^{(1)} \left(-b_{41}^{(1)} B_1^{(1)} - b_{42}^{(1)} D_1^{(1)} - b_{43}^{(1)} F_1^{(1)} \right) \sin(\theta) \right] \lambda d\lambda \\ &- \int_0^\infty \left[c_{44}^{(2)} \left(b_{41}^{(2)} A_1^{(2)} + b_{42}^{(2)} C_1^{(2)} + b_{43}^{(2)} E_1^{(2)} \right) \sin(\theta) \right] \lambda d\lambda = 0\end{aligned}\quad (2.192)$$

$$c_{44}^{(2)} b_{41}^{(2)} A_1^{(2)} + c_{44}^{(1)} b_{41}^{(1)} B_1^{(1)} + c_{44}^{(2)} b_{42}^{(2)} C_1^{(2)} + c_{44}^{(1)} b_{42}^{(1)} D_1^{(1)} + c_{44}^{(2)} b_{43}^{(2)} E_1^{(2)} + c_{44}^{(1)} b_{43}^{(1)} F_1^{(1)} = 0 \quad (2.193)$$

$$\begin{aligned}\sigma_{zz1}^{(1)}(r,0) - \sigma_{zz1}^{(2)}(r,0) &= \int_0^\infty \left[c_{44}^{(1)} \left(+b_{21}^{(1)} B_1^{(1)} + b_{22}^{(1)} D_1^{(1)} \right) \cos(\theta) \right] \lambda d\lambda \\ &- \int_0^\infty \left[c_{44}^{(2)} \left(b_{21}^{(2)} A_1^{(2)} + b_{22}^{(2)} C_1^{(2)} \right) \cos(\theta) \right] \lambda d\lambda = \tilde{\varphi}_1\end{aligned}\quad (2.194)$$

$$c_{44}^{(2)} b_{21}^{(2)} A_1^{(2)} - c_{44}^{(1)} b_{21}^{(1)} B_1^{(1)} + c_{44}^{(2)} b_{22}^{(2)} C_1^{(2)} - c_{44}^{(1)} b_{22}^{(1)} D_1^{(1)} = -\frac{1}{\cos(\theta)} \mathcal{H}_1 \{ \tilde{\varphi}_1 \} J_1(\lambda r) \quad (2.195)$$

The continuity boundary conditions are given by Eqs. 2.130 to 2.132. Substitution of Eqs. 2.142 and 2.143 into the continuity conditions yields:

$$a_1^{(2)} A_1^{(2)} - a_1^{(1)} B_1^{(1)} + a_2^{(2)} C_1^{(2)} - a_2^{(1)} D_1^{(1)} + a_3^{(2)} E_1^{(2)} - a_3^{(1)} F_1^{(1)} = 0 \quad (2.196)$$

$$a_4^{(2)} A_1^{(2)} - a_4^{(1)} B_1^{(1)} + a_5^{(2)} C_1^{(2)} - a_5^{(1)} D_1^{(1)} + a_6^{(2)} E_1^{(2)} - a_6^{(1)} F_1^{(1)} = 0 \quad (2.197)$$

$$a_7^{(2)} A_1^{(2)} + a_7^{(1)} B_1^{(1)} + a_8^{(2)} C_1^{(2)} + a_8^{(1)} D_1^{(1)} = 0 \quad (2.198)$$

Equations 2.191, 2.193, 2.195 and 2.196 to 2.198 form a set of six linear equations, from which the values of A_1 , B_1 , C_1 , D_1 , E_1 and F_1 are obtained:

$$\begin{bmatrix}
a_1^{(2)} & -a_1^{(1)} & a_2^{(2)} & -a_2^{(1)} & a_3^{(2)} & -a_3^{(1)} \\
a_4^{(2)} & -a_4^{(1)} & a_5^{(2)} & -a_5^{(1)} & a_6^{(2)} & -a_6^{(1)} \\
a_7^{(2)} & a_7^{(1)} & a_8^{(2)} & a_8^{(1)} & 0 & 0 \\
c_{44}^{(2)}b_{51}^{(2)} & c_{44}^{(1)}b_{51}^{(1)} & c_{44}^{(2)}b_{52}^{(2)} & c_{44}^{(1)}b_{52}^{(1)} & c_{44}^{(2)}b_{53}^{(2)} & c_{44}^{(1)}b_{53}^{(1)} \\
c_{44}^{(2)}b_{41}^{(2)} & c_{44}^{(1)}b_{41}^{(1)} & c_{44}^{(2)}b_{42}^{(2)} & c_{44}^{(1)}b_{42}^{(1)} & c_{44}^{(2)}b_{43}^{(2)} & c_{44}^{(1)}b_{43}^{(1)} \\
c_{44}^{(2)}b_{21}^{(2)} & -c_{44}^{(1)}b_{21}^{(1)} & c_{44}^{(2)}b_{22}^{(2)} & -c_{44}^{(1)}b_{22}^{(1)} & 0 & 0
\end{bmatrix}
\begin{Bmatrix}
A_1^{(2)} \\
B_1^{(1)} \\
C_1^{(2)} \\
D_1^{(1)} \\
E_1^{(2)} \\
F_1^{(1)}
\end{Bmatrix}
=
\begin{Bmatrix}
0 \\
0 \\
0 \\
0 \\
0 \\
-\frac{\mathcal{H}\{\tilde{\varrho}_1\}J_1(\lambda r)}{\cos(\theta)}
\end{Bmatrix}
\quad (2.199)$$

The solution of this algebraic equation system results in the specific values of A_1 , B_1 , C_1 , D_1 , E_1 and F_1 corresponding to the case of an antisymmetric vertical load at the interface of the two media. A closed-form solution of these equations is too long to be shown here, but it is achievable with the help of some mathematical software. This equation can also be solved numerically. The functions A_1 , B_1 , C_1 , D_1 , E_1 and F_1 involved in these equations are functions of the Hankel space variable λ ; so are the displacement and stress components resulting from them. The substitution of these values of A_1 , B_1 , C_1 , D_1 , E_1 and F_1 into Eqs. 2.142 and 2.143 results in the expressions of displacements and stresses at points of media $d=1,2$ due to antisymmetric vertical loads. Their counterparts in the physical domain are achieved upon their integration according to Eq. 2.142 and 2.143.

For convenience, a little change of notation of the displacement and stress components is introduced to indicate the type of load they refer to. In this work, v_{iz} denotes the displacements in the i -direction ($i=r,\theta,z$) due to antisymmetric vertical loads, while ζ_{ijz} denotes the ij component of stress ($i,j=r,\theta,z$) due to antisymmetric vertical loads. The letters v and ζ are used instead of u and σ to emphasize that these displacements and stresses result from antisymmetric vertical loads, rather than axisymmetric vertical loads (see the end of Subsection 2.3.2.1).

2.4 Description of the loadings

Let ϱ_m represent axisymmetric and antisymmetric loads in the physical domain. The index m is used to emphasize that the axisymmetry or antisymmetry of these loads can be described in the same form of the Fourier series expansion that is shown in Eq. 2.43. ϱ_0 ($m=0$) denotes axisymmetric loads, the intensity of which does not depend on the variable θ (Eq. 2.43 for $m=0$

and Fig. 2.3a). \wp_1 ($m=1$) denotes antisymmetric loads, the intensity of which vary with the cosine of θ (Eq. 2.43 for $m=1$ and Fig. 2.3c).

One way of expressing these loads is by using Hankel transforms:

$$\wp_m = \mathcal{H}_m^{-1} \{ \mathcal{H}_m \{ \wp_m \} \} = \int_0^\infty \mathcal{H}_m \{ \wp_m \} J_m(\lambda r) \lambda d\lambda \quad (2.200)$$

in which \mathcal{H}_m and \mathcal{H}_m^{-1} represent respectively the Hankel transform of order m and its inverse, and J_m represents Bessel functions of order m (Abramowitz and Stegun, 1965).

Consider an axisymmetric load of intensity p_0 applied as a ring of radius s , $\wp_0 = p_0 \delta(r-s)$. The representation of this load in the transformed domain is given by Eq. 2.201. Based on this result, an expression for an analogous load distributed on an annular area with inner and outer radii s_1 and s_2 in the transformed domain can be derived (Eq. 2.202). The symbol $\tilde{\wp}$ with a tilde in Eq. 2.202 stands for distributed loads.

$$\mathcal{H}_0 \{ \wp_0 \} = \int_0^\infty p_0 \delta(r-s) J_0(\lambda r) r dr = p_0 s \cdot J_0(\lambda s) \quad (2.201)$$

$$\mathcal{H}_0 \{ \tilde{\wp}_0 \} = \int_{s_1}^{s_2} p_0 s \cdot J_0(\lambda s) ds = \frac{1}{\lambda} [s_2 J_1(\lambda s_2) - s_1 J_1(\lambda s_1)] p_0 \quad (2.202)$$

Consider now loading configurations in which the amplitude of the load is not uniformly distributed on the ring of radius s . In the first case (Fig. 2.8a), the amplitude varies with the angle θ , but not with the radius s (see also Figs. 2.8c and 2.8d). Because this is an antisymmetric problem with respect to θ , $m=1$.

The concentrated load on the ring is $\wp_1 = p_0 \delta(r-s) \cos(\theta)$ and its representation in the transformed domain is given by Eq. 2.203. Equation 2.204 describes this load when it is distributed on an annular area with inner and outer radii s_1 and s_2 in the transformed domain.

$$\mathcal{H}_1 \{ \wp_1 \} = \int_0^\infty p_0 \delta(r-s) \cos(\theta) J_1(\lambda r) r dr = p_0 s \cdot J_1(\lambda s) \cos(\theta) \quad (2.203)$$

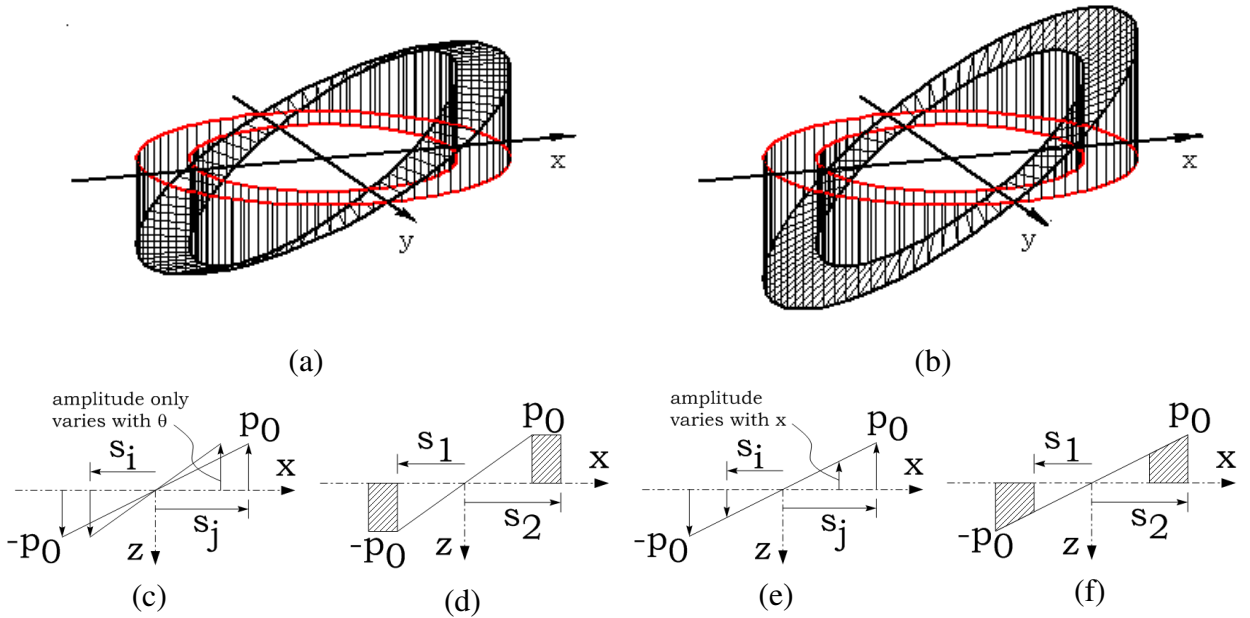


Figure 2.8 Load configurations for antisymmetric vertical loads that vary only with θ and not with r (a, c and d) and that vary linearly with x (b, e and f).

$$\begin{aligned}
 \mathcal{H}_1 \{ \tilde{\varphi}_1 \} = \int_{s_1}^{s_2} p_0 s J_1(\lambda s) \cos(\theta) ds &= \frac{\pi s_2}{2\lambda} [J_1(\lambda s_2) H_0(\lambda s_2) - J_0(\lambda s_2) H_1(\lambda s_2)] p_0 \cos(\theta) \\
 &\quad - \frac{\pi s_1}{2\lambda} [J_1(\lambda s_1) H_0(\lambda s_1) - J_0(\lambda s_1) H_1(\lambda s_1)] p_0 \cos(\theta)
 \end{aligned}
 \tag{2.204}$$

In Eq. 2.204, H_v represents Struve functions of order v (Abramowitz and Stegun, 1965).

Figures 2.8a and 2.8d show a physical interpretation of the distributed load resulting from the integration of $\varphi_1 = p_0 \delta(r-s) \cos(\theta)$.

A simpler case which does not involve Struve functions is obtained by considering that the amplitude of the concentrated load on the ring of radius s varies linearly with its distance x from the y -axis (Fig. 2.8e). The expression of the concentrated load is $\varphi_1 = p_0 \delta(r-s)x$, with $x = r \cdot \cos(\theta)$, and its representation in the transformed domain is given by Eq. 2.205. Its corresponding distributed expression is shown in Eq. 2.206.

$$\mathcal{H}_1\{\varphi_1\} = \int_0^\infty p_0 \delta(r-s) r \cos(\theta) J_1(\lambda r) r dr = p_0 s^2 \cdot J_1(\lambda s) \cos(\theta) \quad (2.205)$$

$$\mathcal{H}_1\{\tilde{\varphi}_1\} = \int_{s_1}^{s_2} p_0 s^2 J_1(\lambda s) \cos(\theta) ds = \frac{1}{\lambda} \left[s_2^2 J_2(\lambda s_2) - s_1^2 J_2(\lambda s_1) \right] p_0 \cos(\theta) \quad (2.206)$$

Figures 2.8b and 2.8f show a physical interpretation of the distributed load resulting from the integration of $\varphi_1 = p_0 \delta(r-s) \cdot r \cdot \cos(\theta)$.

This chapter presented Green's functions to describe the behavior of transversely isotropic media under the effect of different configurations of dynamic loads. Infinite homogeneous three-dimensional full-spaces were considered, as well as bi-material half-space interfaces. In the next chapter, a different technique will be used to describe layered half-spaces. Each layer within the layered system is a finite transversely isotropic medium, the behavior of which is modeled in this present chapter.

3 EXACT STIFFNESS METHOD FOR MULTILAYERED MEDIA

In this chapter, the stiffness-matrix approach is used to compute displacements and stresses of a multilayered transversely isotropic elastic half-space under time-harmonic oscillations. Exact stiffness matrices are obtained for each layer, based on the solutions presented in the preceding chapter. The global stiffness matrix describing the layered system is assembled by considering traction continuity conditions at the interface between adjacent layers of the system.

Consider the three-dimensional multilayered medium shown in Fig. 3.1. Each of the N layers and the underlying half-space is made of a homogeneous transversely isotropic elastic material, the behavior of which is described by Eqs. 2.63 and 2.68. The material constants, mass density and thickness of the n^{th} layer are denoted by $c^{(n)}_{ij}$, $\rho^{(n)}$ and h_n , respectively.

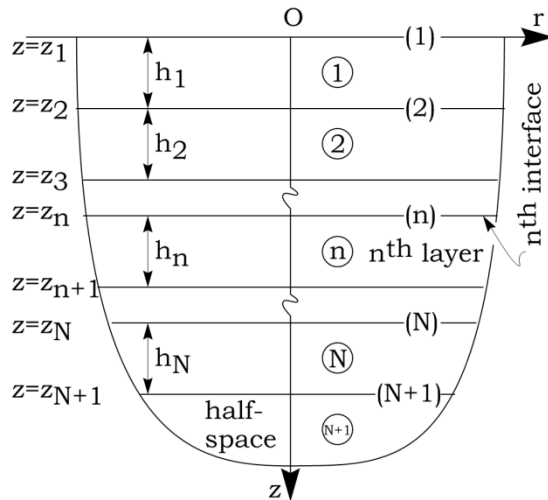


Figure 3.1 Geometry and notation of a multilayered system.

The stiffness-matrix approach is a classical technique for analyzing the behavior of such media. This approach is the same that is used in structural analysis: a stiffness matrix of the layered medium is assembled from the stiffness matrices of the layers and the underlying half-space in the same fashion as the stiffness matrix of a structure is assembled from the elementary stiffness matrices of its components (Gucunski and Peek, 1993; Wang, 1992).

Let $u_{im1}^{*(n)}$ denote the i^{th} displacement component at the top surface of the n^{th} layer ($z=z_n$), and $u_{im2}^{*(n)}$ denote the i^{th} displacement component at the bottom surface of the n^{th} layer ($z=z_{n+1}$). The * superscript indicate a transformed domain. The index m denotes axisymmetric ($m=0$) or antisymmetric problems ($m=1$) with respect to θ . For example, in view of Eq. 2.66 this yields:

$$u_{rm1}^{*(n)} = a_1^{(n)} A_m^{(n)} e^{-\delta^{(n)} \xi_1^{(n)} z_n} + a_1^{(n)} B_m^{(n)} e^{\delta^{(n)} \xi_1^{(n)} z_n} + a_2^{(n)} C_m^{(n)} e^{-\delta^{(n)} \xi_2^{(n)} z_n} + a_2^{(n)} D_m^{(n)} e^{\delta^{(n)} \xi_2^{(n)} z_n} + a_3^{(n)} E_m^{(n)} e^{-\delta^{(n)} \xi_3^{(n)} z_n} + a_3^{(n)} F_m^{(n)} e^{\delta^{(n)} \xi_3^{(n)} z_n} \quad (3.1)$$

$$u_{rm2}^{*(n)} = a_1^{(n)} A_m^{(n)} e^{-\delta^{(n)} \xi_1^{(n)} z_{n+1}} + a_1^{(n)} B_m^{(n)} e^{\delta^{(n)} \xi_1^{(n)} z_{n+1}} + a_2^{(n)} C_m^{(n)} e^{-\delta^{(n)} \xi_2^{(n)} z_{n+1}} + a_2^{(n)} D_m^{(n)} e^{\delta^{(n)} \xi_2^{(n)} z_{n+1}} + a_3^{(n)} E_m^{(n)} e^{-\delta^{(n)} \xi_3^{(n)} z_{n+1}} + a_3^{(n)} F_m^{(n)} e^{\delta^{(n)} \xi_3^{(n)} z_{n+1}} \quad (3.2)$$

The three displacement components from Eqs. 2.65 to 2.67 can be combined in one matrix equation:

$$u_m^{*(n)} = G_m^{(n)} a_m^{(n)} \quad (3.3)$$

where

$$u_m^{*(n)} = \left\langle u_{rm1}^{*(n)} \quad u_{\theta m1}^{*(n)} \quad u_{zm1}^{*(n)} \quad u_{rm2}^{*(n)} \quad u_{\theta m2}^{*(n)} \quad u_{zm2}^{*(n)} \right\rangle^T \quad (3.4)$$

$$a_m^{(n)} = \left\langle A_m^{(n)} \quad B_m^{(n)} \quad C_m^{(n)} \quad D_m^{(n)} \quad E_m^{(n)} \quad F_m^{(n)} \right\rangle^T \quad (3.5)$$

$$G_m^{(n)} = \begin{bmatrix} a_1 e_{1,n}^{-1} & a_1 e_{1,n}^{+1} & a_2 e_{2,n}^{-1} & a_2 e_{2,n}^{+1} & a_3 e_{3,n}^{-1} & a_3 e_{3,n}^{+1} \\ -a_4 e_{1,n}^{-1} & -a_4 e_{1,n}^{+1} & -a_5 e_{2,n}^{-1} & -a_5 e_{2,n}^{+1} & -a_6 e_{3,n}^{-1} & -a_6 e_{3,n}^{+1} \\ -a_7 e_{1,n}^{-1} & a_7 e_{1,n}^{+1} & -a_8 e_{2,n}^{-1} & -a_8 e_{2,n}^{+1} & 0 & 0 \\ a_1 e_{1,n+1}^{-1} & a_1 e_{1,n+1}^{+1} & a_2 e_{2,n+1}^{-1} & a_2 e_{2,n+1}^{+1} & a_3 e_{3,n+1}^{-1} & a_3 e_{3,n+1}^{+1} \\ -a_4 e_{1,n+1}^{-1} & -a_4 e_{1,n+1}^{+1} & -a_5 e_{2,n+1}^{-1} & -a_5 e_{2,n+1}^{+1} & -a_6 e_{3,n+1}^{-1} & -a_6 e_{3,n+1}^{+1} \\ -a_7 e_{1,n+1}^{-1} & a_7 e_{1,n+1}^{+1} & -a_8 e_{2,n+1}^{-1} & a_8 e_{2,n+1}^{+1} & 0 & 0 \end{bmatrix} \quad (3.6)$$

where

$$e_{i,j}^{\pm 1} = e^{\pm \delta^{(n)} \xi_i^{(n)} z_j}, \quad i=1,2; \quad j=1,2,\dots,N+1 \quad (3.7)$$

The upper index (n) in the parameters a_i , $i=1,8$, is omitted in Eq. 3.6 for conciseness.

Analogously, let $\sigma_{ijm1}^{*(n)}$ denote the ij^{th} stress component at the top surface of the n^{th} layer ($z=z_n$), and $\sigma_{ijm2}^{*(n)}$ denote the ij^{th} stress component at the bottom surface of the n^{th} layer ($z=z_{n+1}$). The * superscript indicates a transformed domain. The index m denotes axisymmetric ($m=0$) or antisymmetric problems ($m=1$) with respect to θ . The corresponding matrix equation can be obtained from Eqs. 2.71, 2.73 and 2.74 as:

$$\sigma_m^{*(n)} = F_m^{(n)} a_m^{(n)} \quad (3.8)$$

where

$$\sigma_m^{*(n)} = \left\langle -\sigma_{rzm1}^{*(n)} \quad -\sigma_{\theta zm1}^{*(n)} \quad -\sigma_{zzm1}^{*(n)} \quad \sigma_{rzm2}^{*(n)} \quad \sigma_{\theta zm2}^{*(n)} \quad \sigma_{zzm2}^{*(n)} \right\rangle^T \quad (3.9)$$

$$\frac{F_m^{(n)}}{c_{44}} = \begin{bmatrix} b_{51}e_{1,n}^{-1} & -b_{51}e_{1,n}^{+1} & b_{52}e_{2,n}^{-1} & -b_{52}e_{2,n}^{+1} & b_{53}e_{3,n}^{-1} & -b_{53}e_{3,n}^{+1} \\ -b_{41}e_{1,n}^{-1} & b_{41}e_{1,n}^{+1} & -b_{42}e_{2,n}^{-1} & b_{42}e_{2,n}^{+1} & -b_{43}e_{3,n}^{-1} & b_{43}e_{3,n}^{+1} \\ -b_{21}e_{1,n}^{-1} & -b_{21}e_{1,n}^{+1} & -b_{22}e_{2,n}^{-1} & -b_{22}e_{2,n}^{+1} & 0 & 0 \\ -b_{51}e_{1,n+1}^{-1} & b_{51}e_{1,n+1}^{+1} & -b_{52}e_{2,n+1}^{-1} & b_{52}e_{2,n+1}^{+1} & -b_{53}e_{3,n+1}^{-1} & b_{53}e_{3,n+1}^{+1} \\ b_{41}e_{1,n+1}^{-1} & -b_{41}e_{1,n+1}^{+1} & b_{42}e_{2,n+1}^{-1} & -b_{42}e_{2,n+1}^{+1} & b_{43}e_{3,n+1}^{-1} & -b_{43}e_{3,n+1}^{+1} \\ b_{21}e_{1,n+1}^{-1} & b_{21}e_{1,n+1}^{+1} & b_{22}e_{2,n+1}^{-1} & b_{22}e_{2,n+1}^{+1} & 0 & 0 \end{bmatrix} \quad (3.10)$$

Depending on whether the stresses are being observed on the top or bottom surface of a layer and because of the direction of the normal vector to each surface, the signs of the stress components may differ from those of their corresponding traction components (Fig. 3.2). After a careful consideration of this difference, an expression for the traction vector is obtained:

$$\mathbf{p}_m^{*(n)} = \left\langle p_{rm1}^{*(n)} \quad p_{\theta m1}^{*(n)} \quad p_{zm1}^{*(n)} \quad p_{rm2}^{*(n)} \quad p_{\theta m2}^{*(n)} \quad p_{zm2}^{*(n)} \right\rangle^T = \boldsymbol{\sigma}_m^{*(n)} \quad (3.11)$$

where $p_{im1}^{*(n)}$ denotes the traction acting at the top surface of the n^{th} layer in the i^{th} direction, and $p_{im2}^{*(n)}$ denotes the traction acting at the bottom surface of the n^{th} layer in the i^{th} direction. In this work, the terms of the traction vector were chosen to be positive, while the corresponding corrections of signs were introduced to the stress components (Eq. 3.9). It is convenient that all the terms of Eq. 3.11 are positive while interpreting the traction boundary conditions. This will be detailed later on.

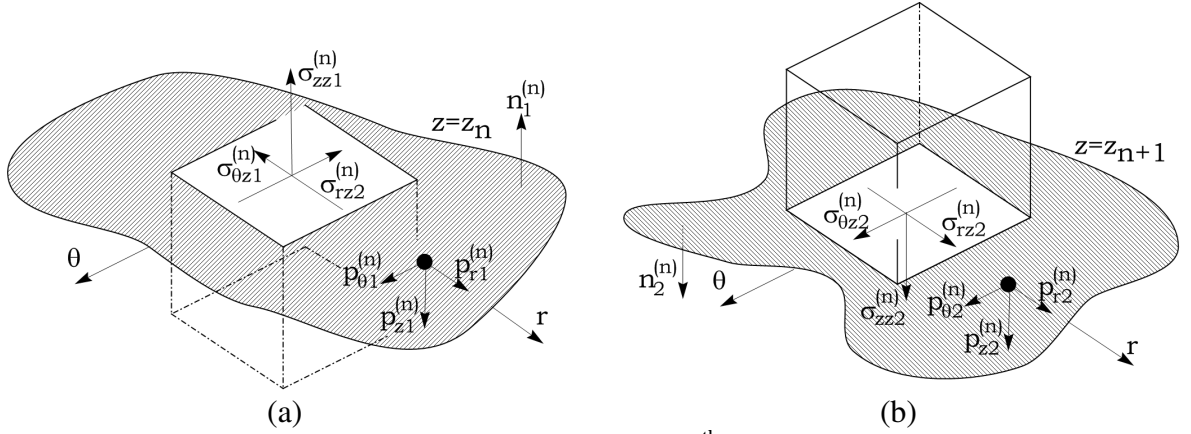


Figure 3.2 Directions of stresses and tractions at the n^{th} interface from the point of view of the (a) top and (b) bottom surfaces of the n^{th} layer when the normal vector to each surface is considered.

3.1 Underlying half-space

Consider the half-space shown in Fig. 3.1 (“layer” $N+1$). For the particular case of this semi-infinite medium, only the terms $A^{(N+1)}_m$, $C^{(N+1)}_m$ and $E^{(N+1)}_m$ are involved in the formulation, in order to satisfy Sommerfeld’s radiation condition (Sommerfeld, 1949). This results in a reduced form of Eqs. 3.3 and 3.8:

$$\mathbf{u}_m^{*(N+1)} = \mathbf{G}_m^{(N+1)} \mathbf{a}_m^{(N+1)} \quad (3.12)$$

where

$$\mathbf{u}_m^{*(N+1)} = \left\langle \mathbf{u}_{rml}^{*(N+1)} \quad \mathbf{u}_{\theta ml}^{*(N+1)} \quad \mathbf{u}_{zml}^{*(N+1)} \right\rangle^T \quad (3.13)$$

$$\mathbf{a}_m^{(N+1)} = \left\langle \mathbf{A}_m^{(N+1)} \quad \mathbf{C}_m^{(N+1)} \quad \mathbf{E}_m^{(N+1)} \right\rangle^T \quad (3.14)$$

$$\mathbf{G}_m^{(N+1)} = \begin{bmatrix} a_1 e_{1,N+1}^{-1} & a_2 e_{2,N+1}^{-1} & a_3 e_{3,N+1}^{-1} \\ -a_4 e_{1,N+1}^{-1} & -a_5 e_{2,N+1}^{-1} & -a_6 e_{3,N+1}^{-1} \\ -a_7 e_{1,N+1}^{-1} & -a_8 e_{2,N+1}^{-1} & 0 \end{bmatrix} \quad (3.15)$$

and

$$\boldsymbol{\sigma}_m^{*(N+1)} = \mathbf{F}_m^{(N+1)} \mathbf{a}_m^{(N+1)} \quad (3.16)$$

where

$$\boldsymbol{\sigma}_m^{*(N+1)} = \left\langle -\boldsymbol{\sigma}_{rzm1}^{*(N+1)} \quad -\boldsymbol{\sigma}_{\theta zm1}^{*(N+1)} \quad -\boldsymbol{\sigma}_{zzm1}^{*(N+1)} \right\rangle^T \quad (3.17)$$

$$\frac{\mathbf{F}_m^{(N+1)}}{c_{44}} = \begin{bmatrix} b_{51} e_{1,N+1}^{-1} & b_{52} e_{2,N+1}^{-1} & b_{53} e_{3,N+1}^{-1} \\ -b_{41} e_{1,N+1}^{-1} & -b_{42} e_{2,N+1}^{-1} & -b_{43} e_{3,N+1}^{-1} \\ -b_{21} e_{1,N+1}^{-1} & -b_{22} e_{2,N+1}^{-1} & 0 \end{bmatrix} \quad (3.18)$$

3.2 Stiffness matrix of the layers and half-space

Consider the vector $\mathbf{a}_m^{(n)}$ involved in Eqs. 3.3 and 3.8, which contains the arbitrary functions $\mathbf{A}_m^{(n)}$, $\mathbf{B}_m^{(n)}$, $\mathbf{C}_m^{(n)}$, $\mathbf{D}_m^{(n)}$, $\mathbf{E}_m^{(n)}$ and $\mathbf{F}_m^{(n)}$. The vector $\mathbf{a}_m^{(n)}$ is common to the expressions of displacements (Eq. 3.3) and stresses of each layer (Eq. 3.8). Equations 3.3 and 3.8 can be combined into:

$$\sigma_m^{*(n)} = F_m^{(n)} a_m^{(n)} = F_m^{(n)} \left(G_m^{(n)} \right)^{-1} u_m^{*(n)} = K_m^{(n)} u_m^{*(n)}; \quad n=1,2,\dots,N \quad (3.19)$$

In Eq. 3.19, the matrix $K_m^{(n)}$ is the stiffness matrix of the layer n .

An analogous definition holds for the half-space. The vector $a_m^{(N+1)}$ involved in Eqs. 3.12 and 3.16 contains the arbitrary functions $A^{(N+1)}_m$, $B^{(N+1)}_m$, $C^{(N+1)}_m$ and $D^{(N+1)}_m$, and it is common to the expressions of displacements (Eq. 3.3) and stresses of the half-space (Eq. 3.8). Equations 3.12 and 3.16 can be combined into:

$$\sigma_m^{*(N+1)} = F_m^{(N+1)} a_m^{(N+1)} = F_m^{(N+1)} \left(G_m^{(N+1)} \right)^{-1} u_m^{*(N+1)} = K_m^{(N+1)} u_m^{*(N+1)} \quad (3.20)$$

In Eq. 3.20, the matrix $K_m^{(N+1)}$ is the stiffness matrix of the half-space (“layer” $N+1$).

Matrices $K_m^{(n)}$ depend on the material properties of the layer n ($n=1,2,\dots,N,N+1$) and its thickness, on the frequency of excitation and on the Hankel space variable λ . The expression of $K_m^{(n)}$ is rather long and has to be determined numerically.

3.3 Stiffness matrix of the multilayered medium

Let \wp_{im}^n denote the external concentrated or distributed load applied at the n^{th} interface of two layers, in the direction of i ($i=r,\theta,z$), such as described in Section 2.4. In view of the sign convention established in Fig. 3.3, the following equation describes the traction discontinuity at that interface:

$$\mathcal{H}_m \left\{ \wp_{im}^n \right\} = p_{im2}^{*(n-1)} + p_{im1}^{*(n)} = \sigma_{im2}^{*(n-1)} - \sigma_{im1}^{*(n)}; \quad i=r,\theta,z \quad (3.21)$$

Additionally, the kinematic continuity condition at the interface of any two layers is given mathematically by:

$$u_{im2}^{*(n-1)} = u_{im1}^{*(n)}; \quad i=r,\theta,z \quad (3.21)$$

Equation 3.21 is applied together with Eqs. 3.19 and 3.20 for all the layers $n=1,2,\dots,N,N+1$ to form the following global stiffness matrix of the multilayered medium:

$$\wp_m^* = K_m u_m^* \quad (3.22)$$

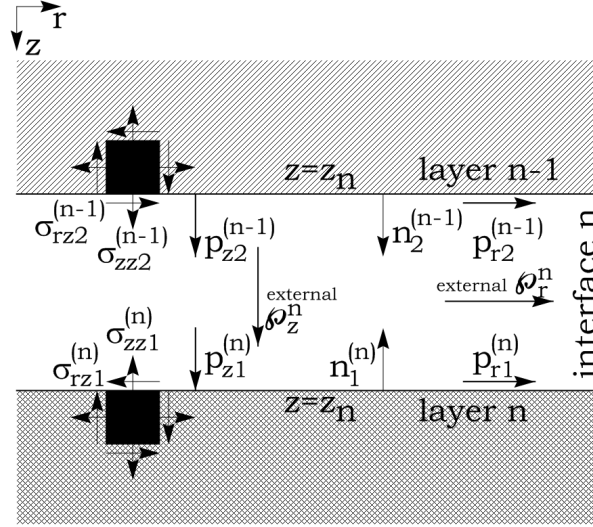


Figure 3.3 Definitions and sign conventions for tractions, stresses and external loads, considering the normal vectors at the free surfaces of each layer. The subscript m is omitted for conciseness.

In Eq. 3.22, $\wp_m^* = \wp_m^*(\lambda)$ is the vector of external loads applied at the layer interfaces, given by Eq. 3.23; $u_m^* = u_m^*(\lambda)$ is the vector of resulting displacements of points of the interfaces, given by Eq. 3.24, and $K_m = K_m(\lambda)$ is the global stiffness matrix of the medium, given by Eq. 3.25. All these terms are in the Hankel transformed domain, and depend on the Hankel space parameter λ .

$$\wp_m^* = \left\langle \wp_{rm}^{*1} \quad \wp_{\theta m}^{*1} \quad \wp_{zm}^{*1} \quad \dots \quad \wp_{rm}^{*(N+1)} \quad \wp_{\theta m}^{*(N+1)} \quad \wp_{zm}^{*(N+1)} \right\rangle^T \quad (3.23)$$

$$u_m^* = \left\langle u_{rm}^*(r, z_1) \quad u_{\theta m}^*(r, z_1) \quad u_{zm}^*(r, z_1) \quad \dots \quad u_{rm}^*(r, z_{N+1}) \quad u_{\theta m}^*(r, z_{N+1}) \quad u_{zm}^*(r, z_{N+1}) \right\rangle^T \quad (3.24)$$

$$K_m = \left[\begin{array}{c} K_m^{(1)} \\ K_m^{(2)} \\ \dots \\ K_m^{(N)} \\ K_m^{(N+1)} \end{array} \right] \quad (3.25)$$

When Eq. 3.22 is assembled, the continuity of displacements at the interfaces, which states that $u_{im2}^{*(n-1)} = u_{im1}^{*(n)}$, is implicitly guaranteed. In the next section, the global stiffness matrix is assembled for an example of three layers plus a half-space. The condition of continuity at the interfaces is explicitly stated, and the resulting stiffness matrix is precisely as shown in Eq. 3.25.

The solution of displacements from Eq. 3.22 must be integrated along λ as described in Eq. 2.63 to obtain the displacements at the layer interfaces in the physical domain.

3.4 Example

Consider the example of multilayered system depicted in Fig. 3.4. The system contains $N=3$ transversely isotropic layers plus an underlying half-space. Only axisymmetric vertical and radial external loads are considered ($m=0$). The index m will be omitted in the formulation of this example for conciseness. The $*$ superscript will also be omitted: all displacement, stress, external load and traction components in this example are in the transformed domain.

In the example of Fig. 3.4, there are 14 unknowns to be determined: $A^{(1)}, B^{(1)}, C^{(1)}, D^{(1)}$ for layer 1 and $A^{(2)}, B^{(2)}, C^{(2)}, D^{(2)}$ for layer 2, $A^{(3)}, B^{(3)}, C^{(3)}, D^{(3)}$ for layer 3 and $A^{(4)}, C^{(4)}$ for the half-space – “layer” 4.

Fourteen boundary conditions or continuity conditions are known. At the free surface (“interface” 1, $z=z_1$),

$$p_{r1}^{(1)} = \wp_r^1 \tag{3.26}$$

$$p_{z1}^{(1)} = \wp_z^1 \tag{3.27}$$

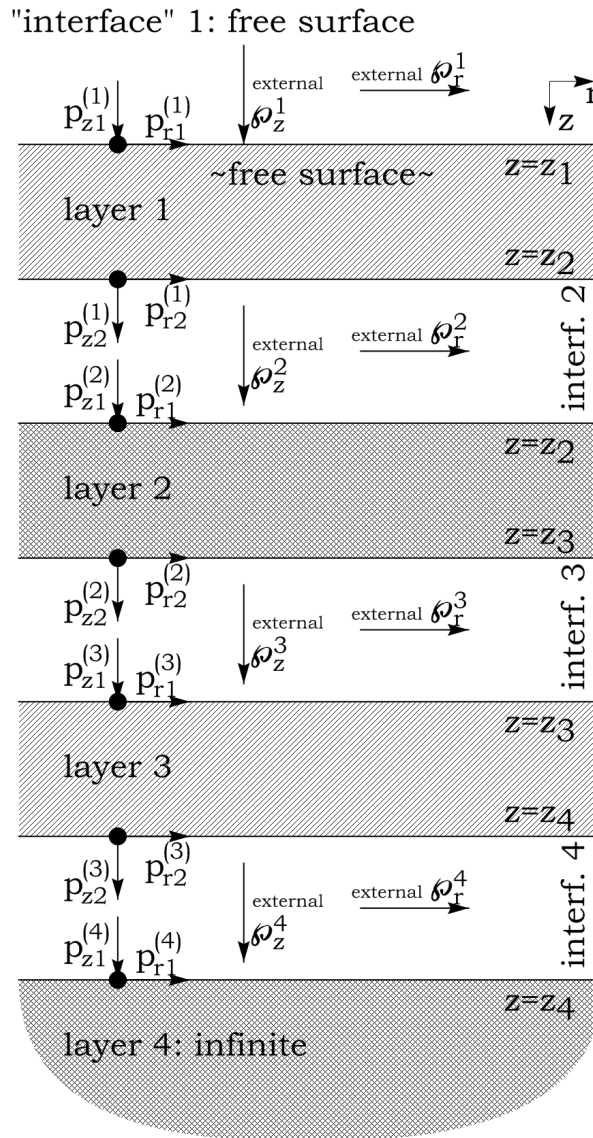


Figure 3.4 Layer and interface numbering, tractions and external forces, for a reduced example of $N=3$ layers plus an underlying infinite half-space.

At interface 2 ($z=z_2$):

$$p_{r2}^{(1)} + p_{r1}^{(2)} = \wp_r^2 \tag{3.28}$$

$$p_{z2}^{(1)} + p_{z1}^{(2)} = \rho z^2 \quad (3.29)$$

$$u_{r2}^{(1)} = u_r^{(1)}(r, z_2) = u_{r1}^{(2)} = u_r^{(2)}(r, z_2) \quad (3.30)$$

$$u_{z2}^{(1)} = u_z^{(1)}(r, z_2) = u_{z1}^{(2)} = u_z^{(2)}(r, z_2) \quad (3.31)$$

At interface 3 ($z=z_3$):

$$p_{r2}^{(2)} + p_{r1}^{(3)} = \rho r^3 \quad (3.32)$$

$$p_{z2}^{(2)} + p_{z1}^{(3)} = \rho z^3 \quad (3.33)$$

$$u_{r2}^{(2)} = u_r^{(2)}(r, z_3) = u_{r1}^{(3)} = u_r^{(3)}(r, z_3) \quad (3.34)$$

$$u_{z2}^{(2)} = u_z^{(2)}(r, z_3) = u_{z1}^{(3)} = u_z^{(3)}(r, z_3) \quad (3.35)$$

At interface 4, corresponding to the surface of the half-space ($z=z_4$):

$$p_{r2}^{(3)} + p_{r1}^{(4)} = \rho r^4 \quad (3.36)$$

$$p_{z2}^{(3)} + p_{z1}^{(4)} = \rho z^4 \quad (3.37)$$

$$u_{r2}^{(3)} = u_r^{(3)}(r, z_4) = u_{r1}^{(4)} = u_r^{(4)}(r, z_4) \quad (3.38)$$

$$u_{z2}^{(3)} = u_z^{(3)}(r, z_4) = u_{z1}^{(4)} = u_z^{(4)}(r, z_4) \quad (3.39)$$

Equation 3.19 is applied for each layer $n=1,4$. For layer $n=1$,

$$k_{11}^{(1)} u_{r1}^{(1)} + k_{12}^{(1)} u_{z1}^{(1)} + k_{13}^{(1)} u_{r2}^{(1)} + k_{14}^{(1)} u_{z2}^{(1)} = -\sigma_{rz1}^{(1)} = p_{r1}^{(1)} \quad (3.40)$$

$$k_{21}^{(1)} u_{r1}^{(1)} + k_{22}^{(1)} u_{z1}^{(1)} + k_{23}^{(1)} u_{r2}^{(1)} + k_{24}^{(1)} u_{z2}^{(1)} = -\sigma_{zz1}^{(1)} = p_{z1}^{(1)} \quad (3.41)$$

$$k_{31}^{(1)}u_{r1}^{(1)} + k_{32}^{(1)}u_{z1}^{(1)} + k_{33}^{(1)}u_{r2}^{(1)} + k_{34}^{(1)}u_{z2}^{(1)} = \sigma_{rz2}^{(1)} = p_{r2}^{(1)} \quad (3.42)$$

$$k_{41}^{(1)}u_{r1}^{(1)} + k_{42}^{(1)}u_{z1}^{(1)} + k_{43}^{(1)}u_{r2}^{(1)} + k_{44}^{(1)}u_{z2}^{(1)} = \sigma_{zz2}^{(1)} = p_{z2}^{(1)} \quad (3.43)$$

For layer n=2,

$$k_{11}^{(2)}u_{r1}^{(2)} + k_{12}^{(2)}u_{z1}^{(2)} + k_{13}^{(2)}u_{r2}^{(2)} + k_{14}^{(2)}u_{z2}^{(2)} = -\sigma_{rz1}^{(2)} = p_{r1}^{(2)} \quad (3.44)$$

$$k_{21}^{(2)}u_{r1}^{(2)} + k_{22}^{(2)}u_{z1}^{(2)} + k_{23}^{(2)}u_{r2}^{(2)} + k_{24}^{(2)}u_{z2}^{(2)} = -\sigma_{zz1}^{(2)} = p_{z1}^{(2)} \quad (3.45)$$

$$k_{31}^{(2)}u_{r1}^{(2)} + k_{32}^{(2)}u_{z1}^{(2)} + k_{33}^{(2)}u_{r2}^{(2)} + k_{34}^{(2)}u_{z2}^{(2)} = \sigma_{rz2}^{(2)} = p_{r2}^{(2)} \quad (3.46)$$

$$k_{41}^{(2)}u_{r1}^{(2)} + k_{42}^{(2)}u_{z1}^{(2)} + k_{43}^{(2)}u_{r2}^{(2)} + k_{44}^{(2)}u_{z2}^{(2)} = \sigma_{zz2}^{(2)} = p_{z2}^{(2)} \quad (3.47)$$

For layer n=3,

$$k_{11}^{(3)}u_{r1}^{(3)} + k_{12}^{(3)}u_{z1}^{(3)} + k_{13}^{(3)}u_{r2}^{(3)} + k_{14}^{(3)}u_{z2}^{(3)} = -\sigma_{rz1}^{(3)} = p_{r1}^{(3)} \quad (3.48)$$

$$k_{21}^{(3)}u_{r1}^{(3)} + k_{22}^{(3)}u_{z1}^{(3)} + k_{23}^{(3)}u_{r2}^{(3)} + k_{24}^{(3)}u_{z2}^{(3)} = -\sigma_{zz1}^{(3)} = p_{z1}^{(3)} \quad (3.49)$$

$$k_{31}^{(3)}u_{r1}^{(3)} + k_{32}^{(3)}u_{z1}^{(3)} + k_{33}^{(3)}u_{r2}^{(3)} + k_{34}^{(3)}u_{z2}^{(3)} = \sigma_{rz2}^{(3)} = p_{r2}^{(3)} \quad (3.50)$$

$$k_{41}^{(3)}u_{r1}^{(3)} + k_{42}^{(3)}u_{z1}^{(3)} + k_{43}^{(3)}u_{r2}^{(3)} + k_{44}^{(3)}u_{z2}^{(3)} = \sigma_{zz2}^{(3)} = p_{z2}^{(3)} \quad (3.51)$$

And for the half-space, “layer” n=4, Eq. 3.20 results in:

$$k_{11}^{(4)}u_{r1}^{(4)} + k_{12}^{(4)}u_{z1}^{(4)} = -\sigma_{rz1}^{(4)} = p_{r1}^{(4)} \quad (3.52)$$

$$k_{21}^{(4)}u_{r1}^{(4)} + k_{22}^{(4)}u_{z1}^{(4)} = -\sigma_{zz1}^{(4)} = p_{z1}^{(4)} \quad (3.53)$$

The boundary conditions from Eqs. 3.26 to 3.39 are applied into Eqs. 3.40 to 3.53. The application of Eqs. 3.26 and 3.27 into Eqs. 3.40 and 3.41 yield:

$$k_{11}^{(1)}u_{r1}^{(1)} + k_{12}^{(1)}u_{z1}^{(1)} + k_{13}^{(1)}u_{r2}^{(1)} + k_{14}^{(1)}u_{z2}^{(1)} = \wp_r^1 \quad (3.54)$$

$$k_{21}^{(1)}u_{r1}^{(1)} + k_{22}^{(1)}u_{z1}^{(1)} + k_{23}^{(1)}u_{r2}^{(1)} + k_{24}^{(1)}u_{z2}^{(1)} = \wp_z^1 \quad (3.55)$$

Then Eqs. 3.42 and 3.44 into 3.28, in view of Eqs. 3.30 and 3.31 yield Eq. 3.56, while Eqs. 3.43 and 3.45 into 3.29, in view of Eqs. 3.30 and 3.31 yield Eq. 3.57.

$$k_{31}^{(1)}u_{r1}^{(1)} + k_{32}^{(1)}u_{z1}^{(1)} + \left(k_{33}^{(1)} + k_{11}^{(2)}\right)u_{r1}^{(2)} + \left(k_{34}^{(1)} + k_{12}^{(2)}\right)u_{z1}^{(2)} + k_{13}^{(2)}u_{r2}^{(2)} + k_{14}^{(2)}u_{z2}^{(2)} = \wp_r^2 \quad (3.56)$$

$$k_{41}^{(1)}u_{r1}^{(1)} + k_{42}^{(1)}u_{z1}^{(1)} + \left(k_{43}^{(1)} + k_{21}^{(2)}\right)u_{r1}^{(2)} + \left(k_{44}^{(1)} + k_{22}^{(2)}\right)u_{z1}^{(2)} + k_{23}^{(2)}u_{r2}^{(2)} + k_{24}^{(2)}u_{z2}^{(2)} = \wp_z^2 \quad (3.57)$$

Equations 3.46 and 3.48 into 3.32, in view of Eqs. 3.34 and 3.35 yield Eq. 3.58, while Eqs. 3.47 and 3.49 into 3.33, considering also 3.34 and 3.35 yield Eq. 3.59.

$$k_{31}^{(2)}u_{r1}^{(2)} + k_{32}^{(2)}u_{z1}^{(2)} + \left(k_{33}^{(2)} + k_{11}^{(3)}\right)u_{r1}^{(3)} + \left(k_{34}^{(2)} + k_{12}^{(3)}\right)u_{z1}^{(3)} + k_{13}^{(3)}u_{r2}^{(3)} + k_{14}^{(3)}u_{z2}^{(3)} = \wp_r^3 \quad (3.58)$$

$$k_{41}^{(2)}u_{r1}^{(2)} + k_{42}^{(2)}u_{z1}^{(2)} + \left(k_{43}^{(2)} + k_{21}^{(3)}\right)u_{r1}^{(3)} + \left(k_{44}^{(2)} + k_{22}^{(3)}\right)u_{z1}^{(3)} + k_{23}^{(3)}u_{r2}^{(3)} + k_{24}^{(3)}u_{z2}^{(3)} = \wp_z^3 \quad (3.59)$$

Equations 3.60 and 3.62 into 3.36, in view of Eqs. 3.38 and 3.39 yield Eq. 3.60, while Eqs. 3.61 and 3.63 into 3.37, in view of Eqs. 3.38 and 3.39 yield Eq. 3.61.

$$k_{31}^{(3)}u_{r1}^{(3)} + k_{32}^{(3)}u_{z1}^{(3)} + \left(k_{33}^{(3)} + k_{11}^{(4)}\right)u_{r1}^{(4)} + \left(k_{34}^{(3)} + k_{12}^{(4)}\right)u_{z1}^{(4)} = \wp_r^4 \quad (3.60)$$

$$k_{41}^{(3)}u_{r1}^{(3)} + k_{42}^{(3)}u_{z1}^{(3)} + \left(k_{43}^{(3)} + k_{21}^{(4)}\right)u_{r1}^{(4)} + \left(k_{44}^{(3)} + k_{22}^{(4)}\right)u_{z1}^{(4)} = \wp_z^4 \quad (3.61)$$

Equations 3.54 to 3.61 are assembled in the following matrix form:

$$\begin{bmatrix}
 k_{11}^{(1)} & k_{12}^{(1)} & k_{13}^{(1)} & k_{14}^{(1)} & 0 & 0 & 0 & 0 \\
 k_{21}^{(1)} & k_{22}^{(1)} & k_{23}^{(1)} & k_{24}^{(1)} & 0 & 0 & 0 & 0 \\
 k_{31}^{(1)} & k_{32}^{(1)} & k_{33}^{(1)} + k_{11}^{(2)} & k_{34}^{(1)} + k_{12}^{(2)} & k_{13}^{(2)} & k_{14}^{(2)} & 0 & 0 \\
 k_{41}^{(1)} & k_{42}^{(1)} & k_{43}^{(1)} + k_{21}^{(2)} & k_{44}^{(1)} + k_{22}^{(2)} & k_{23}^{(2)} & k_{24}^{(2)} & 0 & 0 \\
 0 & 0 & k_{31}^{(2)} & k_{32}^{(2)} & k_{33}^{(2)} + k_{11}^{(3)} & k_{34}^{(2)} + k_{12}^{(3)} & k_{13}^{(3)} & k_{14}^{(3)} \\
 0 & 0 & k_{41}^{(2)} & k_{42}^{(2)} & k_{43}^{(2)} + k_{21}^{(3)} & k_{44}^{(2)} + k_{22}^{(3)} & k_{23}^{(3)} & k_{24}^{(3)} \\
 0 & 0 & 0 & 0 & k_{31}^{(3)} & k_{32}^{(3)} & k_{33}^{(3)} + k_{11}^{(4)} & k_{34}^{(3)} + k_{12}^{(4)} \\
 0 & 0 & 0 & 0 & k_{41}^{(3)} & k_{42}^{(3)} & k_{43}^{(3)} + k_{21}^{(4)} & k_{44}^{(3)} + k_{22}^{(4)}
 \end{bmatrix}
 \begin{Bmatrix}
 u_r^1 \\
 u_z^1 \\
 u_r^2 \\
 u_z^2 \\
 u_r^3 \\
 u_z^3 \\
 u_r^4 \\
 u_z^4
 \end{Bmatrix}
 =
 \begin{Bmatrix}
 \varphi_r^1 \\
 \varphi_z^1 \\
 \varphi_r^2 \\
 \varphi_z^2 \\
 \varphi_r^3 \\
 \varphi_z^3 \\
 \varphi_r^4 \\
 \varphi_z^4
 \end{Bmatrix}
 \quad (3.62)$$

The solution of Eq. 3.62 results in radial and vertical displacements $u_r^{(n)}(r, z_n)$ and $u_z^{(n)}(r, z_n)$ ($n=1,4$) of points of the interfaces of the example depicted in Fig. 3.4 in response to the radial and vertical loads $\varphi_r^{(n)}$ and $\varphi_z^{(n)}$ to which it is subjected. The continuity conditions at the interfaces are stated explicitly, and the resulting global stiffness matrix matches that generalized expression shown in Eq. 3.25.

The displacements involved in Eq. 3.62 are function of the Hankel space variable λ . Their counterparts in the physical domain are achieved upon their integration according to Eq. 2.63.

This chapter presented a method to compute displacements and stresses of a multilayered transversely isotropic elastic half-space. The loadings to which the layered medium is subjected are arbitrary. Time-harmonic concentrated and distributed loads are described in the previous chapter. In the next chapters, the formulation of two different models of circular foundations will be presented. These models will be used with this and the previous chapter's influence functions to study the behavior of rigid and flexible plates embedded in three-dimensional transversely isotropic bi-material and layered systems.

4 MODEL OF AN EMBEDDED RIGID CIRCULAR PLATE

This chapter presents the formulation of a model of rigid circular plates. A set of coupled integral equations, which relates the displacements and the unknown tractions across an arbitrary rigid circular surface inside an elastic medium, is used to describe the embedded disc. These integral equations involve the influence functions corresponding to vertical and transverse displacements, due to unit axisymmetric vertical or antisymmetric transverse and vertical loads, the derivation of which was presented in the previous chapters. This chapter presents a strategy to solve these coupled integral equations by discretizing the circular surface into concentric annular disc elements, on which the traction fields are assumed to vary according to a known shape. The results of vibration of the embedded rigid disc are compared with results from the literature. Original research results of the problem are also presented.

4.1 Problem statement

Consider the time-harmonic excitation of a rigid massless disc of thickness $h=0$ and radius a embedded in the interface of two elastic unbounded three-dimensional media as shown in Fig. 4.1a.

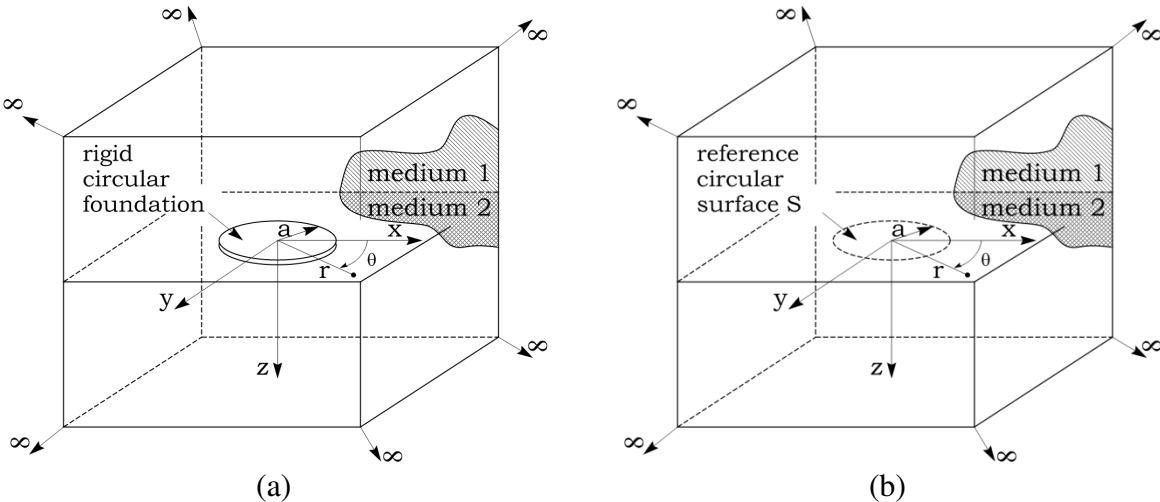


Figure 4.1 (a) Circular plate of radius a buried in the interface of two media and (b) reference surface S of radius a within the interface.

The plate is under the effect of time-harmonic, axisymmetric, either concentrated or distributed vertical ring loads, such as depicted in Fig. 2.3a; or transverse loads (Fig. 2.3b); or antisymmetric vertical loads, which correspond to a net moment about the y-axis (Fig. 2.3c).

The objective of this chapter is to provide a mathematical description of the problem of the rigid plate, which can be used together with the models of transversely isotropic media presented in chapters 2 and 3 to model the problem of the plate embedded in such media.

4.2 Governing equations

Since the disc is massless and $h=0$, its behavior can be modeled solely by considering that a circular surface of the medium, corresponding to the area of the plate, is rigid (Fig. 4.1b).

The displacements w_i of a circular surface S of radius a inside an elastic medium can be related to the interface contact traction t_j through the following integral equation:

$$\int_{s=0}^{s=a} u_{ij}(r, \theta, z=0, s, \omega) t_j(s, \theta, z=0, \omega) ds = w_i(r, \theta, z=0, \omega), \quad i, j=r, \theta, z. \quad (4.1)$$

In Eq. 4.1, $u_{ij}(r, \theta, z=0, s, \omega)$ denotes the displacement of the point P of coordinates $(r, \theta, z=0)$ in the i -direction. It is due a unit ring load in the j -direction concentrated on a ring of radius s . The ring load is dynamic with circular frequency ω . For the case of transversely isotropic interfaces, these displacement components are obtained according to Eq. 2.63. The ring loads that actually act on the surface S are not necessarily unitary as the term $u_{ij}(r, \theta, z=0, s, \omega)$ considers, but they have unknown intensities denoted by t_j ($j=r, \theta, z$), the distribution of which on the surface S is also unknown. The term $w_i(r, \theta, z=0, \omega)$ ($i=r, \theta, z$) denotes the resulting displacement of S at the point P in the i -direction. It is obtained after weighting the displacements $u_{ij}(r, \theta, z=0, s, \omega)$ due to unitary loads by the actual loads t_j which are acting on the whole surface of S ($0 \leq s \leq a$). Equation 4.1 expresses the most general coupled behavior, in which displacements in any direction $i=r, \theta, z$ may occur due to a load in $j=r, \theta, z$. The indices in this equation must be interpreted according to Einstein's summation convention.

Note that for a surface subjected to a vertical load all field components in Eq. 4.1 are independent of θ . In the case of a surface subjected to a horizontal load in the x -direction or a

moment about the y -axis, the θ -dependence of all field variables in the radial and vertical directions is represented by $\cos(\theta)$ and in the θ -direction by $\sin(\theta)$ (Eqs. 2.145 to 2.162).

A solution to Eq. 4.1 by analytical methods is not feasible due to the complexity of the integrand function. A numerical solution is obtained by considering that the surface S is made up of M concentric annular disc elements of inner and outer radii s_{1k} and s_{2k} ($k=1,M$). Figure 4.2 shows an example of this discretization for $M=4$ annular disc elements. The tractions t_j acting on each annular disc element are assumed to be constant in the cases of vertical and transverse loads (Fig. 2.3a and 2.3b). However, for moment loading, the traction in the z -direction is assumed to vary with r and θ across an annular disc element (Figs. 2.3c and 2.8).

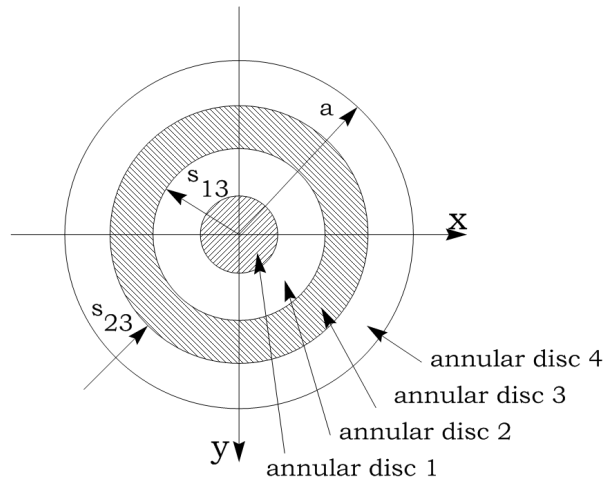


Figure 4.2 Discretization of the region S into concentric annular disc elements for the case of $M=4$.

4.3 Vertical load

Consider a circular surface S inside the material interface shown in Fig. 4.1b, subjected to axisymmetric vertical loads. It is assumed that the influence of radial traction on the vertical displacement of the rigid surface is negligible (Rajapakse, 1988). The radial traction is therefore neglected in the analysis of a vertically loaded surface. Equation 4.1 can be expressed in the following form for a rigid disc under a vertical load by using a set of M concentric annular disc elements:

$$\sum_{k=1}^M u_{zz}(r_i, s_{1k}, s_{2k}, \omega) t_z(r_k, \omega) = w_z(r_i); i=1, M \quad (4.2)$$

The term $u_{zz}(r_i, s_{1k}, s_{2k}, \omega)$ of Eq. 4.2 is defined as follows: in the set of M annular surfaces, consider the one represented by the index k ($k=1, M$), the inner and outer radii of which are s_{1k} and s_{2k} (Fig. 4.3). This surface is subjected to a distributed unit vertical load. The displacement of a point of coordinates r_i ($s_{1i} \leq r_i = (s_{1i} + s_{2i})/2 \leq s_{2i}$) is denominated $u_{zz}(r_i, s_{1k}, s_{2k}, \omega)$ in Eq. 4.2. This displacement is considered to represent the displacement of all the points of the annular surface i ($i=1, M$) in which r_i is contained.

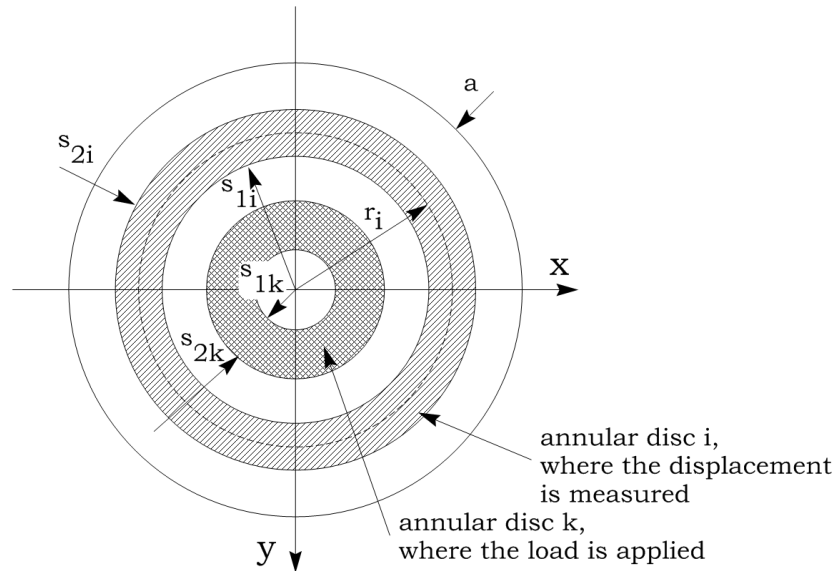


Figure 4.3 Discretization of the region S , showing the annular disc elements i and k .

The derivation of this displacement component $u_{zz}(r_i, s_{1k}, s_{2k}, \omega)$ was described in the previous chapter (Eqs. 2.63 and 2.67).

The vertical load to which the element k is subjected is not necessarily unitary, as the term $u_{zz}(r_i, s_{1k}, s_{2k}, \omega)$ considers, but it has an unknown value denoted by $t_z(r_k)$ in Eq. 4.2. To obtain the displacement $w_z(r_i)$ that each annular surface i ($i=1, M$) actually experiences, the displacements of it due to loads in all other annular surfaces k must be taken into consideration, after being weighed by their respective unknown traction jumps $t_z(r_k)$.

Equation 4.2 results in the actual displacement $w_z(r_i)$ of an arbitrary annular disc element i and presents M unknown tractions $t_z(r_k)$. Equation 4.2 can be repeated for all annular discs $i=1,M$ resulting in the set of M linear equations shown in Eq. 4.3. From the hypothesis that the entire circular surface S behaves like a rigid disc, the vertical displacement of all annular disc elements is the same, e.g., $w_z(r_i)=w_{0z}=1$ ($i=1,M$).

$$\begin{bmatrix} u_{zz}^{1,1} & u_{zz}^{1,2} & & u_{zz}^{1,M} \\ u_{zz}^{2,1} & u_{zz}^{2,2} & & u_{zz}^{2,M} \\ & & \ddots & \\ u_{zz}^{M,2} & u_{zz}^{M,2} & & u_{zz}^{M,M} \end{bmatrix} \begin{Bmatrix} t_z(r_1, \omega) \\ t_z(r_2, \omega) \\ \vdots \\ t_z(r_M, \omega) \end{Bmatrix} = \begin{Bmatrix} w_z(r_1, \omega) = w_{0z} = 1 \\ w_z(r_2, \omega) = w_{0z} = 1 \\ \vdots \\ w_z(r_M, \omega) = w_{0z} = 1 \end{Bmatrix} \quad (4.3)$$

in which

$$u_{zz}^{i,k} = u_{zz}(r_i, s_{1k}, s_{2k}, \omega), \quad i,k=1,M \quad (4.4)$$

Equation 4.3 is solved for the vertical traction jumps acting on each disc element. The total force acting on the circular surface S is given by

$$F_z(\omega) = \sum_{k=1}^M A_k t_z(r_k, \omega) = \sum_{k=1}^M \pi (s_{2k}^2 - s_{1k}^2) t_z(r_k, \omega) \quad (4.5)$$

In Eq. 4.5, A_k is the area of the annular disc element k .

The dynamic vertical compliance of the system comprising the buried rigid surface and its surrounding medium, for each frequency, is defined by:

$$C_{ZZ}(\omega) = w_{0z} a E / F_z(\omega) \quad (4.6)$$

In Eq. 4.6, E is the Young's modulus of one of the two materials of the interface (Fig. 4.1), and a is the outer radius of the rigid surface S . w_{0z} is the displacement of each of its annular disc elements, which in this work is set to be unitary (Eq. 4.3). $F_z(\omega)$ is the total dynamic force (Eq. 4.5) acting on the surface S , in the vertical direction, which causes the annular disc elements to be displaced by w_{0z} . $C_{ZZ}(\omega)$ represents the non-dimensional dynamic vertical compliance

corresponding to the vertical displacement of the surface S, in response to axisymmetric vertical loads applied on the surface of S.

4.4 Transverse and moment loading

Consider the rigid circular surface S shown in Figs. 4.1b and 4.4a, within the interface of two transversely isotropic unbounded media. The surface is subjected to non-axisymmetric transverse loads or concentrated moment about the y-axis.

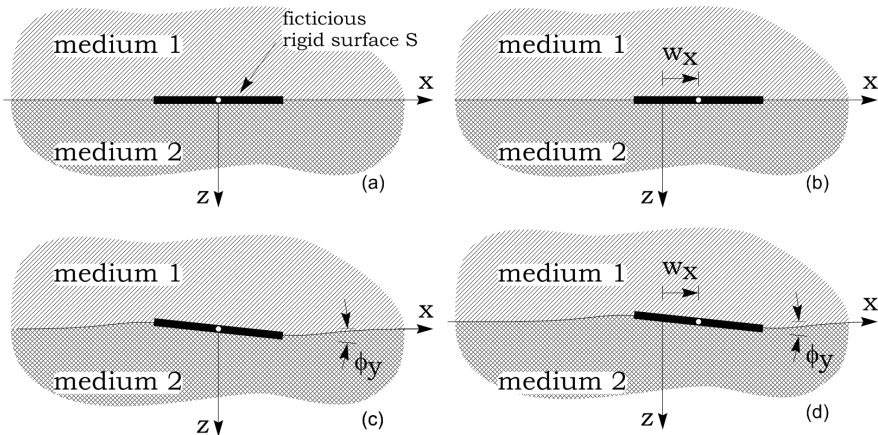


Figure 4.4 (a) Undisturbed media and rigid surface S, (b) pure transverse displacement of the surface S, (c) pure rotation and (d) combined translation and rotation.

If both media 1 and 2 have equal geometrical and material properties, then the transverse displacement of the surface S due to the transverse load is uncoupled from the rotation and vice-versa (Selvadurai and Singh, 1984; Selvadurai; 1980). Transverse loads along the x-direction result in transverse displacements w_x only (Fig. 4.4b), while moments about the y-axis result in rotations ϕ_y only (Fig. 4.4c). For a more general case in which the two media have different material properties or geometrical configurations (such as the case of a plate resting on the surface of a half-space), the surface S undergoes coupled translation and rotation (Luco and Westman, 1971; Luco, 1974; Mesquita, 1989). Pure transverse loads along the x-direction will cause the surface S to be displaced horizontally (w_x) and tilt about the y-axis (ϕ_y) (Fig. 4.4d). Pure moments about the y-axis will correspondingly produce an analogous coupled kinematic response.

In order to describe the horizontal displacement w_x and the rotation ϕ_y of the rigid surface S , it is necessary to define a few terms. First, consider a discretization of the surface S into M concentric annular disc elements. In the set of M annular surfaces, consider the one represented by the index k ($k=1, M$), the inner and outer radii of which are s_{1k} and s_{2k} (Fig. 4.5). This surface is subjected to a uniformly distributed transverse load of unit intensity in the x direction. Consider another annular disc element i ($i=1, M$). The displacements of the central radius of i ($r_i=(s_{1i}+s_{2i})/2$) are taken to represent the whole element i . Due to this unit transverse load applied in the element k , the element i undergoes the combined effect of a transverse displacement denominated $u_{zx}(r_i, s_{1k}, s_{2k}, \omega)$ and a vertical displacement denominated $u_{xx}(r_i, s_{1k}, s_{2k}, \omega)$ (Fig. 4.5).

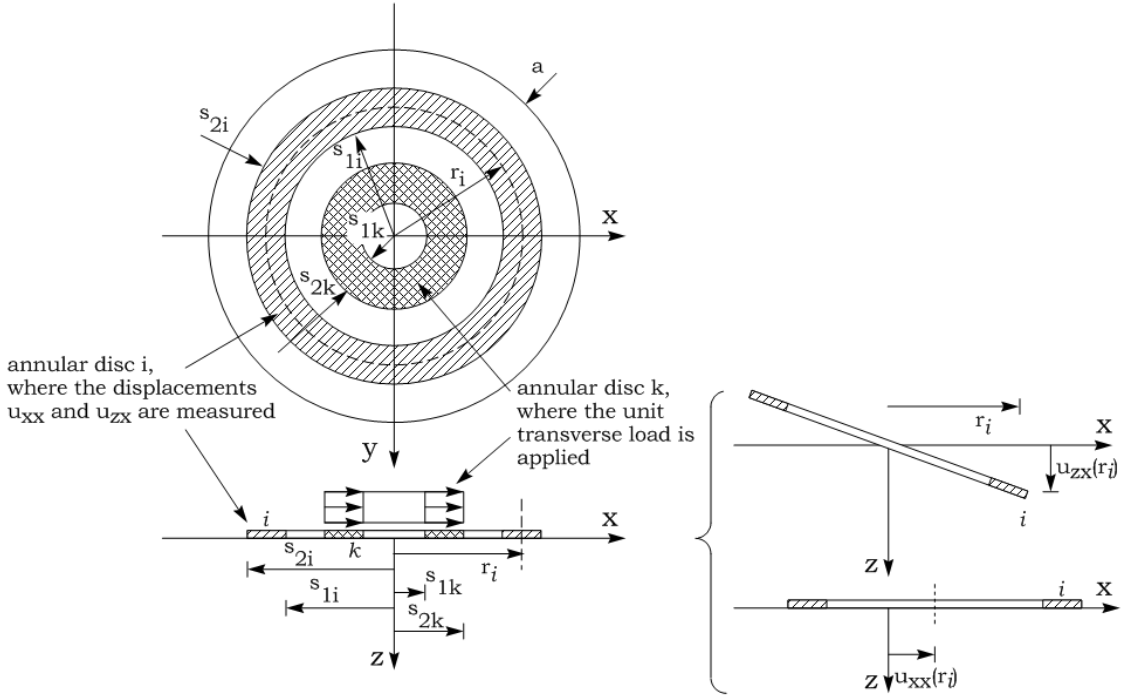


Figure 4.5 Illustration of the terms of transverse and vertical displacement u_{xx} and u_{zx} due to a uniformly distributed transverse load of unit intensity.

On the other hand, consider that the surface of the element k is subjected to a non-axisymmetric vertical load, the intensity of which varies as illustrated in Fig. 2.8, while presenting unit intensity at the point of coordinates $(x=s_{2k}, y=0)$. Due to this antisymmetric vertical load applied in the element k , the element i undergoes the combined effect of a transverse

displacement denominated $v_{xz}(r_i, s_{1k}, s_{2k}, \omega)$ and a vertical displacement denominated $v_{zz}(r_i, s_{1k}, s_{2k}, \omega)$ (Fig. 4.6).

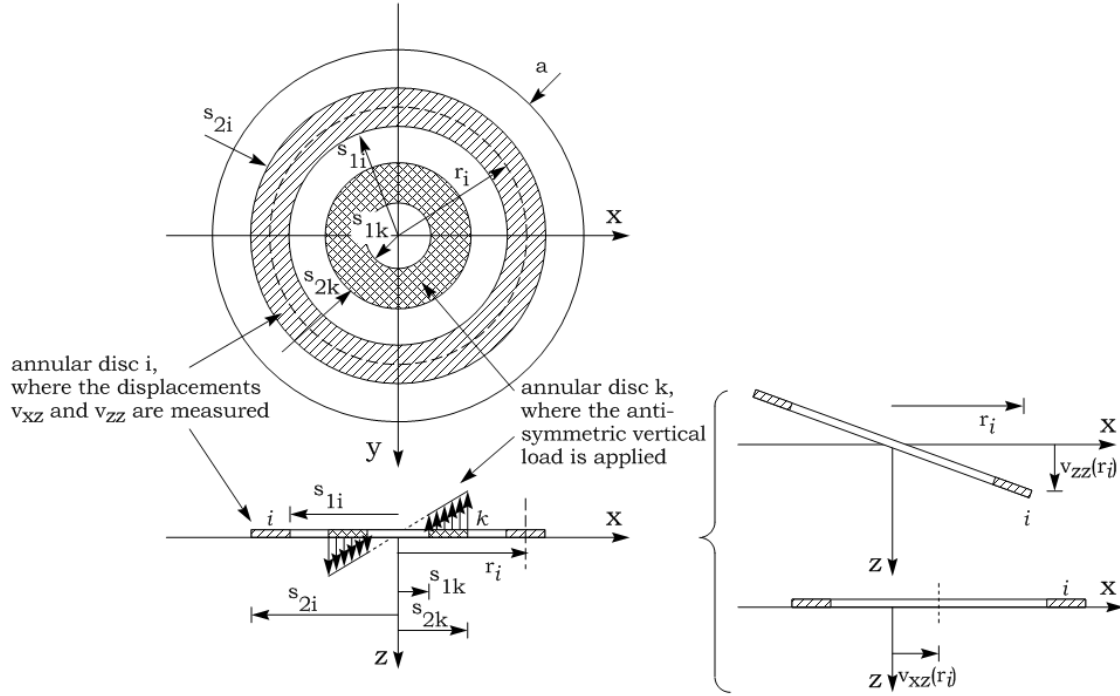


Figure 4.6 Illustration of the terms of transverse and vertical displacement v_{xz} and v_{zz} due to a non-axisymmetric vertical load.

In this work, the letter v is used instead of u in the notation $v_{pz}(r_i, s_{1k}, s_{2k}, \omega)$ ($p=x, z$) to emphasize that these displacements are due to a vertical load that is antisymmetric, as opposed to the displacements $u_{zz}(r_i, s_{1k}, s_{2k}, \omega)$ in Eq. 4.2, which are due to a vertical load that is axisymmetric.

The derivation of all these displacement components is described in the previous chapter. The transverse displacements $u_{xx}(r_i, s_{1k}, s_{2k}, \omega)$ and $v_{xz}(r_i, s_{1k}, s_{2k}, \omega)$ for $y=0$ correspond to the radial displacements $u_{rz}(r_i, s_{1k}, s_{2k}, \omega)$ and $v_{rz}(r_i, s_{1k}, s_{2k}, \omega)$ from Eqs. 2.63 and 2.65 for $\theta=0$.

The vertical and transverse loads to which the element k is subject in a given problem are not necessarily unitary, but they may have unknown values denoted by $t_x(r_k)$ and $t_z(r_k)$. In order to obtain the displacement and rotation $w_x(r_i)$ and $\phi_y(r_i)$ that each annular surface i actually experiences, the displacements and rotations u_{px} and v_{pz} ($p=x, z$) due to unit loads in all other

annular surfaces k ($k=1,M$) must be taken into consideration, after weighed by their respective unknown traction jumps $t_x(r_k)$ and $t_z(r_k)$. This is stated mathematically as:

$$\sum_{k=1}^M u_{zx}(r_i, s_{1k}, s_{2k}, \omega) t_x(r_k, \omega) = w_z^x(r_i) = \phi_y^x(r_i) \cdot r_i \quad (4.7)$$

$$\sum_{k=1}^M v_{zz}(r_i, s_{1k}, s_{2k}, \omega) t_z(r_k, \omega) = w_z^y(r_i) = \phi_y^y(r_i) \cdot r_i \quad (4.8)$$

$$\sum_{k=1}^M u_{xx}(r_i, s_{1k}, s_{2k}, \omega) t_x(r_k, \omega) = w_x^x(r_i) \quad (4.9)$$

$$\sum_{k=1}^M v_{xz}(r_i, s_{1k}, s_{2k}, \omega) t_z(r_k, \omega) = w_x^y(r_i) \quad (4.10)$$

In Eqs. 4.7 to 4.10, it is assumed that the problem has symmetry about the x - z plane, which implies that the resulting moment acts about the y -axis.

For small rotations of each annular disc element i , its vertical displacement $w_z(r_i)$ can be written in terms of its rotation about the y -axis ϕ_y as shown in Eqs. 4.7 and 4.8. In Eqs. 4.7 and 4.8, $\phi_y^x(r_i)$ and $\phi_y^y(r_i)$ denote the rotation of the annular disc i ($i=1,M$) due respectively to the horizontal traction field $t_x(r_k)$ and antisymmetric vertical traction field $t_z(r_k)$. The total rotation $\phi_y(r_i)$ of the annular disc i is a combination of $\phi_y^x(r_i)$ and $\phi_y^y(r_i)$. In Eqs. 4.9 and 4.10, $w_x^x(r_i)$ and $w_x^y(r_i)$ denote the horizontal displacement of the annular disc i ($i=1,M$) due respectively to $t_x(r_k)$ and $t_z(r_k)$. The resulting horizontal displacement $w_x(r_i)$ of the annular disc i is a combination of $w_x^x(r_i)$ and $w_x^y(r_i)$.

Equations 4.7 to 4.10 result in the uncoupled displacements and rotations $w_x^x(r_i)$ and $w_x^y(r_i)$ and $\phi_y^x(r_i)$ and $\phi_y^y(r_i)$ of an arbitrary annular disc element i . They present M unknown tractions $t_x(r_k)$ and $t_z(r_k)$, which are the traction jumps in the transverse and vertical direction acting on all annular disc elements k ($k=1,M$). Equations 4.7 to 4.10 can be repeated for all annular discs $i=1,M$ resulting in four sets of M linear equations shown in Eqs. 4.11 to 4.14. From the hypothesis that the entire circular surface S behaves like a rigid disc, the horizontal displacements

and the rotations of all annular disc elements are the same, e.g., $w_x^x(r_i)=w_{0x}^x=1$ and $\phi_y^y(r_i)=\phi_{0y}^y=1$ ($i=1,M$).

$$\begin{bmatrix} u_{zx}^{1,1} & u_{zx}^{1,2} & & u_{zx}^{1,M} \\ u_{zx}^{2,1} & u_{zx}^{2,2} & & u_{zx}^{2,M} \\ & & \ddots & \\ u_{zx}^{M,2} & u_{zx}^{M,2} & & u_{zx}^{M,M} \end{bmatrix} \begin{Bmatrix} t_x(r_1, \omega) \\ t_x(r_2, \omega) \\ \vdots \\ t_x(r_M, \omega) \end{Bmatrix} = \begin{Bmatrix} \phi_y^x(r_1, \omega) r_1 = \phi_{0y}^x \cdot r_1 = r_1 \\ \phi_y^x(r_2, \omega) r_2 = \phi_{0y}^x \cdot r_2 = r_2 \\ \vdots \\ \phi_y^x(r_M, \omega) r_M = \phi_{0y}^x \cdot r_M = r_M \end{Bmatrix} \quad (4.11)$$

$$\begin{bmatrix} v_{zz}^{1,1} & v_{zz}^{1,2} & & v_{zz}^{1,M} \\ v_{zz}^{2,1} & v_{zz}^{2,2} & & v_{zz}^{2,M} \\ & & \ddots & \\ v_{zz}^{M,2} & v_{zz}^{M,2} & & v_{zz}^{M,M} \end{bmatrix} \begin{Bmatrix} t_z(r_1, \omega) \\ t_z(r_2, \omega) \\ \vdots \\ t_z(r_M, \omega) \end{Bmatrix} = \begin{Bmatrix} \phi_y^y(r_1, \omega) r_1 = \phi_{0y}^y \cdot r_1 = r_1 \\ \phi_y^y(r_2, \omega) r_2 = \phi_{0y}^y \cdot r_2 = r_2 \\ \vdots \\ \phi_y^y(r_M, \omega) r_M = \phi_{0y}^y \cdot r_M = r_M \end{Bmatrix} \quad (4.12)$$

$$\begin{bmatrix} u_{xx}^{1,1} & u_{xx}^{1,2} & & u_{xx}^{1,M} \\ u_{xx}^{2,1} & u_{xx}^{2,2} & & u_{xx}^{2,M} \\ & & \ddots & \\ u_{xx}^{M,2} & u_{xx}^{M,2} & & u_{xx}^{M,M} \end{bmatrix} \begin{Bmatrix} t_x(r_1, \omega) \\ t_x(r_2, \omega) \\ \vdots \\ t_x(r_M, \omega) \end{Bmatrix} = \begin{Bmatrix} w_x^x(r_1, \omega) = w_{0x}^x = 1 \\ w_x^x(r_2, \omega) = w_{0x}^x = 1 \\ \vdots \\ w_x^x(r_M, \omega) = w_{0x}^x = 1 \end{Bmatrix} \quad (4.13)$$

$$\begin{bmatrix} v_{xz}^{1,1} & v_{xz}^{1,2} & & v_{xz}^{1,M} \\ v_{xz}^{2,1} & v_{xz}^{2,2} & & v_{xz}^{2,M} \\ & & \ddots & \\ v_{xz}^{M,2} & v_{xz}^{M,2} & & v_{xz}^{M,M} \end{bmatrix} \begin{Bmatrix} t_z(r_1, \omega) \\ t_z(r_2, \omega) \\ \vdots \\ t_z(r_M, \omega) \end{Bmatrix} = \begin{Bmatrix} w_x^y(r_1, \omega) = w_{0x}^y = 1 \\ w_x^y(r_2, \omega) = w_{0x}^y = 1 \\ \vdots \\ w_x^y(r_M, \omega) = w_{0x}^y = 1 \end{Bmatrix} \quad (4.14)$$

in which

$$u_{px}^{i,k} = u_{px}(r_i, s_{1k}, s_{2k}, \omega), \quad p=x,z; \quad i,k=1,M \quad (4.15)$$

and

$$v_{pz}^{i,k} = v_{pz}(r_i, s_{1k}, s_{2k}, \omega), \quad p=x,z; \quad i,k=1,M \quad (4.16)$$

Equations 4.11 to 4.14 are solved for the horizontal and antisymmetric vertical traction jumps acting on each disc element. The total horizontal force acting on the circular surface S is given by:

$$F_x(\omega) = \sum_{k=1}^M A_k t_x(r_k, \omega) = \sum_{k=1}^M \pi (s_{2k}^2 - s_{1k}^2) t_x(r_k, \omega) \quad (4.17)$$

in which A_k is the area of the annular disc element k .

As for the expression of the total moment acting on the circular surface S , recall that the intensity of the distributed antisymmetric vertical traction jump $t_z(r, \theta)$ was assumed to vary linearly with the x -coordinate (Fig. 2.8d). Its intensity is t_{z0} in the outermost radius a of the disc, i.e.,

$$t_z(r, \theta) = t_{z0} \cdot x/a = t_{z0} \cdot r \cos(\theta)/a \quad (4.18)$$

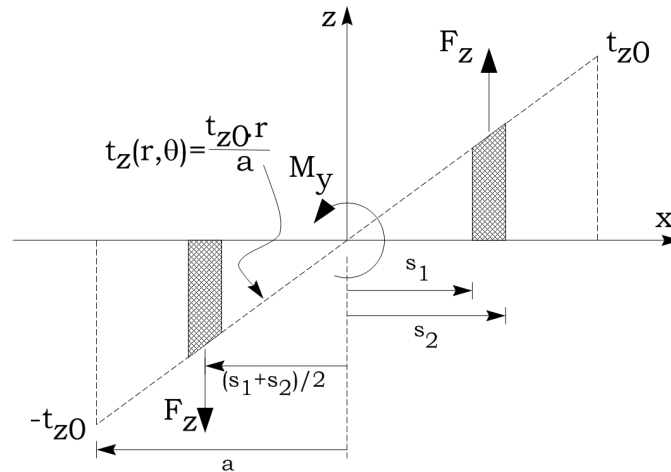


Figure 4.7 Scheme of forces and moments resulting from the antisymmetric traction t_z .

The application of this traction on an infinitesimal annular area dA results in an infinitesimal force dF_z , which in turn results in an infinitesimal moment dM_y acting about the y -axis (Fig. 4.7):

$$dM_y = dF_z \cdot x = [t_z(r, \theta) dA] \cdot x = [t_z(r, \theta) dA] \cdot [r \cos(\theta)] \quad (4.19)$$

Consider one annular disc element k ($k=1,M$) with inner and outer radii s_{1k} and s_{2k} . The intensity of $t_z(r,\theta)$ is $t_z(r_k,\omega)$ and it comes from the solution of Eq. 4.12 in the case of unit rigid rotation or from Eq. 4.14 in the case of unit horizontal displacement. Let the point of coordinate $r_k=(s_{1k}+s_{2k})/2$ be taken to represent this element k . Then, from Eq. 4.18, it comes

$$t_z(r,\theta) = t_z(r_k,\theta) \left(\frac{s_{1k} + s_{2k}}{2} \right) \cos(\theta) / a \quad (4.20)$$

The total moment M_{yk} acting on the element k about the y -axis is obtained upon integration of Eq. 4.19 over the area of the annular disc element:

$$\begin{aligned} M_{yk} &= \int_{A_k} dM_{yk} = \int_{A_k} \left[t_z(r_k,\omega) \left(\frac{s_{1k} + s_{2k}}{2} \right) \cos(\theta) / a \right] [r \cos(\theta)] dA_k \\ &= \frac{t_z(r_k,\omega)}{a} \left(\frac{s_{1k} + s_{2k}}{2} \right) \int_0^{2\pi} \int_{s_{1k}}^{s_{2k}} r \cos^2(\theta) dr d\theta = \frac{\pi}{2a} \left(\frac{s_{1k} + s_{2k}}{2} \right) (s_{2k}^2 - s_{1k}^2) t_z(r_k,\omega) \end{aligned} \quad (4.21)$$

The total moment acting on the entire circular surface S is obtained by considering the contribution of each annular disc element:

$$M_y(\omega) = \sum_{k=1}^M \frac{\pi}{4a} (s_{2k} + s_{1k}) (s_{2k}^2 - s_{1k}^2) t_z(r_k,\omega) \quad (4.22)$$

The transverse and rocking dynamic compliances of the system comprising the two media and the embedded rigid surface are defined for each frequency as:

$$C_{XX}(\omega) = w_{0x}^x a \mu / F_x(\omega) \quad (4.23)$$

$$C_{XM}(\omega) = w_{0x}^x a^2 \mu / M_y(\omega) \quad (4.24)$$

$$C_{MX}(\omega) = \phi_{0y}^x a^2 \mu / F_x(\omega) \quad (4.25)$$

$$C_{MM}(\omega) = \phi_{0y}^y a^3 \mu / M_y(\omega) \quad (4.26)$$

In Eqs. 4.23 and 4.24, $C_{XX}(\omega)$ and $C_{XM}(\omega)$ are compliances which correspond to the kinematic effect of rigid horizontal displacements due to horizontal loads and rocking moments, respectively. Conversely, in Eqs. 4.25 and 4.26, $C_{MX}(\omega)$ and $C_{MM}(\omega)$ are compliances which correspond to the kinematic effect of rigid rotations due to horizontal loads and rocking moments, respectively. ϕ_{0y}^x and ϕ_{0y}^y are the rotations of each of the annular disc elements, which in these particular kinematic problems are all set to be unitary (Eqs. 4.11 and 4.12). w_{0x}^x and w_{0x}^y are the displacement of each of the annular disc elements, which are all set to be unitary (Eqs. 4.13 and 4.14). $F_x(\omega)$ is the total dynamic force (Eq. 4.17) acting on the surface S, in the horizontal direction, which causes the annular disc elements to be displaced by $w_{0x}^x=1$ or rotate by $\phi_{0y}^x=1$. $M_y(\omega)$ is the total rocking moment (Eq. 4.22) acting on the surface S, about the y-axis, which causes the annular disc elements to be displaced by $w_{0x}^y=1$ or rotate by $\phi_{0y}^y=1$. All four compliance terms in this work are defined in their normalized form. In Eqs. 4.23 to 4.26, μ is Lamé's constant of one of the two materials of the interface (Fig. 4.1), and a is the outer radius of the rigid surface S.

$C_{XX}(\omega)$ and $C_{MM}(\omega)$ are known as *direct* compliance terms, since they relate horizontal displacements to horizontal loads and rotations to rocking moments. On the other hand, $C_{XM}(\omega)$ and $C_{MX}(\omega)$ are known as *cross* compliance terms, because they relate horizontal displacements with rocking moments and vice-versa. It has been observed that cross compliances are symmetric quantities, i.e., $C_{XM}(\omega)=C_{MX}(\omega)$ (Mesquita, 1989; Barros, 2006). In a problem in which both media 1 and 2 (Fig. 4.1) have the same geometry and material properties, the traction fields on the top and bottom faces of the surface S are balanced. In that case, the only nonzero compliance terms are the direct ones, $C_{XX}(\omega)$ and $C_{MM}(\omega)$. In any case, the resulting displacement $w_x(\omega)$ and rotation $\phi_y(\omega)$ of the surface under horizontal forces $F_x(\omega)$ and rocking moments $M_y(\omega)$ are:

$$\begin{bmatrix} C_{XX}(\omega) & C_{XM}(\omega) \\ C_{MX}(\omega) & C_{MM}(\omega) \end{bmatrix} \begin{Bmatrix} F_x(\omega) \\ M_y(\omega) \end{Bmatrix} = \begin{Bmatrix} w_x(\omega) \\ \phi_y(\omega) \end{Bmatrix} \quad (4.27)$$

The vibratory response of embedded plates is sometimes presented in terms of the stiffness of the problem, such as shown in Eqs. 4.28. The cross stiffness terms $K_{XM}(\omega)$ and $K_{MX}(\omega)$ are symmetric as well.

$$\begin{Bmatrix} F_x(\omega) \\ M_y(\omega) \end{Bmatrix} = \begin{bmatrix} K_{XX}(\omega) & K_{XM}(\omega) \\ K_{MX}(\omega) & K_{MM}(\omega) \end{bmatrix} \begin{Bmatrix} w_x(\omega) \\ \phi_y(\omega) \end{Bmatrix} = \begin{bmatrix} C_{XX}(\omega) & C_{XM}(\omega) \\ C_{MX}(\omega) & C_{MM}(\omega) \end{bmatrix}^{-1} \begin{Bmatrix} w_x(\omega) \\ \phi_y(\omega) \end{Bmatrix} \quad (4.28)$$

Table 4.1 summarizes the compliance terms presented in sections 4.3 and 4.4. A brief summary of the compliance terms defined in these sections, as well as of the assumed physical hypotheses is:

a) $C_{ZZ}(\omega)$ is the vertical dynamic compliance, corresponding to axisymmetric vertical displacements in response to axisymmetric vertical loads;

b) $C_{XX}(\omega)$ is the direct transverse dynamic compliance, corresponding to horizontal displacements in response to horizontal loads;

c) $C_{MM}(\omega)$ is the direct rocking compliance, corresponding to rotations in response to concentrated moments;

d) The cross compliance terms $C_{XM}(\omega)$ and $C_{MX}(\omega)$ correspond respectively to horizontal displacements due to concentrated moments, and rotation due to horizontal loads;

e) In this work, it is assumed that the axisymmetric vertical displacement due to horizontal and antisymmetric vertical loads (concentrated moment) is negligible, hence the cross compliance terms $C_{ZX}(\omega)$ and $C_{ZM}(\omega)$ are zero;

f) Correspondingly, because of the symmetry that is observed in cross compliance terms, the cross compliances $C_{XZ}(\omega)$ and $C_{MZ}(\omega)$ are also zero;

g) In the particular case in which the media on top and bottom faces of the rigid surface S have equal geometrical and material properties, all cross compliance terms are zero, including $C_{MX}(\omega)$ and $C_{XM}(\omega)$.

Table 4.1 Summary of the terms of direct and cross compliance presented in this chapter.

Kinematic response	Axisymmetric vertical loads	Transverse loads	Concentrated moments
w_z	$C_{ZZ}(\omega) = \frac{w_{0z} a E}{F_z(\omega)}$	$C_{ZX}(\omega) = 0$	$C_{ZM}(\omega) = 0$
w_x	$C_{XZ}(\omega) = 0$	$C_{XX}(\omega) = \frac{w_{0x}^x a \mu}{F_x(\omega)}$	$C_{XM}(\omega) = \frac{w_{0x}^x a^2 \mu}{M_y(\omega)}$
ϕ_y	$C_{MZ}(\omega) = 0$	$C_{MX}(\omega) = \frac{\phi_{0y}^x a^2 \mu}{F_x(\omega)}$	$C_{MM}(\omega) = \frac{\phi_{0y}^y a^3 \mu}{M_y(\omega)}$

4.5 Validation

In the present chapter, the behavior of rigid circular plates under time-harmonic excitations is studied. Excitations in the vertical and transverse directions are considered, as well as rocking moments about the y-axis. Deep embedment of the rigid plate can be modeled by considering that the plate is placed within two unbounded transversely isotropic half-spaces. The model of such bi-material interfaces has been derived in Chapter 2. Shallow embedments of the plate can be represented by considering that the plate is placed within a layered transversely isotropic half-space. The model of layered media has been presented in Chapter 3.

In this section, the model of embedded rigid plates presented in this chapter is compared with existing solutions available in the literature. Pak and Gobert (1992) presented results comprising the vertical vibration of rigid plates at different embedments on isotropic half-spaces. Luco and Westmann (1971) presented solutions for the transverse and rocking vibrations of rigid plates resting on the surface of an isotropic half-space. There are presently no solutions available regarding transverse and rocking vibrations of rigid plates on full-spaces, which is why the present solutions can be compared only qualitatively with those of Luco and Westmann (1971).

Besides these sources, the static solutions provided by Selvadurai and Singh (1984) and Selvadurai (1980) are used to study the convergence of the present solutions with increasing discretization.

4.5.1 Numerical implementation and convergence

The hardest computational task which arises in the solution of the embedded plate comes from the numerical integration of u_{ij} ($i,j=r,\theta,z$) from Eq. 2.63. The same holds for the model of flexible plate formulated in the next chapter. Synge (1957) studied the propagation of Rayleigh waves in transversely isotropic media and proved that Rayleigh waves exist only if the free surface of the material is parallel or perpendicular to the material plane of isotropy. Since this is the case in the present construction of bi-material interface (Fig. 2.2), in which the two unbounded half-spaces are bonded through their plane of isotropy, the configurations of interfacing unbounded half-spaces in this work are characterized by the existence of Rayleigh waves, which possess a finite number of singularities to be integrated (Graff, 1974). Moreover, according to Stoneley (1924), the configuration of two interfacing layers of finite thickness (Fig. 3.1) is characterized by the existence of interface waves, which possess an infinite number of singularities to be integrated (Graff, 1974). In the present implementation, however, no special attention is given to the implementation of integration methods or to the behavior of the integrand. A numerical solver of improper integrals, based on globally adaptive quadratures, which is freely available in numerical packages of the Fortran programming language, is used for this purpose (Piessens, Doncker-Kapenga and Überhuber, 1983). The issue of the singularities is avoided by the inclusion of a small damping in all the material constants according to Christensen's elastic-viscoelastic principle (Christensen, 2010). Equation 4.29 shows an example of the inclusion of the damping factor η in the material parameter c_{11} of a given medium. All other material parameters are defined in an analogous way. The same damping factor η is used in all material parameters.

$$c_{11}^* = c_{11}(1+i\cdot\eta) \quad (4.29)$$

In this work, a hysteretic damping model is implemented, in which the damping factor η is not frequency-dependent (Gaul, 1999).

Pak and Gobert (1992) presented an analytical solution for the static vertical compliance C'_{ZZ} of a rigid circular plate buried in an isotropic full-space (Fig 4.8). The corresponding

solutions for the transverse and rocking case, C'_{XX} and C'_{MM} , were presented by Selvadurai (1980) and Selvadurai and Singh (1984). Their solutions are given by:

$$C'_{ZZ} = \frac{3-4\nu}{64(1-\nu)\mu \cdot w_{0z}a} \quad (4.30)$$

$$C'_{XX} = \frac{7-8\nu}{64(1-\nu)\mu \cdot w_{0x}a} \quad (4.31)$$

$$C'_{MM} = \frac{3(3-4\nu)}{64(1-\nu)\mu \cdot \phi_{0y}a^3} \quad (4.32)$$

In Eqs. 4.30 to 4.32, ν and μ are respectively the Poisson's ratio and Lamé's constant of the isotropic medium, w_{0z} and w_{0x} are longitudinal displacements of the rigid plate in the z - and x -direction, respectively, while ϕ_{0y} is its rotation about the y -axis, and a is the outer radius of the plate.

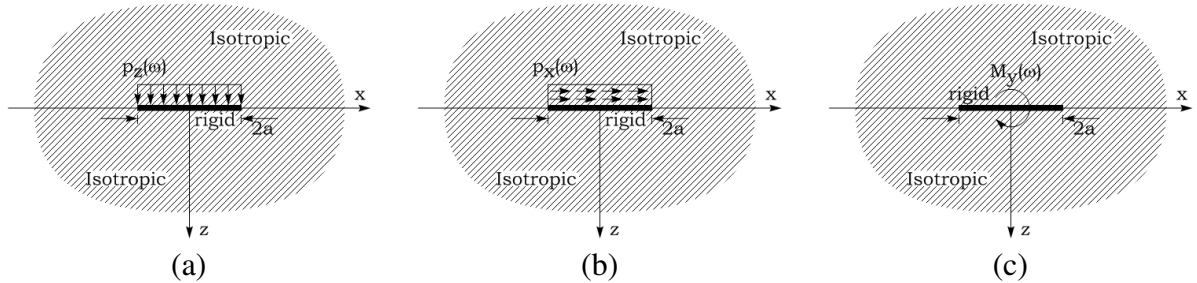


Figure 4.8 Illustrations of a rigid plate inside an isotropic full-space under (a) vertical, (b) transverse and (c) moment static loads.

Table 4.2 shows the error between these analytical solutions and the ones obtained by the present program, as well as the convergence of the present solution with increasing discretization M . In these results, the analytical solutions expressed by C'_{ZZ} , C'_{XX} and C'_{MM} were calculated from Eqs. 4.30 to 4.32 based on a homogeneous isotropic full-space with $\mu=1$ and $\nu=0.25$ containing a model of disc with $a=1$ and $w_{0z}=w_{0x}=\phi_{0y}=1$. The corresponding numerical solutions expressed by $C_{ZZ}(\omega=0)$, $C_{XX}(\omega=0)$ and $C_{MM}(\omega=0)$ were calculated according to Eqs. 4.6, 4.23 and 4.26 for the static case ($\omega=0$).

Table 4.2 Comparison of results with analytical solutions for the static problem.

M	$C_{ZZ}(\omega=0)/C'_{ZZ}$	$C_{XX}(\omega=0)/C'_{XX}$	$C_{MM}(\omega=0)/C'_{MM}$
5	1.03493353664750	1.034255919578913	0.99506657933933
10	1.01678531868697	1.015344450609305	1.00408812350261
20	1.00834989295149	1.006348607114810	1.00221378107221
35	1.00404587193815	1.001912669708005	1.00220942181645
50	1.00227108618090	1.000454275559764	1.00159966342978

The discretization of M=20 disc is chosen throughout this thesis, because it is enough to allow an error of less than 1% in comparison with the analytical solution.

4.5.2 Bi-material interface

4.5.2.1 Vertical vibrations

Figure 4.9 shows the solution of the normalized vertical compliance $C_{ZZ}(\omega)/C_{ZZ}(0)$ of a rigid plate obtained with the present implementation. The plate is placed at the interface of two isotropic half-spaces with Young's modulus $E=2.5$ and Poisson's ratio ν (Fig. 4.8a). These solutions are in agreement with the ones presented by Pak and Gobert (1992) for the embedment of a rigid plate at an infinite depth in an isotropic full-space.

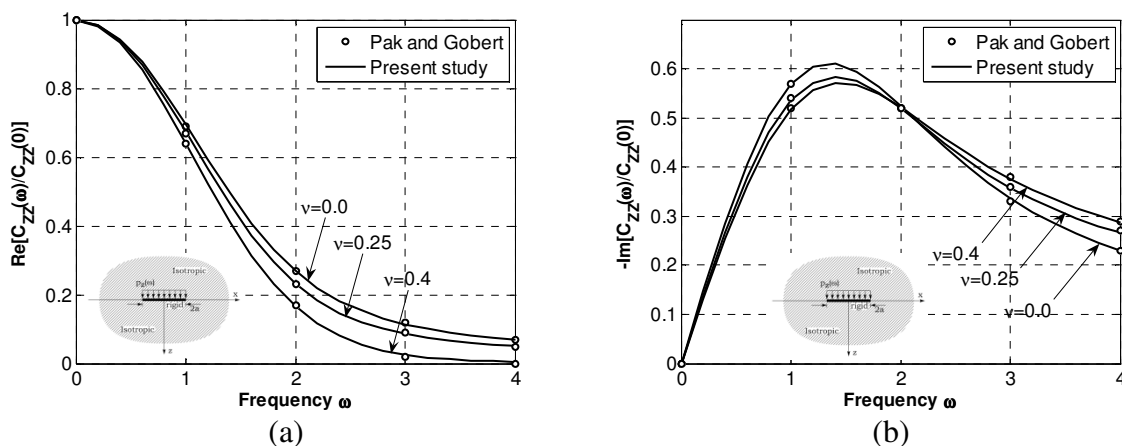


Figure 4.9 Normalized vertical compliance of a rigid plate on an isotropic full-space.

4.5.2.2 Transverse and rocking vibrations

The accuracy of the present implementation on the solution of the transverse and rocking vibration of the plate can be observed in Table 4.2 for the static case.

Figures 4.11 and 4.12 show the direct dynamic transverse and rocking compliance of a rigid plate the interface of two infinite isotropic half-spaces (Figs. 4.8b and 4.8c). The plate is discretized by $M=20$ annular disc elements and its outer radius is $a=1$. Its surrounding medium has material properties $E=2.5$ and $\nu=0.25$. The direct compliances C_{XX} and C_{MM} 4.11 and 4.12 are shown in terms of the normalized frequency $a_0=a \cdot \omega(\rho/c_{44})^{1/2}$.

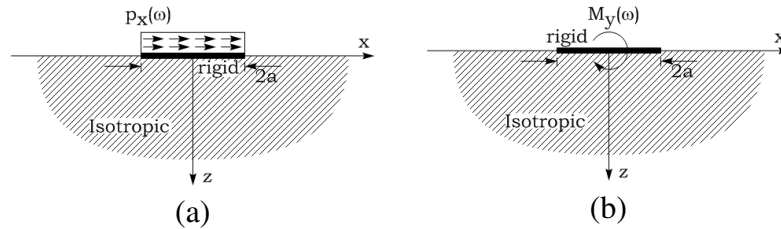


Figure 4.10 Configuration investigated by Luco and Westmann (1971) – rigid plate resting on the surface of an isotropic half-space under (a) transverse load and (b) rocking moment.

These results can be compared only qualitatively with those of a plate resting on the surface of an isotropic half-space provided by Luco and Westmann (1971) (Fig. 4.10).

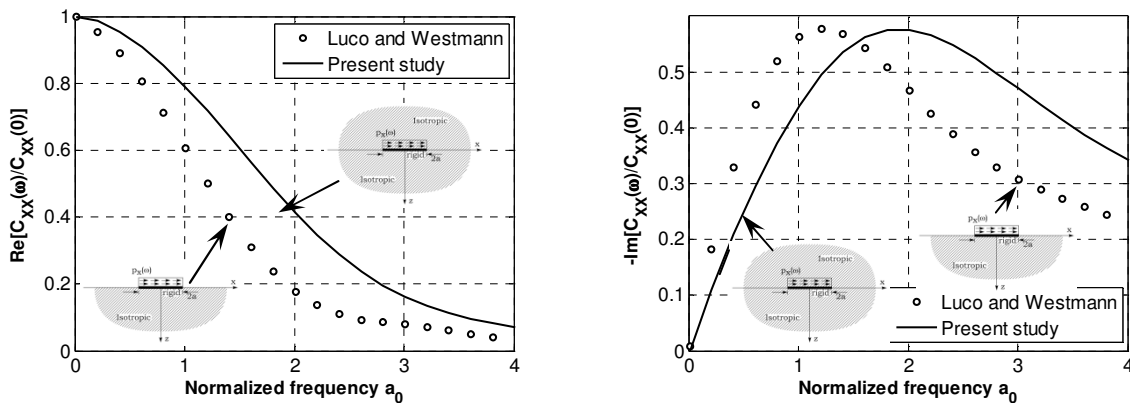


Figure 4.11 Normalized transverse compliance of a rigid plate on an isotropic full-space.

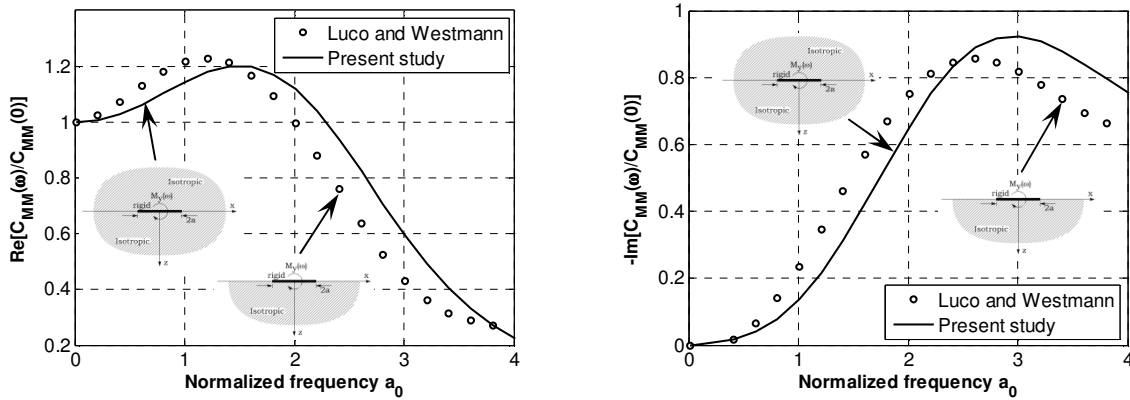


Figure 4.12 Normalized rocking compliance of a rigid plate on an isotropic full-space.

Eskandari-Ghadi, Mirzapour and Ardeshir-Behrestaghi (2011), in their study of the problem of rocking vibration of a rigid plate within bi-material interfaces, disregarded the fact that the transverse and rocking response of such plate is a coupled problem. Since this is a different hypothesis than the one used in this work (see Section 4.4), their results cannot be used as validation source of the cross compliance terms $C_{XM}(\omega)$ and $C_{MX}(\omega)$ formulated in the present work.

4.5.3 Multilayered medium

The present solution of rigid plates embedded in multilayered media can also make use of the work of Pak and Gobert (1992) as validation source.

Figure 4.13a illustrates the case of a rigid plate resting on the surface of an isotropic half-space, on top of which two layers of unit thickness $h_1=h_2=1$ are placed. The two layers and the underlying half-space have material properties $E=2.5$ and $\nu=0.25$. The plate is rigid and has unit outer radius ($a=1$). The normalized vertical dynamic compliance of this system is shown in Fig. 4.14. A discretization of $M=20$ annular disc elements was adopted in these results.

These results agree with the ones presented by Pak and Gobert (1992) regarding the vertical vibration of a rigid circular plate embedded at a depth $H/a=2$ inside an isotropic half-space (Fig. 4.13b).

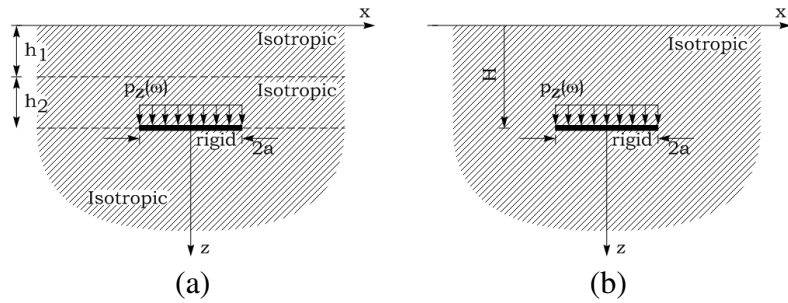


Figure 4.13 Configurations of a rigid plate subjected to vertical loads (a) between a half-space and two layers of the same material and (b) at an arbitrary embedment H inside a half-space.

The compliance shown in Fig. 4.14 is normalized by the vertical static compliance of a plate resting on the surface of the half-space, $C_{ZZ}^0(\omega=0)$, whose closed-form solution was derived by Pak and Gobert (1992).

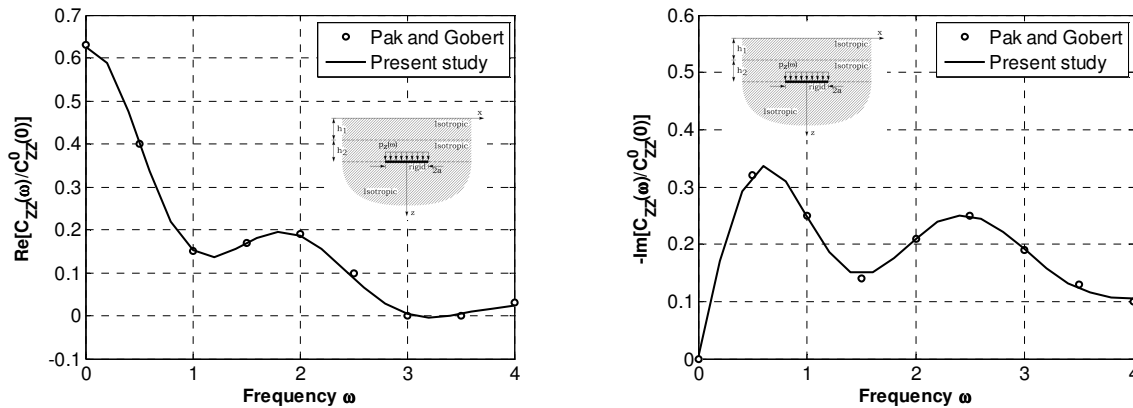


Figure 4.14 Normalized vertical dynamic compliance of a rigid plate between two isotropic layers of unit thickness and an isotropic half-space.

4.6 Numerical results

This section presents original results on the behavior of circular rigid plates obtained in this work. The influence of the inner radius in the vertical, transverse and rocking dynamic compliance of a rigid plate is presented. To isolate the effect of the inner radius, the plate is considered to be buried inside an isotropic full-space. The influence of the composition of bi-material interfaces on the behavior of the plate is also considered. The vertical, transverse and rocking compliances of a rigid plate are presented. Using the formulation of layered media presented in Chapter 3, the problem of a rigid plate at arbitrary embedments inside transversely

isotropic layered half-spaces is also studied. The last part of the section presents a study on the influence of the damping of the surrounding medium.

4.6.1 Influence of the inner radius

Consider the rigid annular plate depicted in Fig. 4.15, embedded at the interface of two infinite isotropic half-spaces. Both media 1 and 2 have Young’s modulus $E=2.5$ and Poisson’s ratio $\nu=0.25$. The inner and outer radii of the plate are b and a , respectively. Figures 4.16, 4.17 and 4.18 show respectively the vertical, transverse and rocking dynamic compliances of this plate for different ratios b/a . The compliances in these figures are calculated according to Eqs. 4.6, 4.23 and 4.26, and are normalized by the static compliances of each case ($C_{ii}(\omega=0)$; $i=Z,X,M$). In all cases, the plate has been discretized by $M=20$ concentric annular disc elements.

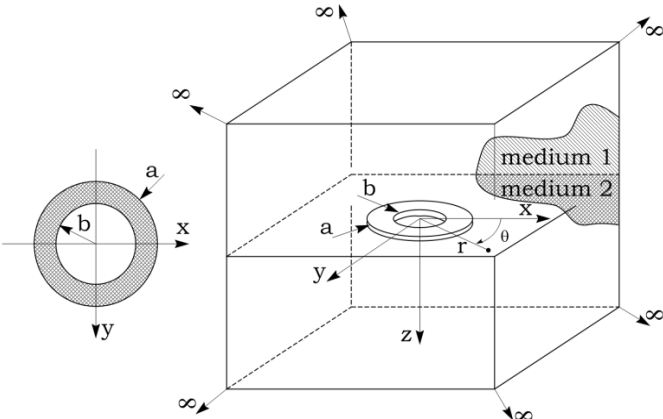


Figure 4.15 Annular plate embedded at the interface of two infinite half-spaces.

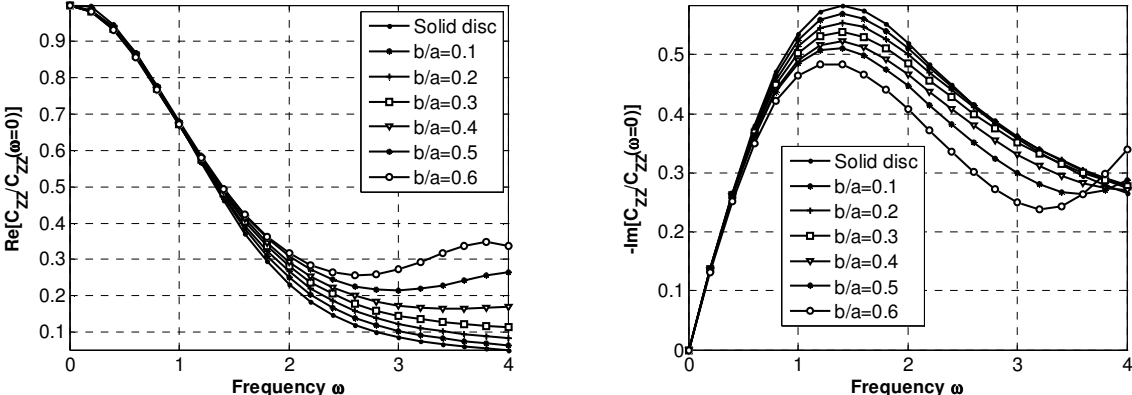


Figure 4.16 Influence of the inner radius b in the normalized compliance of the disc for the case of vertical load.

The case of solid disc ($b=0$) presented in Fig. 4.16 is the same as the one presented in Fig. 4.9, corresponding to the case of a solid disc buried in an unbounded isotropic medium with material properties $E=2.5$ and $\nu=0.25$. It can be seen from Fig. 4.16 that as the surface of the annular plate gets thinner (as b increases), the shape of the curve of normalized compliance differs significantly from that of the solid disc.

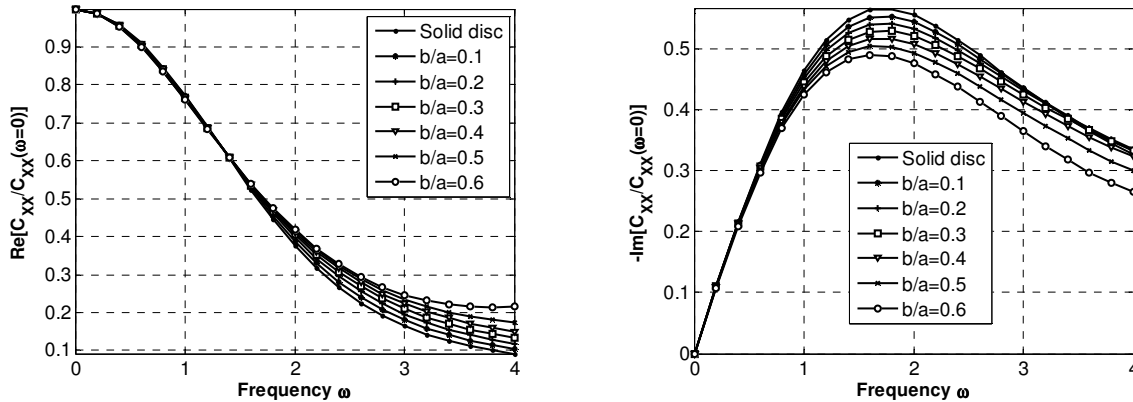


Figure 4.17 Influence of the inner radius b in the normalized compliance of the disc for the case of transverse load.

Both real and imaginary parts of the normalized transverse compliance $C_{XX}(\omega)$, however, suffer a visibly smaller influence of the inner radius than the vertical compliance $C_{ZZ}(\omega)$. This is observed comparing Figs. 4.16 and 4.17. Finally, it can be seen from Fig. 4.18 that the rocking compliance $C_{MM}(\omega)$ is the one that suffers the most the influence of the inner radius b .

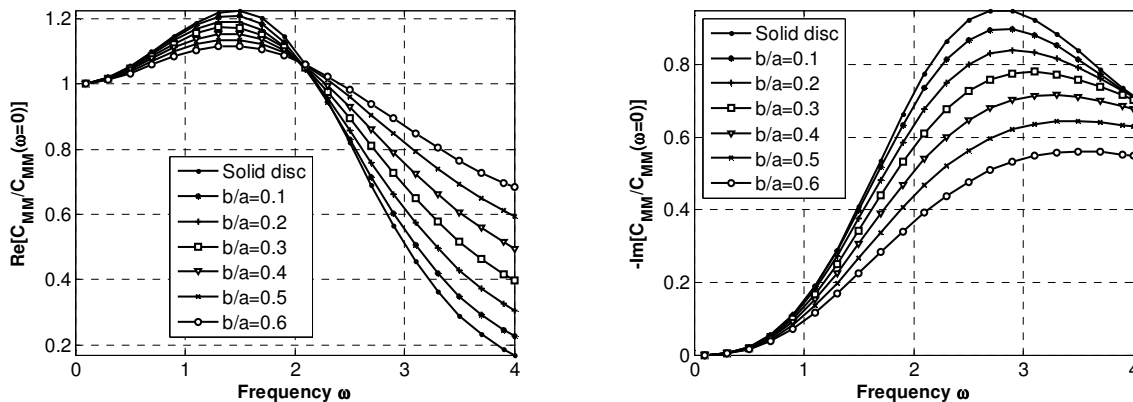


Figure 4.18 Influence of the inner radius b in the normalized compliance of the disc for the case of rocking moment.

4.6.2 Bi-material interface

This section investigates the effect of different bi-material configurations on the vibratory behavior of the rigid plate. Figure 4.19 illustrates the problems. The transversely isotropic materials used in these simulations are taken from Table 2.1, unless stated otherwise. The transverse isotropy of the materials are obtained by varying the anisotropy index n_1 while keeping $n_2=n_3=1$, $c_{44}=1$ and $\nu=0.25$ (Table 2.1). In all cases, the material of medium 2 has $n_1=n_2=n_3=1$, $c_{44}=1$ and $\nu=0.25$, which corresponds to an isotropic material (Table 2.1). All materials for medium 1 are picked from Table 2.1. The mass density of all materials is $\rho=1$ in all cases.

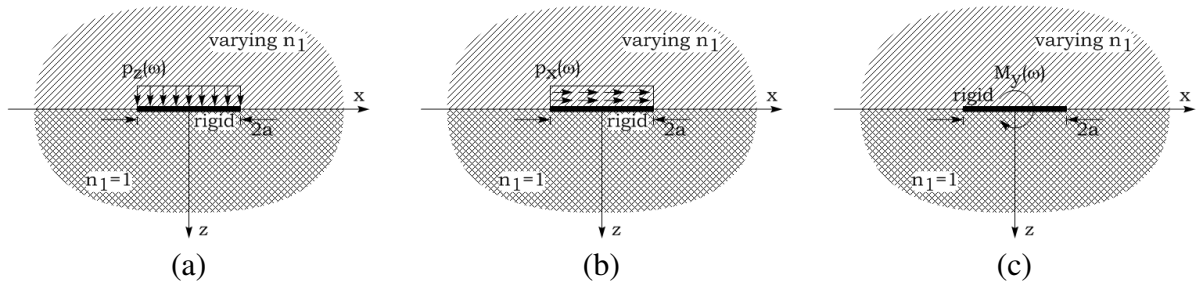


Figure 4.19 Illustration of different bi-material configurations with an embedded rigid plate subjected to (a) vertical and (b) transverse loads and (c) rocking moments.

Figures 4.20, 4.21 and 4.22 show respectively the direct vertical compliance $C_{ZZ}(\omega)$, the direct transverse compliance $C_{XX}(\omega)$ and the direct rocking compliance $C_{MM}(\omega)$. These compliances are determined according to Eqs. 4.6, 4.23 and 4.26, respectively. In all cases, a discretization of $M=20$ concentric annular disc elements was used.

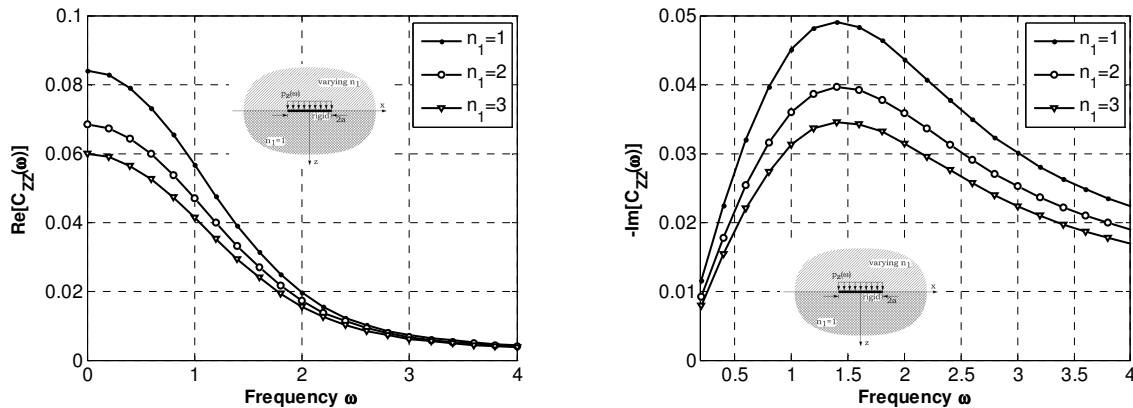


Figure 4.20 Vertical dynamic compliance of the rigid plate for different bi-material constructions. Medium 1 has anisotropy indices $n_2=n_3=1$.

It can be observed from Figs. 4.20 and 4.22 that increasing the anisotropy index n_1 of one of the materials of the bi-material interface has a very significant influence on the vertical and rocking compliances of the system.

It can be seen from Table 2.1 that if only the anisotropy index n_1 is changed, only the Young's modulus normal to the plane of isotropy, E_Z , and the Poisson's ratio ν_{ZX} are influenced. These are material properties related to the direction normal do the plane of isotropy of the transversely isotropic media. In the present problems, this direction corresponds to the vertical direction, since media 1 and 2 interface through their plane of isotropy (Figs. 4.15 and 4.19). The vertical and rocking compliances are intrinsically related to these material properties, because they involve respectively axisymmetric and antisymmetric displacements and loads in the vertical direction (Eqs. 4.6 and 4.26), which is the direction in which the material properties E_Z and ν_{ZX} change. Hence, these compliances are significantly influenced by changes in the index n_1 , even though $n_2=n_3=1$. Moreover, it can be observed that, as the increase of n_1 corresponds to a stiffening of medium 1 vertically by increasing E_Z , larger values of n_1 correspond to smaller amplitudes of these compliance terms (Figs. 4.20 and 4.22). This behavior is physically consistent.

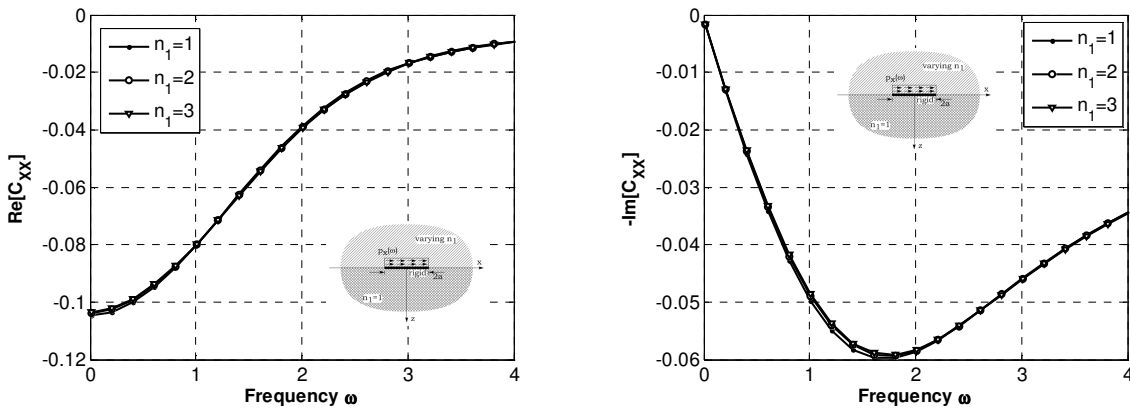


Figure 4.21 Transverse dynamic compliance of the rigid plate for different bi-material constructions. Medium 1 has anisotropy indices $n_2=n_3=1$.

Conversely, the direct transverse compliance $C_{XX}(\omega)$, shown in Fig. 4.21, presents negligible influence from the anisotropy index n_1 , for the case in which $n_2=n_3=1$. This happens because this compliance term relates pure transverse displacements on the plane of isotropy of

the transversely isotropic materials, with transverse loads applied on the same plane (Eq. 4.23). Since the material properties of that plane (E and ν) do not change with n_1 (Table 2.1), it is natural that the compliance $C_{XX}(\omega)$ is not influenced by changes solely in n_1 .

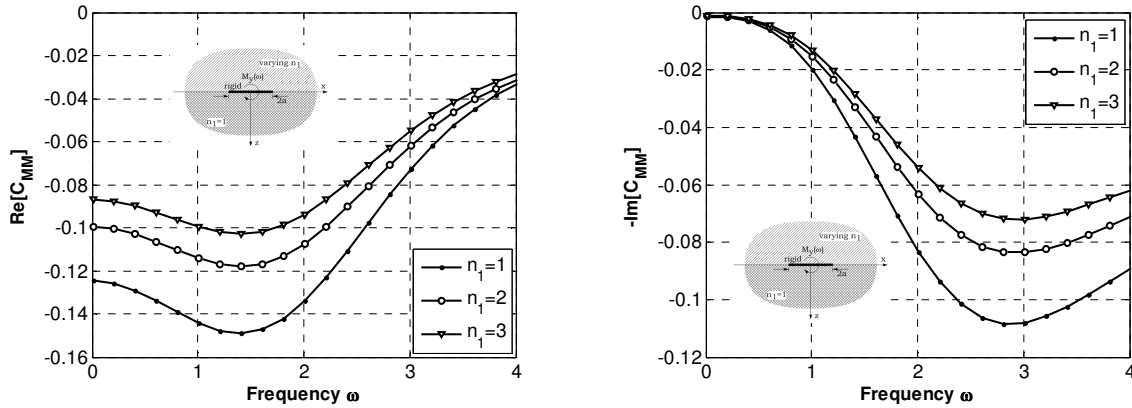


Figure 4.22 Rocking dynamic compliance of the rigid plate for different bi-material constructions. Medium 1 has anisotropy indices $n_2=n_3=1$.

In order to show this more clearly, consider a different bi-material configuration, in which not only n_1 , but all the anisotropy indices of medium 1 vary according to $n_1=n_2=n_3$, while $c_{44}=1$ and $\nu=0.25$ (Table 4.3). The material properties of medium 2 are $n_1=n_2=n_3=1$, $c_{44}=1$ and $\nu=0.25$ (isotropic material). All materials from Table 4.3 satisfy the constraints of Eq. 2.14.

Table 4.3 Transversely isotropic materials used in the results of Figs. 4.23 to 4.25.

n_1	n_2	n_3	c_{11}	c_{12}	c_{13}	c_{33}	E	E_z	ν	ν_{zx}
1	1	1	3.0000	1.0000	1.0000	3.0000	2.5	2.5000	0.25	0.2500
2	2	2	5.6254	1.6254	1.8127	11.2508	5.0	10.3444	0.25	0.2500
3	3	3	8.1727	2.1727	2.0576	24.5180	7.5	23.6996	0.25	0.1989
4	4	4	10.7784	2.7784	2.1946	43.1135	10.0	42.4030	0.25	0.1619

Figures 4.23 to 4.25 show the corresponding direct compliance terms. Notice that now, in these cases in which the material properties on the plane of isotropy (E and ν) also vary, there is a significant influence on the direct transverse compliance $C_{XX}(\omega)$ (Fig. 4.24). The curve in Fig. 4.24 corresponding to the isotropic material ($n_1=1$) evidently matches that from Fig. 4.21, and can be used as a reference. The direct vertical and rocking compliances $C_{ZZ}(\omega)$ and $C_{MM}(\omega)$ (Figs.

4.23 and 4.25) also present different results than those that were observed in Figs. 4.20 and 4.22. However, it is not easy to make a general remark regarding the specific influence of each of these anisotropy indices on the compliance terms, since their influence on the material properties of the medium vary so much. It is straightforward to see that an increase in the anisotropy index n_1 physically means that the material gets stiffer vertically than it is horizontally. This physical interpretation is lost when changes in the other anisotropy indices are made simultaneously.

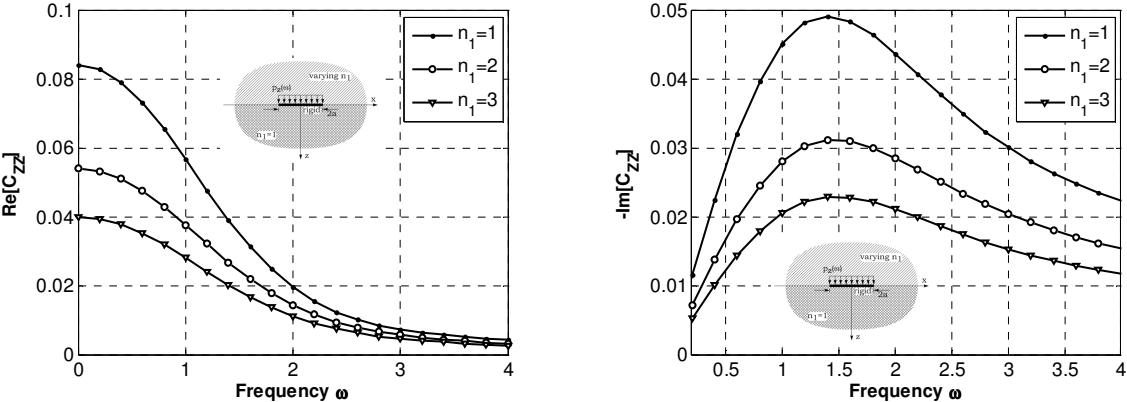


Figure 4.23 Vertical dynamic compliance of the rigid plate for different bi-material constructions. Medium 1 has anisotropy indices $n_1=n_2=n_3$.

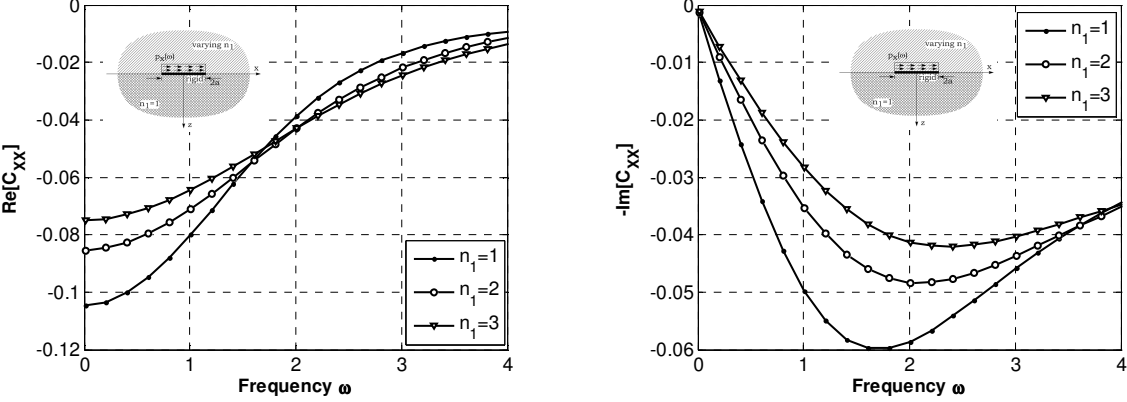


Figure 4.24 Transverse dynamic compliance of the rigid plate for different bi-material constructions. Medium 1 has anisotropy indices $n_1=n_2=n_3$.

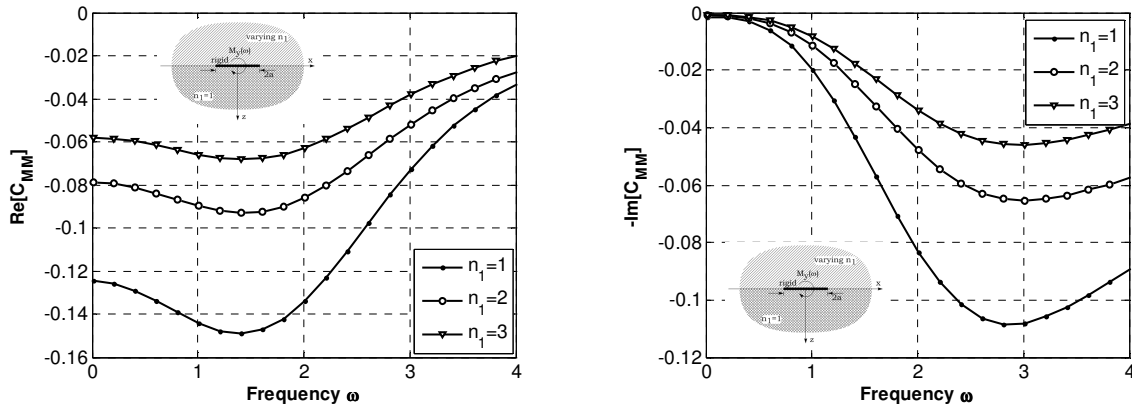


Figure 4.25 Rocking dynamic compliance of the rigid plate for different bi-material constructions. Medium 1 has anisotropy indices $n_1=n_2=n_3$.

Consider again the bi-material configurations described earlier, in which medium 1 has material properties $c_{44}=1$ and $\nu=0.25$, while its anisotropy indices are $n_2=n_3=1$ (Table 2.1). Medium 2 has material properties $c_{44}=1$ and $\nu=0.25$, while $n_1=n_2=n_3=1$ (isotropic material). These material properties are the same ones used in Figs. 4.20 to 4.22, and it was observed that the anisotropy index n_1 has negligible influence on the direct transverse compliance $C_{XX}(\omega)$ of the system rigid plate – surrounding medium. Observe, however, the influence of this anisotropy index on the cross compliance terms $C_{MX}(\omega)$ and $C_{XM}(\omega)$, which are shown in Figs. 4.26 and 4.27.

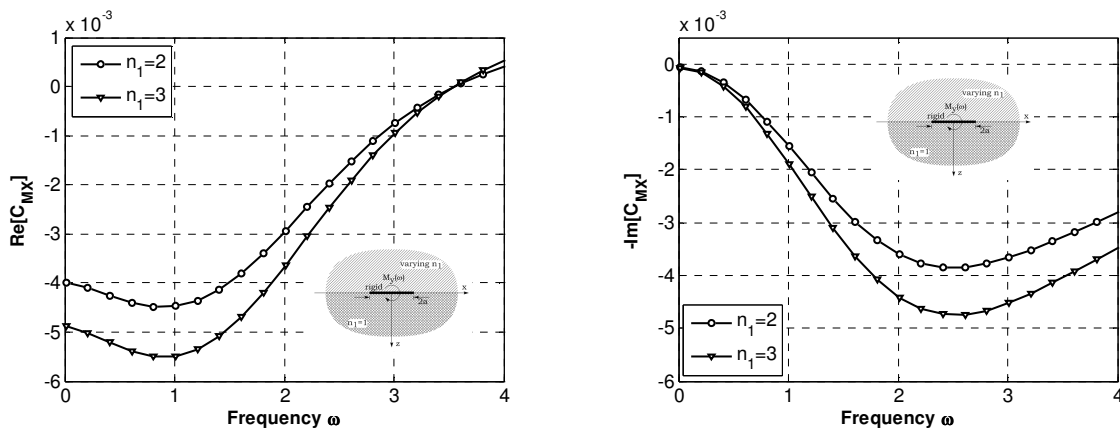


Figure 4.26 Cross compliance $C_{MX}(\omega)$ of the rigid plate for different bi-material constructions. Medium 1 has anisotropy indices $n_2=n_3=1$.

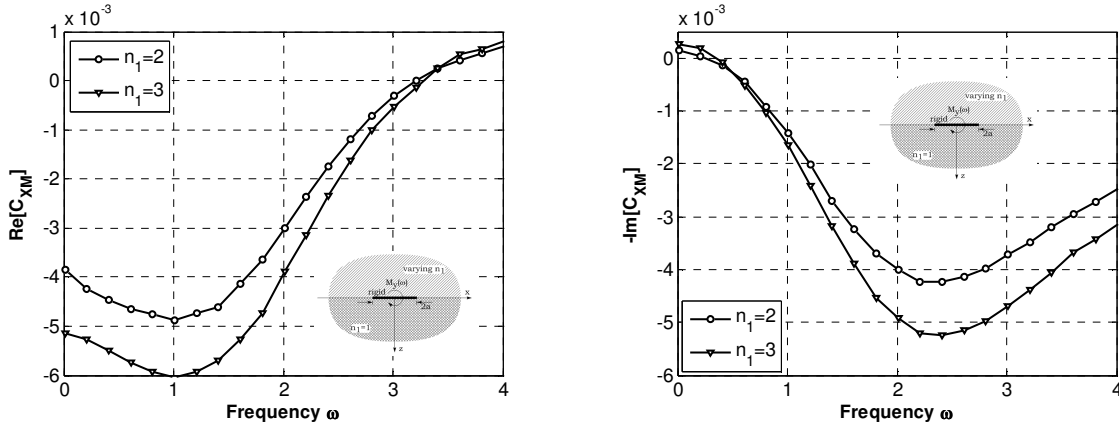


Figure 4.27 Cross compliance $C_{XM}(\omega)$ of the rigid plate for different bi-material constructions. Medium 1 has anisotropy indices $n_2=n_3=1$.

Consider the case of the cross compliance term $C_{MX}(\omega)$ (Fig. 4.26). It comprises the influence of transverse loads to rigid rotations (Eq. 4.25). Such transverse loads are applied on the plane of isotropy. The material properties on the plane of isotropy are E and ν , which do not vary in the two cases shown in Fig. 4.26. Nevertheless, there is a significant difference in the two curves of $C_{MX}(\omega)$. This difference comes from the fact that the transverse and rocking behaviors of the embedded plate, in this bi-material case, are coupled, and it is a reasonable justification of why the cross compliance terms must also be taken into consideration in the cases of bi-material interfaces. An analogous but somewhat more complicated interpretation holds for the cross compliance term $C_{XM}(\omega)$ (Fig. 4.27).

Notice that the amplitudes of the cross compliance terms $C_{MX}(\omega)$ and $C_{XM}(\omega)$ are much smaller than their direct compliance counterparts $C_{XX}(\omega)$ and $C_{MM}(\omega)$. This happens simply because the horizontal displacement of the plate due to a unit horizontal load (C_{XX}) is much larger than its rotation due to a unit horizontal load (C_{MX}). Analogously, the rotation of the plate due to a unit concentrated moment (C_{MM}) is much larger than its horizontal displacement due to a unit concentrated moment (C_{XM}).

4.6.3 Multilayered system

In this section, the problem of vertical vibrations of a rigid plate embedded in layered media is studied. Three different layered systems are considered (Fig. 4.28 and Tables 4.4 and

4.5). In all cases, the plate is embedded between two layers of thickness h_i ($i=1,2$) and a half-space. In all cases, the layers and the half-space have $c_{44}=1$ and $\nu=0.25$, while their other properties are obtained by varying the anisotropy index n_1 . The other anisotropy indices are $n_2=n_3=1$. The material of the layers and their thicknesses in each case are shown in Table 4.4. The material properties of materials m_1 , m_2 and m_3 are shown in Table 4.5. The mass density of all materials is $\rho=1$ in all cases.

Table 4.4 Multilayered media configurations used in this section.

Layer	Case A	Case B	Case C
1	Material m_1 ; $h_1=0.5$	Material m_3 ; $h_1=0.5$	Material m_3 ; $h_1=0.3$
2	Material m_1 ; $h_2=0.5$	Material m_2 ; $h_2=0.5$	Material m_2 ; $h_2=0.7$
half-space	Material m_1 ; $h_3=\infty$	Material m_1 ; $h_3=\infty$	Material m_1 ; $h_3=\infty$

Table 4.5 Material properties used in this section.

Material	n_1	n_2	n_3	c_{11}	c_{12}	c_{13}	c_{33}	E	E_Z	ν_Z
m_1	1.0	1.0	1.0	3.0000	1.0000	1.0000	3.0000	2.5	2.5000	0.2500
m_2	1.5	1.0	1.0	2.8284	0.8284	0.8284	4.2426	2.5	3.8673	0.2265
m_3	2.0	1.0	1.0	2.7749	0.7749	0.7749	5.5497	2.5	5.2114	0.2183

(*) for all materials, $c_{44}=1.0$, $\nu=0.25$ and $\rho=1$.

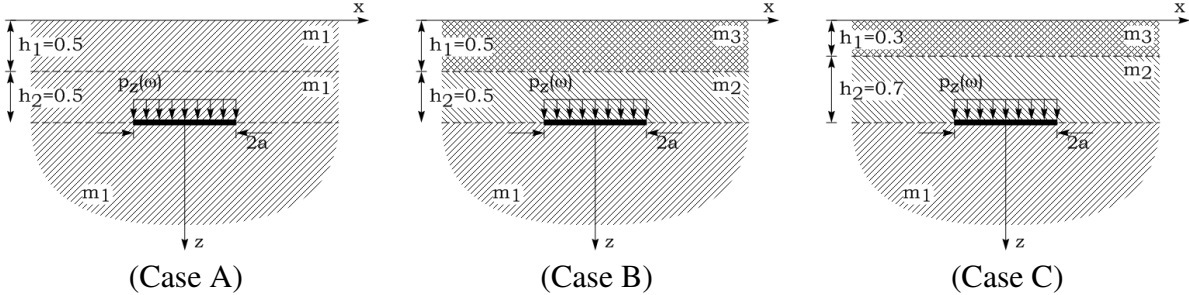


Figure 4.28 Illustration of different layered system configurations with an embedded plate subjected to vertical loads.

It can be observed from Fig. 4.29 that, for the material configurations chosen, there is a significant change in the vertical compliance of the system when the materials of the layers are

changed altogether (Case A versus Cases B and C). The difference is less noticeable when the relative thickness of the layers changes, but the material composition of the layers is the same (Case B versus Case C).

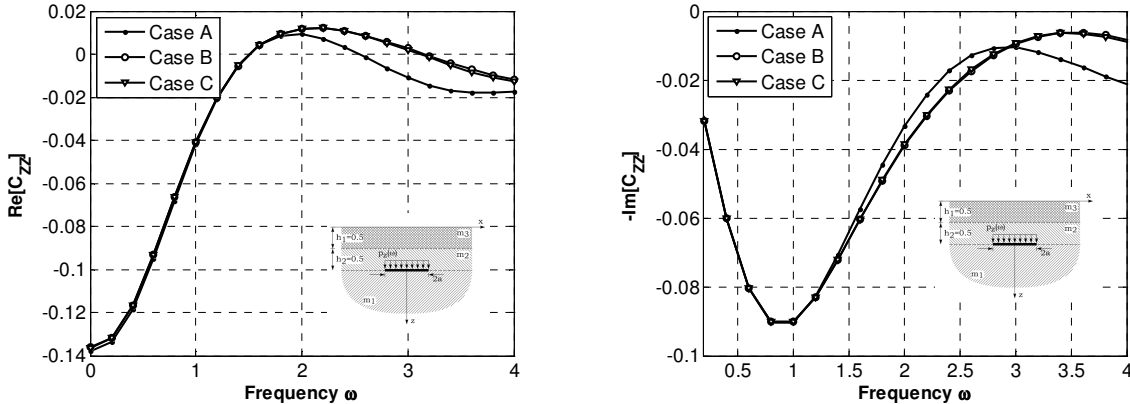


Figure 4.29 Vertical dynamic compliance of the rigid plate for three layered systems.

4.6.4 Influence of the damping

In this section the influence of the damping coefficient of the surrounding medium on the dynamic transverse and rocking compliance of the embedded plates is presented. In this work, a model of hysteretic damping is introduced in the formulation according to the elastic-viscoelastic correspondence principle (Christensen, 2010) (Section 4.5.1).

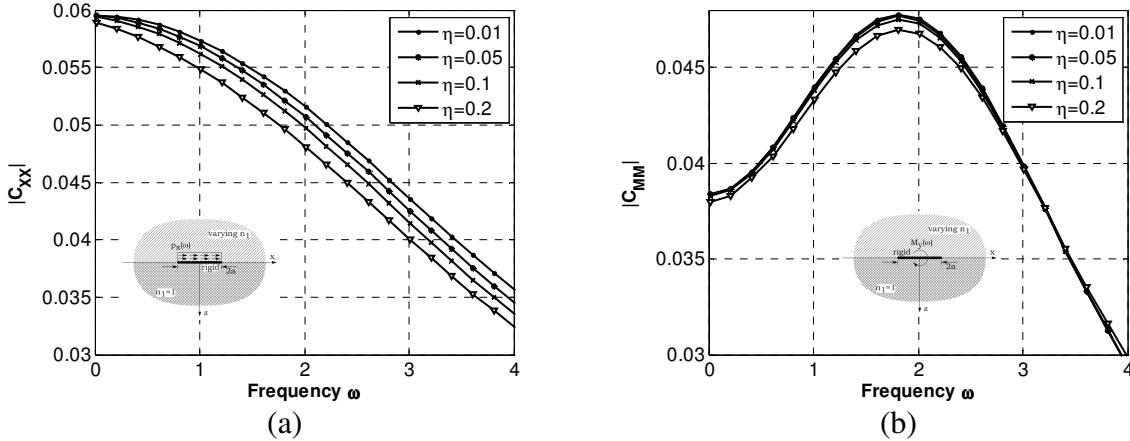


Figure 4.30 Influence of the damping coefficient on the frequency behavior of the rigid plate.

Bi-material constructions shown in Figs. 4.19b and 4.19c are considered. In all cases, both media have $c_{44}=1$ and $\nu=0.25$, and for medium 1, $n_1=n_2=n_3=4$, while $n_1=n_2=n_3=2$ for medium 2 (Table 4.3). The damping coefficient of both media is varied between $\eta=0.01$ and $\eta=0.2$, which are introduced in the material properties of the media according to Eq. 4.29.

Figure 4.30 shows the direct transverse and rocking compliances of the system rigid plate – bi-material interface.

Higher damping coefficients stiffen the surrounding domain and cause an overall decrease in the displacement amplitude compared to the ones with smaller damping coefficients. This amplitude decay is supported by Gaul (1999). These results indicate that the strategy adopted in this work to represent the material attenuation in the transversely isotropic materials produces physically consistent results.

In this chapter, a model of rigid circular plates was presented. A discretized relation of traction and displacements was used to represent the rigid plate. The present implementation shows convergence with increasing discretization, as well as good agreement with previous results for both static and dynamic problems in different loading configurations. The influence of the inner radius in the vertical, transverse and rocking compliance of a rigid plate was studied. The vertical, transverse and rocking vibration of rigid plates in different transversely isotropic bi-material interfaces was presented. It was shown that the cross compliance terms cannot be disregarded in the cases of bi-material interfaces, because of the fact that the transverse and rocking behavior of such media is coupled. The corresponding case of a rigid plate embedded in a multilayered medium was presented in terms of the vertical compliance of the system plate – surrounding medium. Finally, a study was presented on the influence of the damping factor introduced to the media. The results indicate that the methodology of inclusion of the damping factor in the material constants produces physically consistent results. In the next chapter, a variational formulation is used to model the flexure of an elastic plate.

5 MODEL OF AN EMBEDDED ELASTIC CIRCULAR PLATE

This chapter presents the formulation of a model of flexible circular plates. Kirchhoff theory of thin plates under small deflections is adopted. A trial function for the deflection profile of the plate is described by power series, each term of which is multiplied by an in principle unknown generalized coordinate. An extra term is included in the deflection profile to comply with the effect of a concentrated load. An energy functional is established. This energy functional includes the strain energy of the flexible plate, which is obtained by considering the deflection profile defined previously. It also includes the strain energy of the medium in which the plate is embedded, which is obtained by considering the traction field that arises from the deflection of the plate. The energy functional finally includes the potential energy of the concentrated and distributed loads that are applied on the plate. The minimization of this energy functional according to the principle of minimum potential energy, under the constraint that it must satisfy the boundary conditions at the plate edge, results in the generalized coordinates which correspond to the deflection profile of the plate. The results of static flexure and vertical vibrations of the embedded flexible plate are compared with results from the literature. Original research results of the problem are presented.

5.1 Problem statement

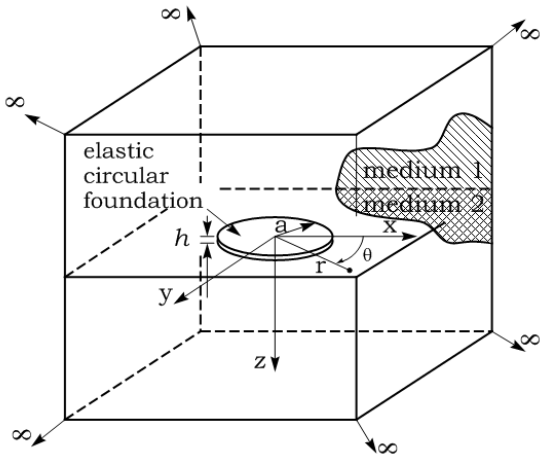


Figure 5.1 Elastic solid circular plate of radius a and thickness h buried in the interface of two transversely isotropic media.

Consider an elastic, solid circular plate, with outer radius a , thickness h , Young's modulus E_p , Poisson ratio ν_p , embedded at the interface of two transversely isotropic media, such as depicted in Fig. 5.1.

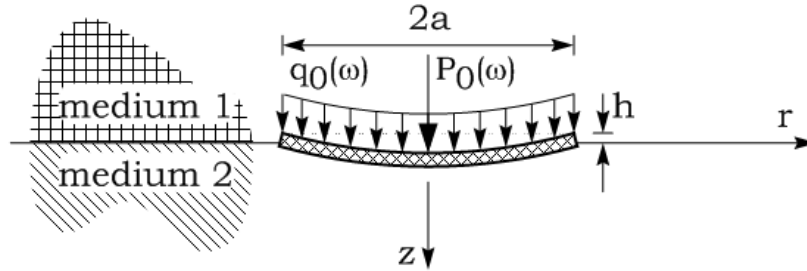


Figure 5.2 Elastic solid circular plate under the effect of distributed and/or concentrated vertical loads.

The plate is under the effect of time-harmonic axisymmetric concentrated and/or distributed vertical loads, such as depicted in Fig. 5.2.

The objective of this chapter is to provide a mathematical description of the problem of elastic plate, which can be used together with the models of transversely isotropic media presented in chapters 2 and 3 to model the problem of the plate embedded in those media.

5.2 Governing equations and boundary conditions

The model of elastic plate adopted in this work comes from the classical plate theory, or Kirchhoff theory. This model is based on hypotheses similar to those used in the thin beam theory – or Euler-Bernoulli beam theory. It considers that the thickness h of the plate is small, compared with its radius a , and that the plate undergoes small deflections (Timoshenko and Woinowsky-Krieger, 1964). In the Kirchhoff theory, it is assumed that:

- a) the middle surface remains undeformed during bending (Fig 5.3);
- b) points lying initially on a normal to the middle flat surface of the plate remain normal to the middle bent surface of the plate after bending (Fig. 5.3) and
- c) the state of normal stresses on the middle surface can be disregarded.

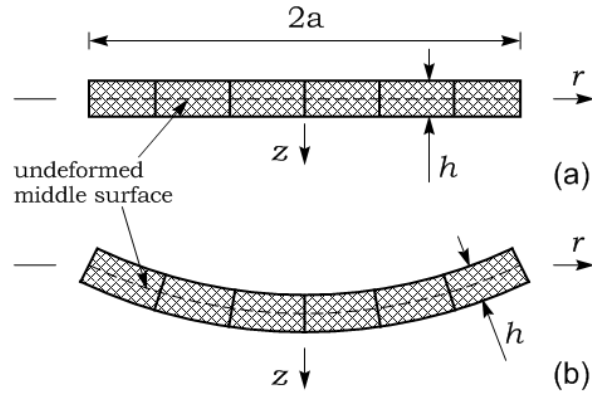


Figure 5.3 Deflection pattern assumed by the Kirchhoff theory: (a) undeformed plate and (b) deformed plate, showing the undeformed middle surface and that normals to it remain normals after deflection.

Under these assumptions, all stress components can be expressed by the deflection $w(r)$ of the plate ($0 \leq r \leq a$). The deflection must satisfy the linear partial differential equation presented in Eq. 5.1, together with the boundary conditions of the problem. If there are forces acting on the middle plane of the plate, the first hypothesis does not hold anymore, and additional terms must be included in Eq. 5.1 to take into account the effect of these forces. The consequence is that this theory of plates works only for loads applied perpendicularly to the surface of the plate. Notice that the mass of the plate is not taken into account.

The linear partial differential equation that relates the deflection $w(r)$ of the plate and the loading $q(r)$ applied on it is (Timoshenko and Woinowsky-Krieger, 1964):

$$D \nabla^4 w(r) = q(r); 0 \leq r \leq 1 \quad (5.1)$$

in which

$$D = E_p h^3 / \left[12 (1 - \nu_p^2) \right] \quad (5.2)$$

and

$$\nabla^4 = \frac{\partial^4}{\partial r^4} + \frac{2}{r} \frac{\partial^3}{\partial r^3} - \frac{1}{r^2} \frac{\partial^2}{\partial r^2} + \frac{1}{r^3} \frac{\partial}{\partial r} \quad (5.3)$$

In Eq. 5.1, $q(r)$ is an arbitrary axisymmetric load applied perpendicularly to the surface of the plate. The term D in Eq. 5.2 is known as the bending (or flexural) rigidity of the plate. The term ∇^4 is known as biharmonic operator. In the present case of axisymmetric bending, it involves only derivatives with respect to the variable r . In a more general case of bending, it would also involve derivatives with respect to θ .

From the classical plate theory, $M_r(r)$, which is the bending moment that acts along the circumferential section of the plate, and $Q(r)$, which is the shear force acting on the cylindrical section of radius r , for an arbitrary deflection profile $w(r)$, are given by Eqs. 5.4 and 5.5 (Timoshenko and Woinowsky-Krieger, 1964).

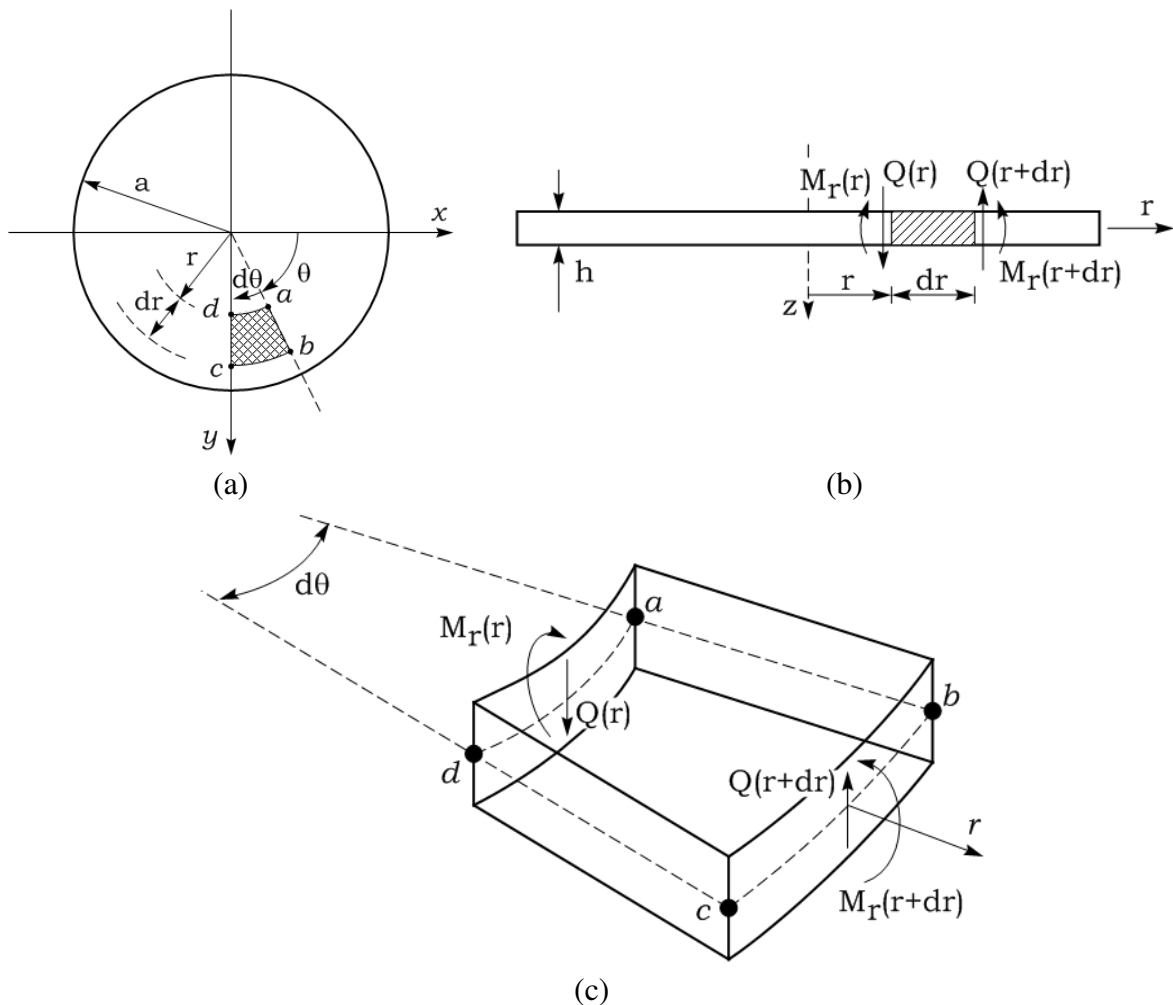


Figure 5.4 Illustration of the moment $M_r(r)$ and the shear force $Q(r)$ acting on an arbitrary section of the elastic plate. Part (a) shows the surface of the whole plate, part (b) shows an arbitrary cross-section which passes through the center of the plate and part (c) shows an element of the body of the plate.

$$M_r(r) = -D \left[\frac{d^2}{dr^2} w(r) + \frac{\nu_p}{r} \frac{d}{dr} w(r) \right] \quad (5.4)$$

$$Q(r) = D \left[\frac{d^3}{dr^3} w(r) + \frac{1}{r} \frac{d^2}{dr^2} w(r) - \frac{1}{r^2} \frac{d}{dr} w(r) \right] \quad (5.5)$$

Figure 5.4 gives a physical interpretation of these quantities and the sign convention adopted in the present work. The sign convention established in Fig. 5.4 implies that positive moments $M_r(r)$ and positive shear forces $Q(r)$ result in positive deflections $w(r)$ (Eq. 5.1). Positive deflections correspond to bending the plate towards positive values of the z -coordinate (downward in Fig. 5.4b).

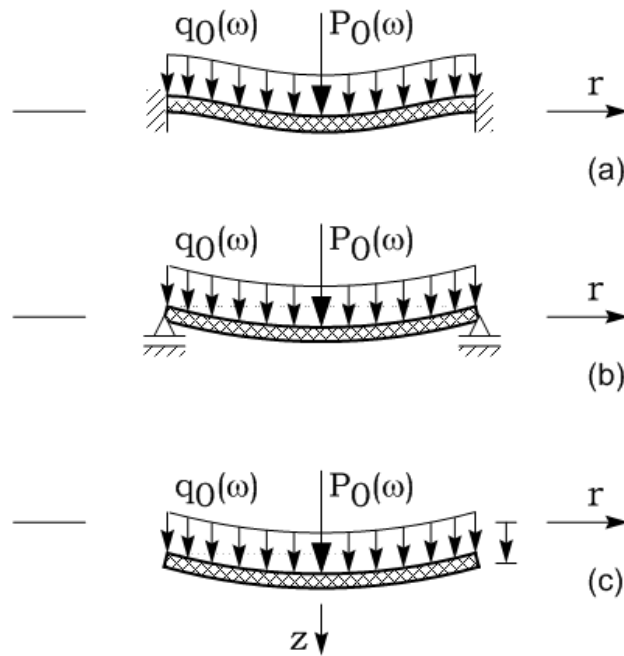


Figure 5.5 Different boundary conditions at the plate edge, showing (a) clamped edge, (b) simply supported edge and (c) free edge.

Figure 5.5 shows some of the possible configurations (boundary conditions) that a circular plate can present. Figure 5.5a corresponds to the case of the plate clamped all around. This configuration is mathematically described by:

$$w(r=1) = 0 \quad (5.6)$$

$$\left. \frac{d}{dr} w(r) \right|_{r=1} = 0 \quad (5.7)$$

Figure 5.5b corresponds to the case of a simply supported edge, the mathematical description of which is:

$$w(r=1) = 0 \quad (5.8)$$

$$M_r(r=1) = 0 \quad (5.9)$$

Finally, Fig. 5.5c represents the configuration of a plate with free edge, whose corresponding boundary conditions are:

$$M_r(r=1) = 0 \quad (5.10)$$

$$Q(r=1) = 0 \quad (5.11)$$

Rajapakse (1988), Wan (2003), Selvadurai (1979c) and others investigated extensively the representation of an embedded plate with different sets of boundary conditions. The configuration of free edge is capable of representing accurately the case of an elastic plate resting on the surface of a half-space (Rajapakse, 1988). On the other hand, it is difficult to specify the exact boundary conditions that correspond to the case of a plate buried in an elastic medium, such as the case shown in Fig. 5.1. The precise condition depends on the way in which the plate edge is bonded to the surrounding medium (Rajapakse, 1988). The boundary conditions expressed in Eqs. 5.10 and 5.11 (Fig. 5.5c) correspond to the most relaxed case. The most extreme case corresponds to the configuration of the plate clamped all around (Eqs. 5.6 and 5.7 and Fig. 5.4a). According to Rajapakse (1988), the boundary conditions corresponding to the case of clamped plate are inappropriate to represent the buried plate. While Selvadurai (1979) described the buried plate without imposing boundary conditions on the plate edge, Rajapakse (1988) concluded that there is negligible difference in the representation of this problem if Kirchhoff boundary conditions are

imposed. Kirchhoff boundary conditions correspond to a free edge of the plate (Fig. 5.4c and Eqs. 5.10 and 5.11) (Timoshenko and Woinowsky-Krieger, 1964; Kirchhoff, 1850; Rajapakse, 1988).

5.3 Variational formulation

A methodology of solution for the deflection profile $w(r)$ from Eq. 5.1, based on the boundary conditions established in Eqs. 5.10 and 5.11 was proposed by Rajapakse (1988). It consists in a variational formulation, which involves establishing an energy functional comprising the strain energy of the flexible plate and of its surrounding medium. In order to determine the strain energy of the plate, a trial solution of its deflection profile is created.

Consider a solid circular elastic plate with unit radius $a=1$ and thickness h , Young's modulus E_p and Poisson's ratio ν_p (Fig. 5.1). The plate is under the effect of a vertical concentrated load of intensity P_0 and of a uniformly distributed vertical load of intensity q_0 (Fig. 5.2). A trial solution for the deflection profile of the plate due to these loads can be described by:

$$w(r) = w^*(r) + \sum_{n=0}^N w_n(r) = a_0 r^2 \log(r) + \sum_{n=0}^N \alpha_n r^{2n}; 0 \leq r \leq 1 \quad (5.12)$$

in which

$$a_0 = P_0 / (8\pi D) \quad (5.13)$$

$$D = E_p h^3 / \left[12(1 - \nu_p^2) \right] \quad (5.14)$$

The summation in Eq. 5.12 comprises an approximation for the deflection of the plate by power series. Each power profile r^{2n} is weighted by a generalized coordinate α_n ($n=0, N$). The term outside the summation is incorporated to cover the effect of singular stress due to the concentrated load P_0 .

Figure 5.6a illustrates a few terms of the power series involved in Eq. 5.12. They are the profiles given by $w^*(r) = a_0 r^2 \log(r)$ and $w_n(r) = \alpha_n r^{2n}$ obtained if $a_0 = \alpha_n = 1$ ($n=0, N$). Figure 5.6b shows the resulting deflection profile obtained with the summation of all the terms shown in Fig.

5.6a according to Eq. 5.12. Any deflection profile can be approximated by changing the values of the generalized coordinates α_n . The values of α_n that result in the actual deflection of the plate depend on some physical condition which represents the problem of embedded plate.

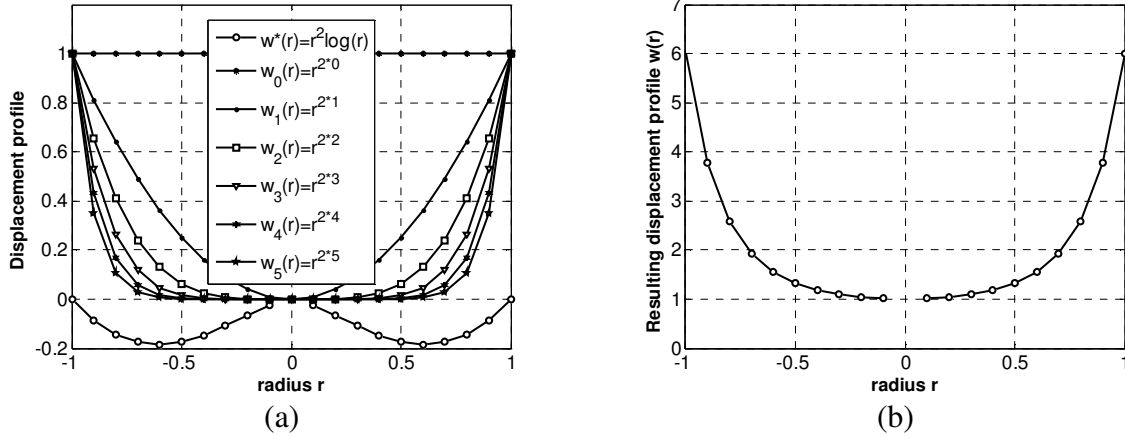


Figure 5.6 (a) Each of the terms of the power series involved in Eq. 5.12, for the case of $a_0 = \alpha_n = 1$ ($n=0, N$), and (b) the resulting deflection profile from the summation of all these terms.

In view of the deflection profile established by Eq. 5.12, the expressions of bending moment $M_r(r)$ and shear force $Q(r)$ presented in Eqs. 5.4 and 5.5 become:

$$M_r(r) = -D \left\{ a_0 \left[3 + 2 \log(r) + \nu_p + 2\nu_p \log(r) \right] + \sum_{n=1}^N \alpha_n \left[2n(2n-1) + 2n\nu_p \right] r^{2n-2} \right\} \quad (5.15)$$

$$Q(r) = D \left[\frac{4a_0}{r} + \sum_{n=1}^N 4n^2(2n-2) \alpha_n r^{2n-3} \right] \quad (5.16)$$

Substitution of the first boundary conditions of free edge (Eq. 5.10) in Eq. 5.15 yields:

$$M_r(1) = -D \left\{ a_0 \left[3 + \nu_p \right] + \sum_{n=1}^N \alpha_n \left[2n(2n-1) + 2n\nu_p \right] \right\} = 0 \quad (5.17)$$

$$\sum_{n=1}^N \alpha_n \left[2n(2n-1) + 2n\nu_p \right] = -a_0 (3 + \nu_p) \quad (5.18)$$

Substitution of the second boundary condition of free edge (Eq. 5.11) in Eq. 5.16 yields:

$$Q(1) = D \left[4a_0 + \sum_{n=1}^N 4n^2 (2n-2) \alpha_n \right] = 0 \quad (5.19)$$

$$\sum_{n=1}^N 4n^2 (2n-2) \alpha_n = -4a_0 \quad (5.20)$$

Equations 5.18 and 5.20 can be combined in a matrix equation involving a $2 \times (N+1)$ matrix [B] and a 2×1 vector {R} such that:

$$[B]\{\alpha\} = \{R\} \quad (5.21)$$

in which

$$B_{11} = B_{12} = B_{22} = 0 \quad (5.22)$$

$$B_{21} = 2(1 + \nu_p) \quad (5.23)$$

$$B_{1j} = \left[4(j-1)^2 - 2(1 - \nu_p)(j-1) \right]; \quad 3 \leq j \leq (N+1) \quad (5.24)$$

$$B_{2j} = 4(j-1)^2 (2j-4); \quad 3 \leq j \leq (N+1) \quad (5.25)$$

$$R = \left\langle -a_0(3 + \nu_p) \quad -4a_0 \right\rangle^T \quad (5.26)$$

$$\{\alpha\} = \langle \alpha_1 \quad \alpha_2 \quad \cdots \quad \alpha_N \rangle^T \quad (5.27)$$

5.3.1 Strain energy of the flexible plate

The strain energy U_p of a thin elastic circular plate under flexural deformations is given by Eq. 5.28 (Timoshenko and Woinowsky-Krieger, 1964; Rajapakse, 1988).

$$U_p = \int_0^1 \pi D \left[\left(\frac{d^2}{dr^2} w(r) + \frac{1}{r} \frac{d}{dr} w(r) \right)^2 - \frac{2(1-\nu_p)}{r} \frac{d^2}{dr^2} w(r) \frac{d}{dr} w(r) \right] r dr \quad (5.28)$$

In view of the deflection profile $w(r)$ from Eq. 5.12, this strain energy can be expressed in a matrix form involving the generalized coordinates α , as shown in Eq. 5.29.

$$U_p = \pi D (3 + \nu_p) a_0^2 + \langle Q^p \rangle \{ \alpha \} + \{ \alpha \}^T [K^p] \{ \alpha \} \quad (5.29)$$

In Eq. 5.29, $\langle Q^p \rangle$ is a $(N+1) \times 1$ vector and $[K^p]$ an $(N+1) \times (N+1)$ matrix, the terms of which are:

$$Q_1^p = 0 \quad (5.30)$$

$$Q_i^p = 4\pi D a_0 [3i - 5 + (i-1)\nu_p]; \quad 2 \leq i \leq (N+1) \quad (5.31)$$

$$K_{ij}^p = K_{ji}^p = 0 \quad (5.32)$$

$$K_{ij}^p = \frac{4(i-1)(j-1)\pi D}{2i+2j-6} [4(i-1)(j-1) - 2(1-\nu_p)(2i-3)]; \quad 2 \leq i, j \leq (N+1) \quad (5.33)$$

5.3.2 Strain energy of the surrounding medium

The strain energy U_h of an elastic medium of volume V is given by (Fung, 1965):

$$U_h = \frac{1}{2} \int_V \sigma_{ij} \epsilon_{ij} dV \quad (5.34)$$

Any interface within such elastic medium is subjected to contact tractions to resist the external loads that are applied to it. Consider vertical loads applied on the surface of a circular

plate of unit radius $a=1$ within the medium, in such a way that the resulting deflection of the plate is described by Eq. 5.12. Let $t_z(r)$ represent the resulting traction field due to these loads. It is assumed that the influence of radial tractions on the vertical displacement of the plate is negligible (Rajapakse, 1988). Then Eq. 5.34 results in (Fung and Tong, 2001; Fung, 1965):

$$U_h = \frac{1}{2} \int_0^1 2\pi r \cdot t_z(r) w(r) dr \quad (5.35)$$

The strain energy of the elastic medium shown in Eq. 5.35 is a general expression that in principle has no relation with the particular deflection profile established in Eq. 5.12. However, it can be determined what is the traction field $t_z(r)$ in Eq. 5.35 that results in the deflection profile from Eq. 5.12.

Let $t^*(r)$ represent the portion of $t_z(r)$ responsible for vertical displacements of the form $w^*(r)=a_0r^2\log(r)$ (Fig. 5.6a), which is the parcel of the displacement profile that is outside the summation in Eq. 5.12. Then, let $t_{nz}(r)$ be responsible for each term $w_n(r)=\alpha_n r^{2n}$ of the power series inside the summation in Eq. 5.12 (Fig. 5.6a). There are evidently $N+1$ different terms of $t_{nz}(r)$ ($n=0,N$), each corresponding to a term of the power series. Figure 5.6a shows six different terms of that power series. There is one traction profile $t_{nz}(r)$ corresponding to each of them, hence the index n in $t_{nz}(r)$. An expression for the traction field $t_z(r)$ evidently involves all these terms:

$$t_z(r) = t^*(r) + \sum_{n=0}^N t_{nz}(r) \quad (5.36)$$

A solution to Eq. 5.36 by analytical methods is not feasible due to the complexity of each of the terms $t^*(r)$ and $t_{nz}(r)$. A numerical solution is obtained by considering that the plate is made up of M concentric annular discs elements of inner and outer radii s_{1k} and s_{2k} ($k=1,M$). Figure 4.3 shows an example of this discretization for $M=5$ annular disc elements. The tractions $t^*(r_k)$ and $t_{nz}(r_k)$ acting on each annular disc element are assumed to be uniformly distributed. This same strategy was used in Section 4.3 when dealing with the problem of the rigid plate under vertical load. In that section, the traction field involved in Eq. 4.1 was also unknown. A discretized version of that equation was presented in Eq. 4.2. In Eq. 4.2, it is stated that the displacement of

all the annular disc elements is the same, w_{0z} , since the plate was rigid. For the present problem of flexible plate, the displacement of each element varies across the plate.

Recall that the traction field $t^*(r)$ is responsible for displacements of the form $w^*(r)=a_0r^2\log(r)$. For the discretized plate, the following expression holds for this traction field:

$$\sum_{k=1}^M u_{zz}(r_i, s_{1k}, s_{2k}, \omega) t^*(r_k, \omega) = w^*(r_i) = a_0 r_i^2 \log(r_i); i=1, M \quad (5.37)$$

The term $u_{zz}(r_i, s_{1k}, s_{2k}, \omega)$ in Eq. 5.37 is defined in Section 4.3. Equation 5.37 results in the deflection profile $w^*(r_i)=a_0r_i^2\log(r_i)$ of the annular disc element i ($i=1, M$) and involves M unknown traction components $t^*(r_k)$ ($k=1, M$). Equation 5.37 can be repeated for all annular disc elements $i=1, M$ resulting in a set of M linear equations:

$$\begin{bmatrix} u_{zz}^{1,1} & u_{zz}^{1,2} & & u_{zz}^{1,M} \\ u_{zz}^{2,1} & u_{zz}^{2,2} & & u_{zz}^{2,M} \\ & & \ddots & \\ u_{zz}^{M,2} & u_{zz}^{M,2} & & u_{zz}^{M,M} \end{bmatrix} \begin{Bmatrix} t^*(r_1, \omega) \\ t^*(r_2, \omega) \\ \vdots \\ t^*(r_M, \omega) \end{Bmatrix} = \begin{Bmatrix} w^*(r_1, \omega) = a_0 r_1^2 \log(r_1) \\ w^*(r_2, \omega) = a_0 r_2^2 \log(r_2) \\ \vdots \\ w^*(r_M, \omega) = a_0 r_M^2 \log(r_M) \end{Bmatrix} \quad (5.38)$$

Or, solving for $t^*(r_k)$,

$$\begin{Bmatrix} t^*(r_1, \omega) \\ t^*(r_2, \omega) \\ \vdots \\ t^*(r_M, \omega) \end{Bmatrix} = a_0 \begin{Bmatrix} T^*(r_1, \omega) \\ T^*(r_2, \omega) \\ \vdots \\ T^*(r_M, \omega) \end{Bmatrix} = a_0 \begin{bmatrix} u_{zz}^{1,1} & u_{zz}^{1,2} & & u_{zz}^{1,M} \\ u_{zz}^{2,1} & u_{zz}^{2,2} & & u_{zz}^{2,M} \\ & & \ddots & \\ u_{zz}^{M,2} & u_{zz}^{M,2} & & u_{zz}^{M,M} \end{bmatrix}^{-1} \begin{Bmatrix} r_1^2 \log(r_1) \\ r_2^2 \log(r_2) \\ \vdots \\ r_M^2 \log(r_M) \end{Bmatrix} \quad (5.39)$$

in which

$$u_{zz}^{i,k} = u_{zz}(r_i, s_{1k}, s_{2k}, \omega), i, k=1, M \quad (5.40)$$

Another way of presenting Eq. 5.39 is:

$$t^*(r_k, \omega) = a_0 T^*(r_k, \omega) = a_0 k_{zz}(r_i, s_{1k}, s_{2k}, \omega) \cdot r_i^2 \log(r_i) \quad (5.41)$$

in which $k_{zz}(r_i, s_{1k}, s_{2k}, \omega)$ are the coefficients of the inverse matrix of $u_{zz}(r_i, s_{1k}, s_{2k}, \omega)$, i.e.,

$$\begin{bmatrix} k_{zz}^{1,1} & k_{zz}^{1,2} & k_{zz}^{1,M} \\ k_{zz}^{2,1} & k_{zz}^{2,2} & k_{zz}^{2,M} \\ & \ddots & \\ k_{zz}^{M,2} & k_{zz}^{M,2} & k_{zz}^{M,M} \end{bmatrix} = \begin{bmatrix} u_{zz}^{1,1} & u_{zz}^{1,2} & u_{zz}^{1,M} \\ u_{zz}^{2,1} & u_{zz}^{2,2} & u_{zz}^{2,M} \\ & \ddots & \\ u_{zz}^{M,2} & u_{zz}^{M,2} & u_{zz}^{M,M} \end{bmatrix}^{-1} \quad (5.42)$$

Equation 5.39 is solved for the vertical traction jumps $t^*(r_k)$ acting on each disc element $k=1, M$, involving the term a_0 .

Recall that the traction field $t_{nz}(r)$ is responsible for displacements of the form $w_n(r) = \alpha_n r^{2n}$. For the discretized plate, Eq. 5.43 holds for the traction field $t_{nz}(r)$. Now, a different expression of $t_{nz}(r)$ is obtained for each n , corresponding to the generalized coordinate α_n ($n=0, N$).

$$\sum_{k=1}^M u_{zz}(r_i, s_{1k}, s_{2k}, \omega) t_{nz}(r_k, \omega) = w_n(r_i) = \alpha_n r_i^{2n}; \quad i=1, M; \quad n=0, N \quad (5.43)$$

Equation 5.43 results in the deflection profile $w_n(r_i) = \alpha_n r_i^{2n}$ of the annular disc element i ($i=1, M$) and it involves M unknown traction components $t_{nz}(r_k)$ ($k=1, M$). Equation 5.43 can be repeated for all annular disc elements $i=1, M$, thus resulting in a set of M linear equations:

$$\begin{bmatrix} u_{zz}^{1,1} & u_{zz}^{1,2} & u_{zz}^{1,M} \\ u_{zz}^{2,1} & u_{zz}^{2,2} & u_{zz}^{2,M} \\ & \ddots & \\ u_{zz}^{M,2} & u_{zz}^{M,2} & u_{zz}^{M,M} \end{bmatrix} \begin{Bmatrix} t_{nz}(r_1, \omega) \\ t_{nz}(r_2, \omega) \\ \vdots \\ t_{nz}(r_M, \omega) \end{Bmatrix} = \begin{Bmatrix} w_n(r_1, \omega) = \alpha_n r_1^{2n} \\ w_n(r_2, \omega) = \alpha_n r_2^{2n} \\ \vdots \\ w_n(r_M, \omega) = \alpha_n r_M^{2n} \end{Bmatrix} \quad (5.44)$$

Or, solving for $t_{nz}(r_k)$,

$$\begin{Bmatrix} t_{nz}(r_1, \omega) \\ t_{nz}(r_2, \omega) \\ \vdots \\ t_{nz}(r_M, \omega) \end{Bmatrix} = \alpha_n \begin{Bmatrix} T_{nz}(r_1, \omega) \\ T_{nz}(r_2, \omega) \\ \vdots \\ T_{nz}(r_M, \omega) \end{Bmatrix} = \alpha_n \begin{bmatrix} u_{zz}^{1,1} & u_{zz}^{1,2} & u_{zz}^{1,M} \\ u_{zz}^{2,1} & u_{zz}^{2,2} & u_{zz}^{2,M} \\ & \ddots & \\ u_{zz}^{M,2} & u_{zz}^{M,2} & u_{zz}^{M,M} \end{bmatrix}^{-1} \begin{Bmatrix} r_1^{2n} \\ r_2^{2n} \\ \vdots \\ r_M^{2n} \end{Bmatrix} \quad (5.45)$$

Another way of representing Eq. 5.45 is:

$$t_{nz}(r_k, \omega) = \alpha_n T_{nz}(r_k, \omega) = \alpha_n k_{zz}(r_i, s_{1k}, s_{2k}, \omega) r_i^{2n} \quad (5.46)$$

For example, the traction field $t_{0z}(r_k)$, responsible for the parcel $w_0(r_i) = \alpha_0 r_i^{2 \cdot 0}$ of the deflection profile is obtained from (n=0):

$$\begin{bmatrix} u_{zz}^{1,1} & u_{zz}^{1,2} & u_{zz}^{1,M} \\ u_{zz}^{2,1} & u_{zz}^{2,2} & u_{zz}^{2,M} \\ & & \ddots \\ u_{zz}^{M,2} & u_{zz}^{M,2} & u_{zz}^{M,M} \end{bmatrix} \begin{Bmatrix} t_{0z}(r_1, \omega) \\ t_{0z}(r_2, \omega) \\ \vdots \\ t_{0z}(r_M, \omega) \end{Bmatrix} = \begin{Bmatrix} w_0(r_1, \omega) = \alpha_0 r_1^{2 \cdot 0} = \alpha_0 \\ w_0(r_2, \omega) = \alpha_0 r_2^{2 \cdot 0} = \alpha_0 \\ \vdots \\ w_0(r_M, \omega) = \alpha_0 r_M^{2 \cdot 0} = \alpha_0 \end{Bmatrix} \quad (5.47)$$

Or, solving for $t_{0z}(r_k)$,

$$\begin{Bmatrix} t_{0z}(r_1, \omega) \\ t_{0z}(r_2, \omega) \\ \vdots \\ t_{0z}(r_M, \omega) \end{Bmatrix} = \alpha_0 \begin{Bmatrix} T_{0z}(r_1, \omega) \\ T_{0z}(r_2, \omega) \\ \vdots \\ T_{0z}(r_M, \omega) \end{Bmatrix} = \alpha_0 \begin{bmatrix} u_{zz}^{1,1} & u_{zz}^{1,2} & u_{zz}^{1,M} \\ u_{zz}^{2,1} & u_{zz}^{2,2} & u_{zz}^{2,M} \\ & & \ddots \\ u_{zz}^{M,2} & u_{zz}^{M,2} & u_{zz}^{M,M} \end{bmatrix}^{-1} \begin{Bmatrix} r_1^{2 \cdot 0} = 1 \\ r_2^{2 \cdot 0} = 1 \\ \vdots \\ r_M^{2 \cdot 0} = 1 \end{Bmatrix} \quad (5.48)$$

The traction field $t_{1z}(r_k)$, responsible for the parcel $w_1(r_i) = \alpha_1 r_i^{2 \cdot 1}$ of the deflection profile is obtained from (n=1):

$$\begin{bmatrix} u_{zz}^{1,1} & u_{zz}^{1,2} & u_{zz}^{1,M} \\ u_{zz}^{2,1} & u_{zz}^{2,2} & u_{zz}^{2,M} \\ & & \ddots \\ u_{zz}^{M,2} & u_{zz}^{M,2} & u_{zz}^{M,M} \end{bmatrix} \begin{Bmatrix} t_{1z}(r_1, \omega) \\ t_{1z}(r_2, \omega) \\ \vdots \\ t_{1z}(r_M, \omega) \end{Bmatrix} = \begin{Bmatrix} w_1(r_1, \omega) = \alpha_1 r_1^{2 \cdot 1} \\ w_1(r_2, \omega) = \alpha_1 r_2^{2 \cdot 1} \\ \vdots \\ w_1(r_M, \omega) = \alpha_1 r_M^{2 \cdot 1} \end{Bmatrix} \quad (5.49)$$

Or, solving for $t_{1z}(r_k)$,

$$\begin{Bmatrix} t_{1z}(r_1, \omega) \\ t_{1z}(r_2, \omega) \\ \vdots \\ t_{1z}(r_M, \omega) \end{Bmatrix} = \alpha_1 \begin{Bmatrix} T_{1z}(r_1, \omega) \\ T_{1z}(r_2, \omega) \\ \vdots \\ T_{1z}(r_M, \omega) \end{Bmatrix} = \alpha_1 \begin{bmatrix} u_{zz}^{1,1} & u_{zz}^{1,2} & & u_{zz}^{1,M} \\ u_{zz}^{2,1} & u_{zz}^{2,2} & & u_{zz}^{2,M} \\ & & \ddots & \\ u_{zz}^{M,2} & u_{zz}^{M,2} & & u_{zz}^{M,M} \end{bmatrix}^{-1} \begin{Bmatrix} r_1^{2 \cdot 1} \\ r_2^{2 \cdot 1} \\ \vdots \\ r_M^{2 \cdot 1} \end{Bmatrix} \quad (5.50)$$

and so on up to $n=N$.

The dependence of the traction fields $t^*(r)$ and $t_{nz}(r)$ on the composition of the elastic medium (whether it is a homogeneous full-space or a bimaterial interface or a multilayered system) is encompassed by the kernel function $u_{zz}(r_i, s_{1k}, s_{2k}, \omega)$.

From Eq. 5.36, it holds, for each ring k ($k=1, M$), that

$$t_z(r_k, \omega) = t^*(r_k, \omega) + \sum_{n=0}^N t_{nz}(r_k, \omega); k=1, M \quad (5.51)$$

$$t_z(r_k, \omega) = a_0 T^*(r_k, \omega) + \sum_{n=0}^N \alpha_n T_{nz}(r_k, \omega); k=1, M \quad (5.52)$$

$$t_z(r_k, \omega) = a_0 k_{zz}(r_i, s_{1k}, s_{2k}, \omega) r_i^2 \log(r_i) + \sum_{n=0}^N \alpha_n k_{zz}(r_i, s_{1k}, s_{2k}, \omega) r_i^{2n}; k=1, M \quad (5.53)$$

The substitution of the traction field $t_z(r)$ from Eq. 5.53 into Eq. 5.35, yields after a laborious simplification, the strain energy of the elastic medium U_h represented in terms of generalized coordinates (Rajapakse, 1988):

$$U_h = \{\alpha\}^T [K^h] \{\alpha\} + \langle Q^h \rangle \{\alpha\} + \sum_{k=1}^M \pi r_k T^*(r_k) a_0^2 r_k^2 \log(r_k) \Delta r_k \quad (5.54)$$

In Eq. 5.54, $\Delta r_k = s_{2k} - s_{1k}$ is the width of each annular disc element. $[K^h]$ is an $(N+1) \times (N+1)$ matrix and $\langle Q^h \rangle$ an $(N+1) \times 1$ vector, the terms of which are respectively given by:

$$K_{ij}^h = \sum_{k=1}^M T_{(i-1)z}(r_k) \pi \Delta r_k \cdot r_k^{2j-1}; 1 \leq i, j \leq (N+1) \quad (5.55)$$

$$Q_i^h = \sum_{k=1}^M \left[T^*(r_k) r_k^{2(i-1)} a_0 + \pi r_k^3 \log(r_k) T_{(i-1)z}(r_k) \right] \Delta r_k a_0; 1 \leq i \leq (N+1) \quad (5.56)$$

5.3.3 Variational formulation of the embedded plate

Let E_p and E_q denote respectively the potential energy of the centrally applied concentrated force P_0 and of the uniformly distributed loading q_0 . Equations 5.57 and 5.58 describe E_p and E_q in terms of generalized coordinates (Rajapakse, 1988).

$$E_p = P_0 \alpha_0 \quad (5.57)$$

$$E_q = 2\pi q_0 \sum_{n=0}^N \alpha_n / (2n + 2) \quad (5.58)$$

Consider the strain energy of an elastic medium, U_h (Eq. 5.54), and of a flexible plate, U_p (Eq. 5.29), derived in the previous subsections. The total potential energy function U of the system comprising the flexible plate and its surrounding medium, under the effect of P_0 and/or q_0 is given by:

$$U = U_h + U_p - E_p - E_q \quad (5.59)$$

Or, in terms of generalized coordinates:

$$U = \{\alpha\}^T \left[K^h \right] \{\alpha\} + \{\alpha\}^T \left[K^p \right] \{\alpha\} + \langle Q^h \rangle \{\alpha\} + \langle Q^p \rangle \{\alpha\} \\ + \sum_{j=1}^M \pi r_j T_{zj}^* a_0^2 \log(r_j) \Delta r_j + \pi D (3 + \nu_p) a_0^2 - P_0 \alpha_0 - 2\pi q_0 \sum_{n=0}^N \alpha_n / (2n + 2) \quad (5.60)$$

The principle of minimum potential energy can be used to determine the generalized coordinates involved in Eq. 5.60. The specific values of these coordinates that correspond to the

plate with free edge boundary conditions (Eq. 5.21) can be obtained by establishing the following minimization problem:

$$\text{Problem P: } \begin{cases} \text{Minimize} & f(\alpha) = U & \text{(Eq. 5.60)} \\ \text{subject to} & g(\alpha) = [B]\{\alpha\} - \{R\} = 0 & \text{(Eq. 5.21)} \end{cases}$$

According to classical mathematical programming, this problem can be put as the following penalized problem PP (Nash, 2010):

$$\text{Problem PP: Minimize } \bar{U} = f(\alpha) + \lambda \cdot h(\alpha)$$

in which $h(\alpha)$ is a penalty function and λ is the penalty parameter. A common choice for the penalty function is the quadratic form (Rajapakse, 1988; Nash, 2010), $h(\alpha) = \frac{1}{2} \cdot g^2(\alpha)$. The constrained energy functional to be minimized then becomes:

$$\bar{U} = U + \frac{1}{2} \lambda [[B]\{\alpha\} - \{R\}]^T [[B]\{\alpha\} - \{R\}] \quad (5.61)$$

The value of λ must be such that the constraints are satisfied as its value increases. Rajapakse (1988) has investigated the influence of the parameter λ on the numerical stability of this energy functional and concluded that, for a particular but representative model of rigid and flexible plates embedded in an isotropic half-space, values of λ within the fairly wide range $1 \leq \lambda \leq 10^5$ provide stable expressions of Eq. 5.61.

The generalized coordinates α_n ($n=0, N$) which satisfy the boundary conditions at the plate edge arise upon application of the problem PP into Eq. 5.61:

$$\frac{\partial}{\partial \alpha_n} \bar{U} = 0; n=0, N \quad (5.62)$$

The substitution of Eq. 5.61 into Eq. 5.62 yields the equation system in Eq. 5.63. This system is written in a convenient matrix form for numerical implementation:

$$[K^s] \{\alpha\} = \{F\} \quad (5.63)$$

in which

$$[\mathbf{K}^s] = [\mathbf{K}^p] + [\mathbf{K}^p]^T + [\mathbf{K}^h] + [\mathbf{K}^h]^T + \lambda [\mathbf{B}]^T [\mathbf{B}] \quad (5.64)$$

$$\{\mathbf{F}\} = \langle \pi q_0 / i \rangle^T + \langle P_0 \delta_{li} \rangle^T + \lambda [\mathbf{B}]^T \{\mathbf{R}\} - \langle \mathbf{Q}^p \rangle^T - \langle \mathbf{Q}^h \rangle^T \quad (5.65)$$

In Eqs. 5.63 to 5.65, $[\mathbf{K}^h]$ is an $(N+1) \times (N+1)$ matrix and $\langle \mathbf{Q}^h \rangle$ an $(N+1) \times 1$ vector, which come from the description of the strain energy of the elastic medium, such as given by Eqs. 5.55 and 5.56. $[\mathbf{K}^p]$ an $(N+1) \times (N+1)$ matrix and $\langle \mathbf{Q}^p \rangle$ is an $(N+1) \times 1$ vector, which come from the description of the strain energy of the elastic plate, such as given by Eqs. 5.30 to 5.33. $[\mathbf{B}]$ is a $2 \times (N+1)$ matrix and $\{\mathbf{R}\}$ is a 2×1 vector, which contain a description of the boundary conditions of the plate, such as given by Eqs. 5.22 to 5.26. P_0 and q_0 are respectively the point load and the uniformly distributed load that are applied on the surface of the plate. In Eq. 5.65, δ_{ij} is the Krönecker delta, $\delta_{ij}=1$ if $i=j$ and $\delta_{ij}=0$ otherwise.

The numerical solution of Eq. 5.63, which depends on the material properties and configuration of the system of elastic plate and its surrounding medium, results in the generalized coordinates α_n ($n=0, N$), from which the deflection profile of the plate is obtained (Eq. 5.12).

5.4 Implementation

The present formulation of flexible plate has been presented in a convenient matrix form in order to allow a straightforward numerical implementation. A basic algorithm for solving Eq. 5.63, which was implemented in the present work, is:

a) Consider the Green's function describing the behavior of a material interface. For instance, the previous chapters presented solutions for the vertical displacement of bi-material and layered media under distributed axisymmetric vertical loads. For the case of a bi-material interface, this displacement is given by Eqs. 2.95 and 2.104, after solving Eq. 2.120. For the case of a multilayered system, this displacement is given by Eq. 3.22;

b) Consider a circular surface at that interface, discretized by M concentric annular disc elements;

c) Determine $u_{zz}(r_i, s_{1k}, s_{2k}, \omega)$ for all these elements, which is the vertical displacement of the point of coordinates r_i due to an axisymmetric vertical load distributed on the area which goes from s_{1k} to s_{2k} ($i, k=1, M$). It is convenient to assemble these results in an $M \times M$ matrix, such as shown in Eqs. 5.38 and 5.44;

d) Using this matrix and Eq. 5.39, determine the traction vector $T^*(r_k)$, $k=1, M$, which is one vector of length M . The radii r_i ($i=1, M$) in the right-hand-side of Eq. 5.39 are the central coordinate of each annular disc element (Fig. 4.3);

e) Using the same matrix and Eq. 5.45, determine the traction vectors $T_{nz}(r_k)$, $k=1, M$, $n=0, N$. It is necessary to apply Eq. 5.45 $N+1$ times (such as Eqs. 5.48 and 5.50), each of them resulting in a different vector $T_{nz}(r_k)$, each of length M ;

f) Using $T^*(r_k)$ and $T_{nz}(r_k)$, determine $[K^h]$ and $\langle Q^h \rangle$ according to Eqs. 5.55 and 5.56;

g) Determine vector $\langle Q^p \rangle$ from Eqs. 5.30 and 5.31;

h) Determine matrix $[K^p]$ from Eqs. 5.32 and 5.33;

i) Determine matrix $[B]$ from Eqs. 5.22 to 5.25;

j) Determine vector $\{R\}$ from Eq. 5.26;

k) Choose a penalty parameter λ ;

l) Assemble matrix $[K^s]$ according to Eq. 5.64;

m) Assemble vector $\{F\}$ according to Eq. 5.65;

n) Solve Eq. 5.63 for the vector $\{\alpha\}$;

o) Determine the deflection profile $w(r)$ by substituting $\{\alpha\}$ into Eq. 5.12, or if necessary, the moment $M_r(r)$ and shear force $Q(r)$ from Eqs. 5.15 and 5.16.

5.5 Validation

In the present chapter, the behavior of a flexible circular plate under time-harmonic vertical excitations is studied. Deep embedment of the plates is modeled by bonded transversely isotropic half-spaces (Chapter 2), while shallow embedments are represented by layered transversely isotropic half-spaces (Chapter 3).

In this section, the models of embedded flexible plates developed in this work are compared with existing solutions available in the literature. The main validation source is the

results provided by Rajapakse (1988). Rajapakse (1988) studied the static flexure of flexible plates at different depths of embedment on isotropic half-spaces.

5.5.1 Convergence

The influence functions u_{ij} ($i,j=r,\theta,z$), used in Eqs. 5.38 and 5.44, come from the solution of the bi-material interface or the layered system, such as presented in Chapters 2 and 3. These functions are exactly the same ones used in the implementation of the rigid plate (Chapter 4), and their convergence with increasing discretization has been presented in Table 4.2. The discretization of $M=20$ discs is chosen throughout this thesis, because, according to Table 4.2, it enables an error of less than 1% with the analytical solution in the representative model of rigid plates.

5.5.2 Bi-material interface

Figures 5.8 and 5.9 show solutions from the present implementation for cases of flexible plates. Figure 5.8 presents results of deflection of a flexible plate due to a centrally applied concentrated load of intensity P_0 (Fig. 5.7a). In Fig. 5.9, a uniformly distributed load of intensity q_0 is considered (Fig. 5.7b).

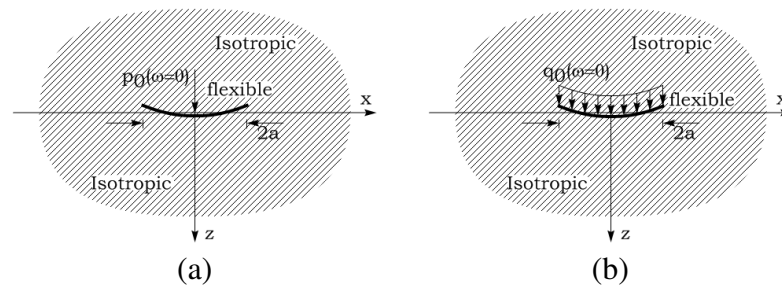


Figure 5.7 Illustrations of a flexible plate inside an isotropic full-space under (a) concentrated and (b) distributed static vertical loads.

These results are shown in terms of the dimensionless central displacement $w^*(r=0)$, differential deflection w^*_d , normalized moment acting at the center of the plate $M^*_r(r=0)$ and relative rigidity K_r , defined by (Rajapakse, 1988):

$$w^*(r) = \frac{a \cdot w(r) E_s}{P_0 (1 - \nu_s^2)} \text{ or } w^*(r) = \frac{w(r) E_s}{a \cdot q_0 (1 - \nu_s^2)} \quad (5.66)$$

$$M_r^*(r) = \frac{M_r(r)}{q_0 \cdot a^2} \quad (5.67)$$

$$w_d^* = \frac{a E_s [w(0) - w(1)]}{P_0 (1 - \nu_s^2)} \quad (5.68)$$

$$K_r = (1 - \nu_s^2) \frac{E_p}{E_s} \left(\frac{h}{a} \right)^3 \quad (5.69)$$

In Eqs. 5.66 to 5.69, E_p and ν_p are the Young's modulus and Poisson's ratio of the elastic plate, and h and a are its thickness and outer radius. E_s and ν_s are the Young's modulus and Poisson's ratio of the surrounding medium. The non-normalized deflection $w(r)$ and the moment $M_r(r)$ come respectively from Eqs. 5.12 and 5.15.

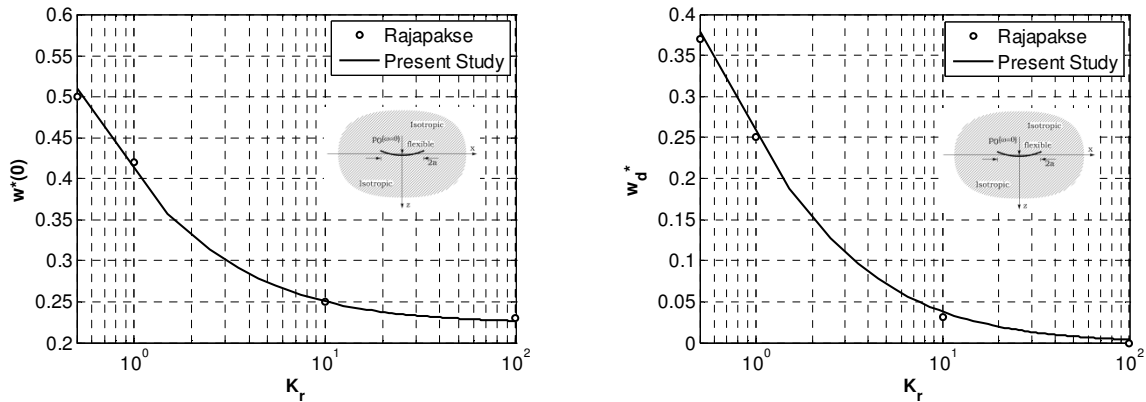


Figure 5.8 Normalized displacement and differential deflection of a flexible plate under concentrated load.

The results in Figs. 5.8 and 5.9 obtained with the present implementation consider a plate of $\nu_p=0.3$, discretized by $M=20$ discs, in the interface of two isotropic half-spaces with $E_s=2.5$ and $\nu_s=0.25$. $N=6$ generalized coordinates are used for the deflection profile (Eq. 5.12), since this number guarantees accurate computation of the stress resultants on the plate (Rajapakse, 1988).

These results agree with the ones presented by Rajapakse (1988) for the behavior of a flexible plate at infinite depth within an isotropic half-space.

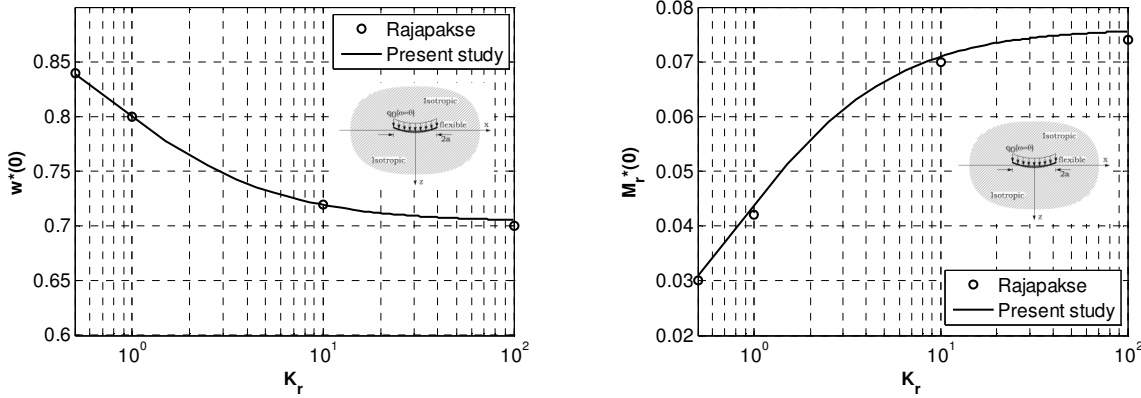


Figure 5.9 Normalized displacement and moment of a flexible plate under uniformly distributed load.

5.5.3 Multilayered medium

The behavior of an elastic plate embedded at different depths within an isotropic half-space is shown in Figs. 5.11 and 5.12.

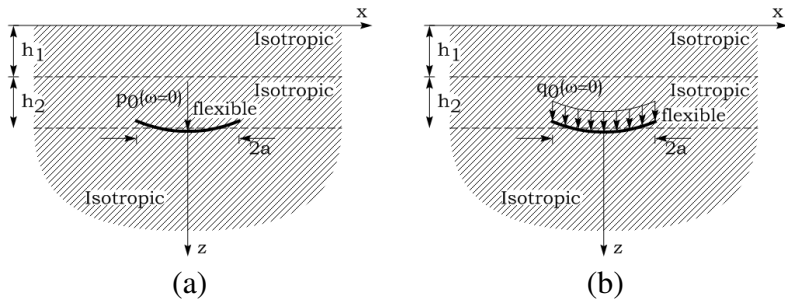


Figure 5.10 Configurations of a flexible plate subjected to (a) concentrated and (b) distributed vertical loads between a half-space and two layers of the same material.

Figure 5.11 presents the normalized central displacement and differential displacement of a flexible circular plate under the effect of a centrally applied concentrated static force P_0 (Fig. 5.10a). The plate has unit outer radius $a=1$ and Poisson's ratio $\nu_p=0.3$. The normalizations in these results are defined in Eqs. 5.66 to 5.69. A discretization of $M=20$ annular disc elements and $N=6$ generalized coordinates are used in this analysis. The different depths of embedment H/a are

obtained by piling layers of unit thickness on top of the plate, i.e., an embedment at a depth $H/a=L$ is obtained by placing the plate between a half-space and L layers of unit thickness. All the L layers and the underlying half-space have material properties $E_s=2.5$ and $\nu_s=0.25$. These results are supported by Rajapakse (1988), who studied the bending of a plate embedded in an arbitrary depth within an isotropic half-space.

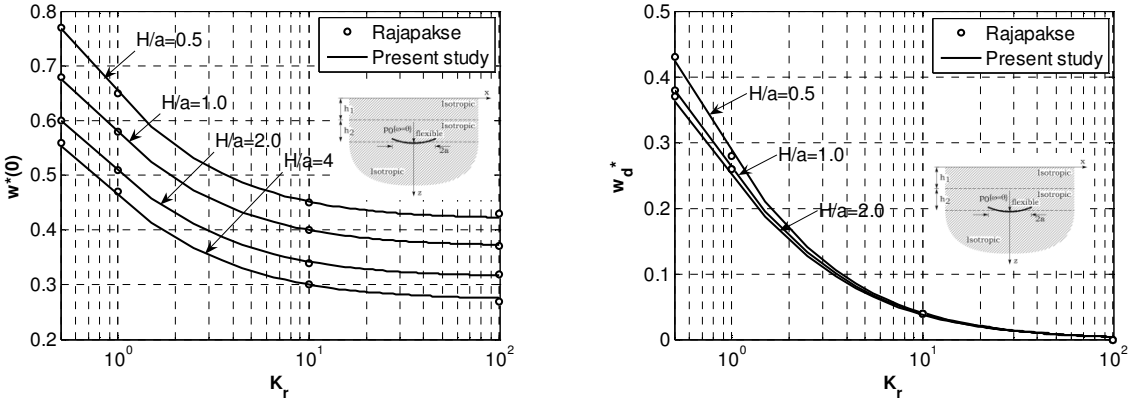


Figure 5.11 Behavior of an elastic plate at different embedments within an isotropic half-space, due to a centrally applied point load P_0 .

The results for the analogous case of a flexible plate under the effect of a uniformly distributed load q_0 (Fig. 5.10b) are presented in Fig. 5.12.

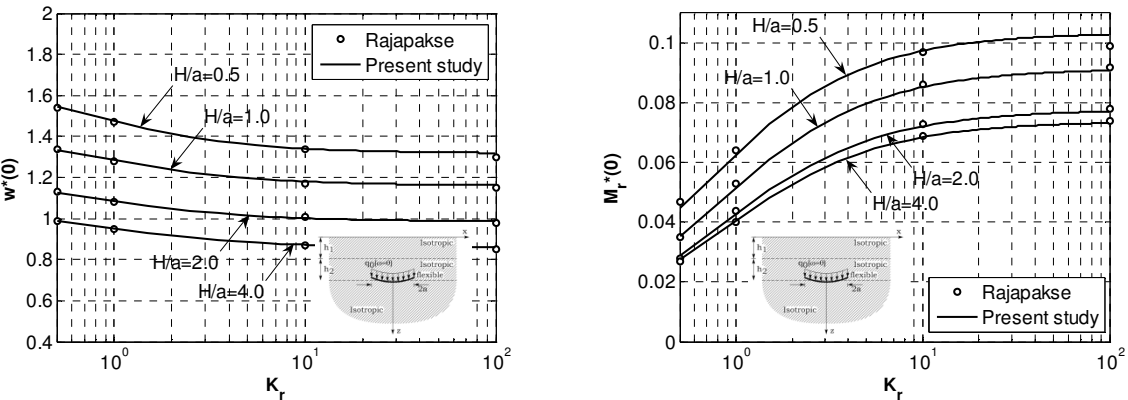


Figure 5.12 Behavior of an elastic plate at different embedments within an isotropic half-space, due to a uniformly distributed load q_0 .

In this section, the presented formulations of elastic plates embedded at bi-material interfaces and multilayered systems were compared with similar problems from the literature, to which it has shown good agreement.

5.6 Numerical results

This section presents original results of the behavior of embedded elastic plates obtained in this work. The influence of the composition of bi-material interfaces (Chapter 2) on the static and dynamic flexure of the plate is considered. Using the formulation of layered media presented in Chapter 3, the problem of flexible plates at arbitrary embedments inside transversely isotropic layered half-spaces is also studied. A brief investigation on the ability of the present formulation to comply with the boundary conditions of the plate is presented.

5.6.1 Bi-material interface

This section shows the effect of different bi-material configurations on the static and dynamic flexure of the flexible plates. Figure 5.13 illustrates the problem. The transversely isotropic materials used in these simulations are taken from Table 2.1. The transverse isotropy of the materials are obtained by varying the anisotropy index n_1 while keeping $n_2=n_3=1$, $c_{44}=1$ and $\nu=0.25$ (Table 2.1). In all cases, the material of medium 2 (Fig. 5.1) has $n_1=n_2=n_3=1$, $c_{44}=1$ and $\nu=0.25$, which corresponds to an isotropic material (Table 2.1). All materials for medium 1 are picked from Table 2.1. The mass density of all materials is $\rho=1$ in all cases.

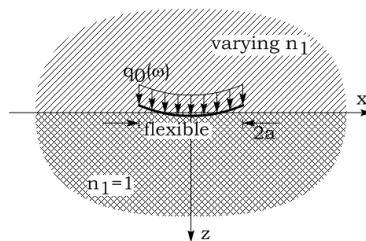


Figure 5.13 Illustration of different bi-material configurations with an embedded flexible plate subjected to a uniformly distributed vertical load.

Figure 5.14 shows the deflection profile of the plate for the frequencies $\omega=0.2$ and $\omega=1.0$, while Fig. 5.15 shows results for the frequencies $\omega=2.0$ and $\omega=4.0$. All four cases consider a

uniformly distributed vertical load on the surface of the plate. The plate material has Young's modulus $E=2.5$ and Poisson's ratio $\nu=0.25$. It has thickness $h=0.001$ and outer radius $a=1$. The bi-material configurations considered are the same as the ones used in Figs. 5.6 to 5.8. The plate is discretized by $M=20$ concentric annular disc elements. $N=6$ generalized coordinates are used (Eq. 5.12).

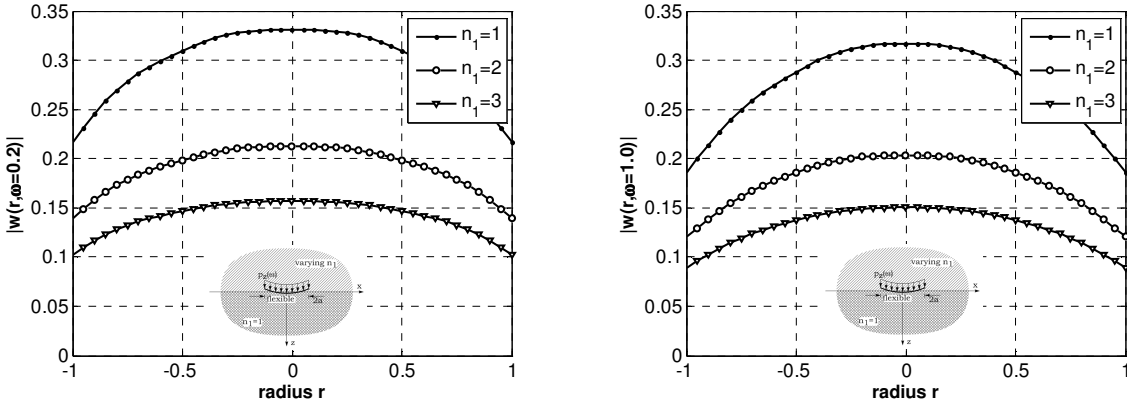


Figure 5.14 Deflection profile of a flexible plate for different bi-material constructions for the frequencies $\omega=0.2$ and $\omega=1.0$, for the case of a uniformly distributed load.

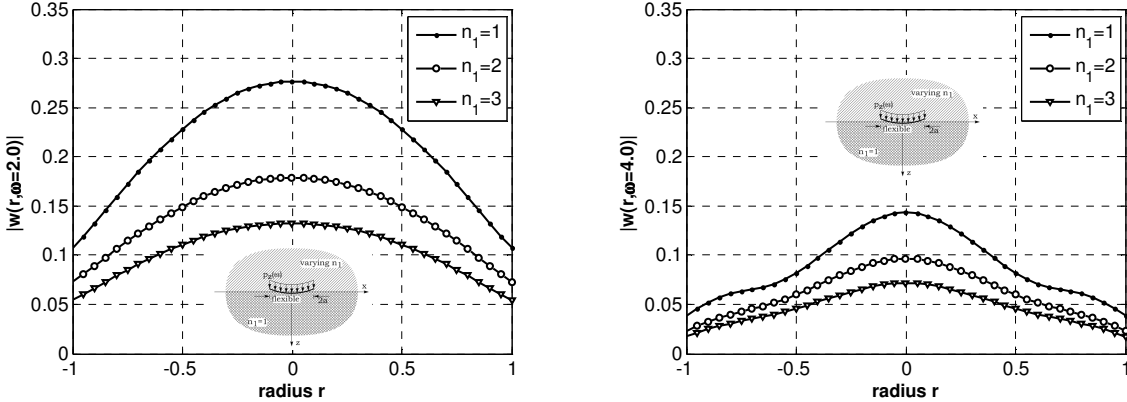


Figure 5.15 Deflection profile of a flexible plate for different bi-material constructions for the frequencies $\omega=2.0$ and $\omega=4.0$, for the case of a uniformly distributed load.

The deflection of the plate for four different frequencies is presented in the same scale in Figs. 5.14 and 5.15. An increase in the anisotropy index n_1 stiffens medium 1 vertically by increasing the Young's modulus E_Z (Table 2.1), i.e., an increase in n_1 stiffens medium 1

vertically. Therefore, it is physically consistent that an increase in n_1 corresponds to a decrease in the deflection of the plate, which is observed in all these results.

From Figs. 5.14 and 5.15, it can also be seen that different frequencies of excitation have a larger influence on the amplitude of the deflection of the plate than they have on the shape of its deflection. Figures 5.14 to 5.15 also show that an increase on the frequency of excitation corresponds to an overall decrease of the amplitude of displacement, which is physically consistent. This is shown more clearly in Fig. 5.16. The results of Fig. 5.16 correspond to the same bi-material constructions that were used in Figs. 5.14 and 5.15. An elastic plate with thickness $h=0.001$ and outer radius $a=1$ is used. The figure shows how the central displacement $w(r=0)$ of the plate varies with the frequency of excitation.

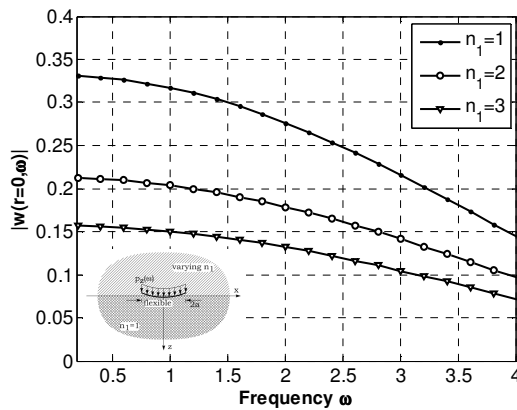


Figure 5.16 Central deflection of a flexible plate for different bi-material constructions, for the case of a uniformly distributed load.

In all the cases of flexible plate in the present and in the succeeding section, it was necessary to minimize the energy functional involving the strain energy of the plate and its surrounding medium (Eq. 5.51). The penalized energy functional involves a penalty factor λ , in order to guarantee that the boundary conditions at the plate edge are satisfied (Eq. 5.21). It was observed that, in all the cases of flexible plate in this chapter, the value of λ has very little influence on the accuracy and numerical stability of the solution of the constrained minimization problem. This has also been observed by Rajapakse (1988) for the case of different depths of embedment of the plate within an isotropic half-space. The value $\lambda=10^4$ was used in all the experiments presented in this chapter.

5.6.2 Multilayered system

In this section, the bending of an elastic plate embedded in layered media is studied. Three different layered systems are considered (Fig. 5.17 and Tables 5.1 and 5.2). In all cases, the plate is embedded between two layers of thickness h_i ($i=1,2$) and a half-space. In all cases, the layers and the half-space have $c_{44}=1$ and $\nu=0.25$, while their other properties are obtained by varying the anisotropy index n_1 . The other anisotropy indices are $n_2=n_3=1$. The material of the layers and their thicknesses in each case are shown in Table 5.1. The material properties of the materials m_1 , m_2 and m_3 are shown in Table 5.2. The mass density of all materials is $\rho=1$ in all cases.

Table 5.1 Multilayered media configurations used in this section.

Layer	Case A	Case B	Case C
1	Material m_1 ; $h_1=0.5$	Material m_3 ; $h_1=0.5$	Material m_3 ; $h_1=0.3$
2	Material m_1 ; $h_2=0.5$	Material m_2 ; $h_2=0.5$	Material m_2 ; $h_2=0.7$
half-space	Material m_1 ; $h_3=\infty$	Material m_1 ; $h_3=\infty$	Material m_1 ; $h_3=\infty$

Table 5.2 Multilayered media configurations used in this section.

Material *	n_1	n_2	n_3	c_{11}	c_{12}	c_{13}	c_{33}	E	E_Z	ν_Z
m_1	1.0	1.0	1.0	3.0000	1.0000	1.0000	3.0000	2.5	2.5000	0.2500
m_2	1.5	1.0	1.0	2.8284	0.8284	0.8284	4.2426	2.5	3.8673	0.2265
m_3	2.0	1.0	1.0	2.7749	0.7749	0.7749	5.5497	2.5	5.2114	0.2183

(*) for all materials, $c_{44}=1.0$, $\nu=0.25$ and $\rho=1$.

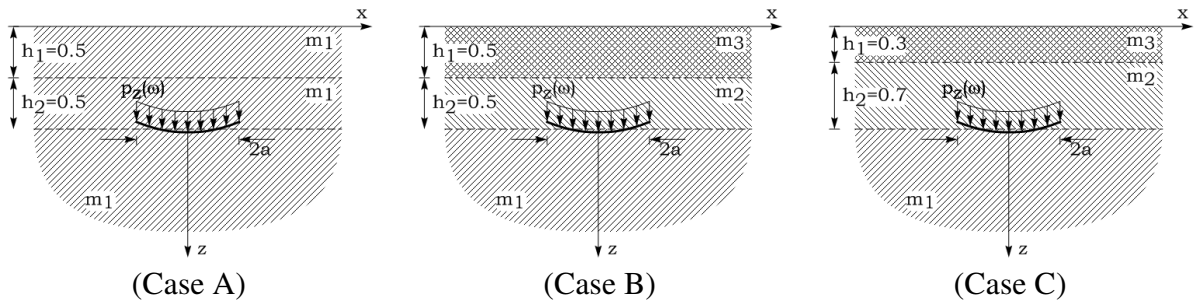


Figure 5.17 Illustration of different layered system configurations with an embedded plate subjected to vertical loads.

Figures 5.18, 5.19 and 5.20 show respectively the deflection profile $w(r)$ of the plate, the circumferential moment $M_r(r)$ and the shear force $Q(r)$ acting on it, for the frequencies $\omega \approx 0.0$ and $\omega = 4.0$. The deflection $w(r)$, the moment $M_r(r)$ and the shear force $Q(r)$ are determined according to Eqs. 5.12, 5.15 and 5.16. All cases consider a uniformly distributed vertical load on the surface of the plate. The plate material has Young's modulus $E=2.5$ and Poisson's ratio $\nu=0.25$. It has thickness $h=0.001$ and outer radius $a=1$. The plate is discretized with $M=20$ concentric annular disc elements. $N=6$ generalized coordinates are used in the deflection profile (Eq. 5.12). The same behavior observed in the case of the embedded rigid plate (Section 4.6.3) is also observed in these results, i.e., that the change in material composition has a more significant influence in the behavior of the plate than a change in the relative thickness of the layers, for the present configurations of embedment. This difference becomes more pronounced for a larger frequency.

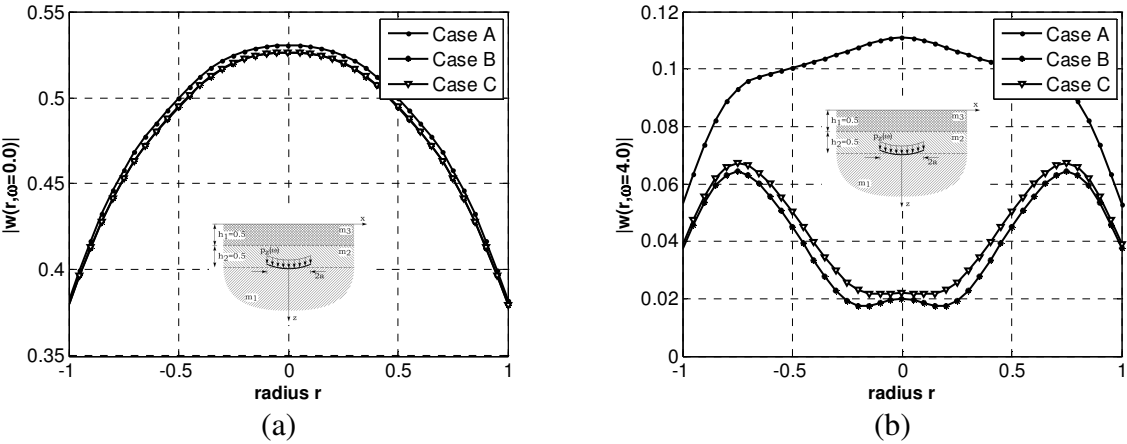


Figure 5.18 Deflection profile of a flexible plate for different layered systems for the frequencies (a) $\omega \approx 0.0$ and (b) $\omega = 4.0$.

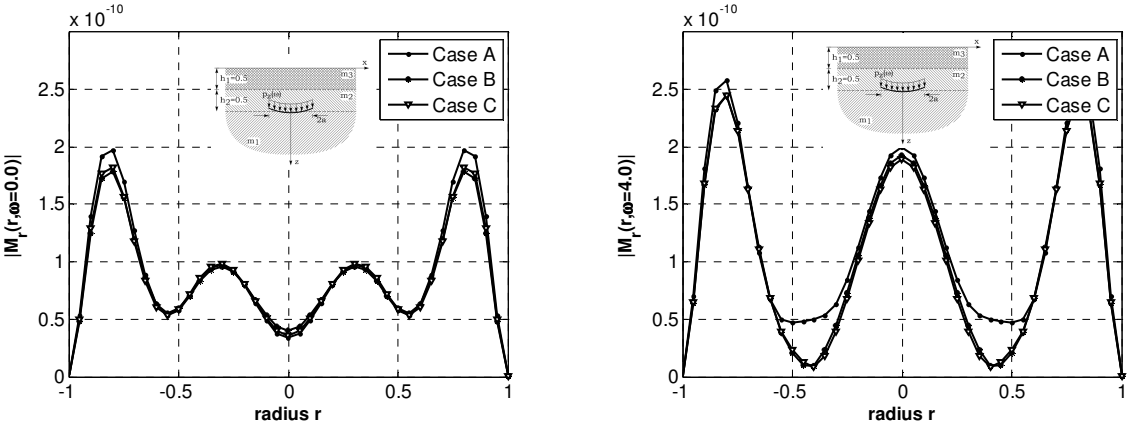


Figure 5.19 Moment $M_r(r)$ acting on a flexible plate for different layered systems for the frequencies $\omega \approx 0.0$ and $\omega = 4.0$.

For these layered system configurations, there is little change in the shear force acting on the plate (Fig. 5.20).

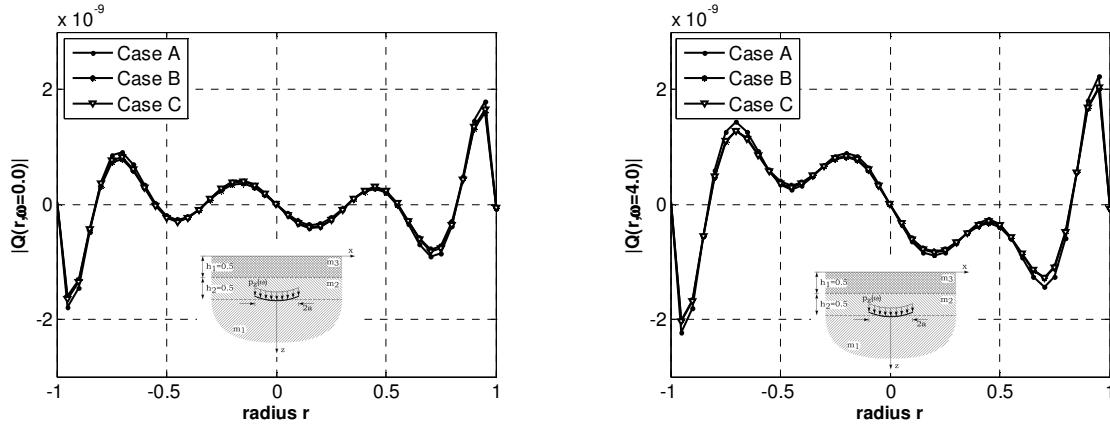


Figure 5.20 Shear force $Q(r)$ acting on a flexible plate for different layered systems for the frequencies $\omega=0.0$ and $\omega=4.0$.

Notice that in all cases the moment $M_r(r)$ and the shear force $Q(r)$ satisfy the boundary conditions of free edge established in Eqs. 5.10 and 5.11. Moreover, the deflections of the plates shown in Figs. 5.14, 5.15 and 5.18 are different from zero at the plate edges ($w(r=1) \neq 0$), which physically agrees with the boundary conditions of free edge (Fig. 5.5c).

Figure 5.18b enables an interesting physical interpretation of the problem. It is straightforward to identify, from that figure, that the most flexible layered problem (Case A) results in the largest displacement amplitudes. In cases B and C, the two layers on top of the plate are stiffer than those in Case A (Fig. 5.17). It can be seen that the displacement amplitude in both cases is smaller for these cases than for Case A, as expected (Fig 5.18b). Moreover, from Case B to Case C, the only difference is that the relative thickness of the layers changes toward the most flexible medium (layer 2). That is, the layered system in Case C is less stiff than in Case B. Consequently, Case C results in a larger displacement amplitude of the plate than Case B (Fig. 5.18b). This behavior is physically consistent and it holds for all results in this section, even though it is more clearly seen in Fig. 5.18b.

In this chapter, a model of thin elastic plates under small deflections was presented. It was shown that the flexible plate can be accurately represented by establishing a variational problem, in which an energy functional involving the strain energy of the plate and of its surrounding medium is minimized according to the principle of minimum potential energy. The influence functions from Chapters 2 and 3 were used to represent transversely isotropic bi-material and layered media in which the plate is considered to be embedded. The present implementation has been validated with a representative source from the literature. The deflection profile of the embedded flexible plate was studied for different bi-material configurations. For the case of a layered system, three different constructions were considered. The behavior of a flexible plate embedded in such media was presented in terms of the deflection, moment and shear force across the plate. It was observed that the present results satisfy the boundary conditions established for the plate.

6 CONCLUDING REMARKS

This chapter shows a summary of what has been presented in this research work. It reviews the main findings, achievements and conclusions of this study.

In the first chapter, it was seen that there are well-established solutions for the displacement and stress fields of different models of continua. Different methods have been used successfully to obtain these solutions corresponding to two- and three-dimensional unbounded domains (full-spaces), and semi-infinite domains possessing a free-surface (half-spaces). Solutions exist for the cases of isotropic or transversely isotropic media, in rectangular or cylindrical coordinates. Some methods to obtain such solutions involve a space transform such as Hankel transforms, together with other techniques such as expanding in Fourier series some specific variables of interest which are involved in the formulation. On the other hand, another group of methods have arisen, which describe the behavior of rigid and flexible circular plates under different types of loadings. These models and the abovementioned solutions have been used to describe the behavior of plates embedded within isotropic and transversely isotropic full- and half-spaces. Little concern has been given to the case of plates embedded in bi-material transversely isotropic media, as well as layered half-spaces, especially the dynamic cases. These are the problems investigated in this study.

In Chapter 2, a classical Green's function of transversely isotropic full-spaces was reviewed. An extension for the bi-material case was provided, as well as simplified particularizations of the main solution for the axisymmetric and antisymmetric cases. It was shown that stress boundary conditions for the case of non-axisymmetric transverse loads can be established based solely on axisymmetric loads (Section 2.3.2.2), and that a case of concentrated moment can be described as an antisymmetric vertical load. It was observed that all loading cases result in equation systems with lengthy analytical solutions. A convenient alternative is to solve these systems numerically. The solution of the displacement fields in these media involves numerical integration of singular integrands, a problem that was successfully averted by including a small damping in the material parameters.

The corresponding solution for a two-dimensional layered half-space was also derived by Wang (1992). In Chapter 3, an extension of his work to the three-dimensional case has been presented. At the end of the chapter, an example was provided, which emphasizes the resemblance of the method to the finite element approach to structural analysis. The example was also useful to understand that the preceding general solution implicitly guarantees the continuity of displacements between the layers.

In Chapter 4, a model of rigid circular plate was introduced. It was seen that a rigid massless plate can be represented by considering a rigid circular surface of the surrounding medium. The tractions acting across this surface can be accurately computed by discretizing it, on each discrete part of which the tractions are assumed to be constant. The chapter showed that the present solution is capable of reproducing accurately previous results from the literature, in which rigid plates embedded in isotropic full-spaces and half-spaces had been considered. Some original research results were presented. It was seen that the aspect ratio of the outer and inner radius of a plate have a significant influence on its behavior, and that the way in which it affects each of the different types of vibration is not obvious *a priori*. It was seen that the transverse isotropy of the media influences each type of vibration differently. Even though one type of transverse isotropy may not influence a specific type of direct compliance term, in a bi-material interface it may influence its cross compliance counterpart. This happens because, in a bi-material interface, the transverse and rocking behaviors of the rigid plate are coupled, and this shows that cross compliance terms must be taken into consideration for a proper analysis of bi-material interfaces. From all the studies, it was observed that a discretization of $M=20$ concentric annular disc elements is enough to provide accurate computation of the traction fields across the plate.

In Chapter 5, a model of elastic plate was presented. Kirchhoff theory of thin plates under small deflections was adopted. A trial solution for the linear partial differential equation which describes the deflection of plate was defined in terms of a power series. In order to obtain the actual deflection of the plate, a variational problem was established. An energy functional involving the strain energy of the plate and of its surrounding medium was defined. The minimization of this functional, under the constraint that it must satisfy the boundary conditions at the plate edge, results in the deflection profile of the plate. The chapter showed that the present solution is capable of reproducing accurately previous results from the literature, in which the

vertical flexure of elastic plates embedded in isotropic full-spaces and half-spaces had been considered. It was observed from the numerical results that the strategy of describing the flexible plate as a variational problem is also capable of producing physically consistent descriptions of the problem also for the cases of transversely isotropic bi-material and layered constructions. The formulation is capable of complying with the imposed boundary conditions. The fairly large range of input data in which the formulation is stable makes it apt to be used in practical engineering problems. For the case of the flexible plate, $N=6$ generalized coordinates was observed to be enough to provide an accurate description of the deflection profile of the plate. When minimizing the energy functional involving the strain energy of the plate and its surrounding medium, it was seen that the convergence of the minimization problem has a negligible dependence of the penalty factor λ , which is responsible for ensuring that the boundary conditions at the plate edge are satisfied. This observation holds for all material constructions that were used in this work.

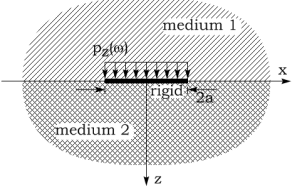
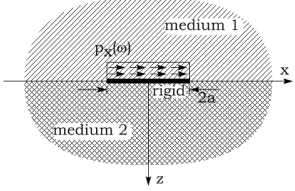
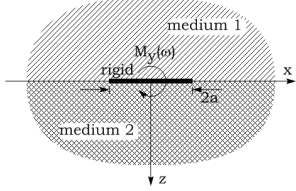
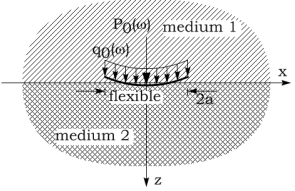
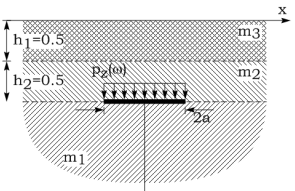
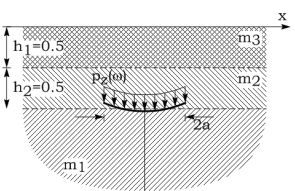
From Chapters 4 and 5, it was observed that the present models are capable of reproducing accurately physical behaviors of embedded plates in elastic media, such as:

- a) stiffening the surrounding medium results in smaller amplitudes of displacement of the plates;
- b) larger frequencies result in a decay in the amplitude of displacement of the plates;
- c) higher damping coefficients stiffen the media and cause an overall decrease in the displacement amplitude compared to the ones with smaller damping coefficients;
- d) in a layered system, changing the relative thickness of the layers so that the stiffer medium is thicker results in an overall stiffer layered medium, which ultimately results in smaller amplitudes of displacement of the plate embedded in it.

Briefly, this work has presented reliable models to study the vertical, transverse and rocking dynamic response of rigid massless circular plates embedded at the interface of two transversely isotropic, three-dimensional, linear viscoelastic half-spaces, or embedded at an arbitrary depth within a multilayered transversely isotropic, three-dimensional, linear viscoelastic half-space. This work also provided a model to study the behavior of elastic circular foundations

embedded in such media. The models that were created in this work are illustrated in Table 6.1. In Table 6.1, the cells containing figures indicate the cases which were formulated and implemented in this work. The cells marked by “Requires implementation” correspond to models that can be obtained after a careful computational implementation of the formulation that was described in this work. The cells marked by “Requires formulation” correspond to models that require a totally different formulation than the ones presented in this work. The models used here to describe the vertical vibrations are based on the theory of plates, the hypotheses of which disregard transverse and rocking behaviors (see hypothesis in Section 5.2). A model of boundary elements would be adequate to treat those cases.

Table 6.1 Models of embedded plates which have been presented in the present work

		Vertical load	Transverse load	Rocking moment
Bi-material	Rigid plate			
	Flexible Plate		Requires formulation.	Requires formulation.
Multilayer	Rigid Plate		Requires implementation.	Requires implementation.
	Flexible Plate		Requires formulation.	Requires formulation.

Since transversely isotropic media provide reasonably good models of soil materials, the presented solutions contribute to the study and design of rigid and flexible circular foundations

and anchors embedded in layered soil. The bi-material solution can be used as an approximation to the case of deeply buried foundations, while the layered system can be used to model foundations at arbitrary embedments, or even resting on the surface of the soil. Different layered constructions involving rocks, clays, ice and other soil materials can be used, and their material attenuation can be included in the model as well. The present model enables practical investigations of the vertical, transverse and rocking vibrations of the foundation embedded in such media.

6.1 Further developments

It is straightforward to see that an immediate development of this work involves the implementation of the cases of coupled transverse and rocking vibrations of the rigid plate in the layered half-space.

An important improvement on the model of flexible plate would be the introduction of a dynamic model of the plate, which takes the mass of the plate into consideration, in order to allow the study of its vibration modes and resonance, for instance. A new set of Ansatz functions to the deflection profile of the plate (Eq. 5.2), aiming to model annular plates, would also be of interest to practical applications.

Further attention could be given to the implementation in order to make it more computationally cost-effective.

If the material attenuation turns out to be a major concern when modeling a practical problem, it would be interesting to introduce an improved damping model. The hysteretic model, which was introduced in the formulation primarily to bypass the problem of the singularities in the integrands, has the pay-off of introducing non-causal responses into the problem.

7 REFERENCES

- Abramowitz, Milton; Stegun, Irene A., eds. *Handbook of Mathematical Functions with Formulas, Graphs, and Mathematical Tables*, New York: Dover, pp. 496, 1965.
- Adolph, M. Síntese de Funções de Green e Estados Auxiliares Viscoelastodinâmicos em Meios Tridimensionais Ilimitados com Auxílio de Transformada de Radon (Synthesis of viscoelastodynamic Green functions and auxiliary states for three-dimensional unbounded domains with aid of the Radon transform). Ph.D. Thesis. State University of Campinas, Unicamp, Brazil, 2006.
- Adolph, M., Mesquita, E., Carvalho, E. R., Romanini, E. Numerically evaluated displacement and stress solutions for a 3D viscoelastic half space subjected to a vertical distributed surface stress loading using the Radon and Fourier transforms. *Communications in Numerical Methods in Engineering* v.23, pp787-804, 2007.
- Anderson, D. L. Elastic Wave Propagation in Layered Anisotropic Media. *Journal of Geophysical Research*, vol. 66, issue 9, pp. 2953-2963, 1961.
- Arnold, R. N., Bycroft, G. N. and Warburton, G. B. Forced vibrations of a body on an infinite elastic solid. *Journal of Applied Mechanics*. ASME. Vol. 22, p. 391-406, 1955.
- Baran, P. A. and Sweezy, P. M. *Monopoly capital: An essay on the American economic and social order*. Harmondsworth: Penguin Books, 1968.
- Barnett, D. M. and Lothe, J. Consideration of the existence of surface wave (Rayleigh wave) solution in anisotropic elastic crystals. *J. Physiscs*, F4(5), 671-686, 1974.
- Barros, P. L. A. *Elastodinâmica de meios transversalmente isotrópicos: Funções de Green e o Método dos Elementos de Contorno na análise da interação solo-estrutura* (Elastodynamics of Transversely Isotropic Media: Green's Functions and Boundary Element Method Analysis of the Soil-Structure Interaction). Ph.D. Thesis, State University of Campinas, Campinas, Brazil, 1997.

- Barros, P. L. A. Impedances of rigid cylindrical foundations embedded in transversely isotropic soils. *International Journal for Numerical and Analytical Methods in Geomechanics*, **30**:683-702, 2006.
- Barros, P. L. A. and Mesquita, E. Elastodynamic Green's Functions for Orthotropic Plane Strain Continua with inclined Axis of Symmetry. *International Journal for Solids and Structures*, **36**:4767-4788, 1999.
- Barros, P. L. A and Mesquita, E. A Non-Singular Version of the Indirect Boundary Element Method Applied to the Stationary Response of Elastic Domains. *Proceedings 13th ASCE Engineering Mechanics Conference*, 13-16 June, , Johns Hopkins University, Baltimore, Maryland, USA, 6 pp., 1999b.
- Barros, P. L. A. Mesquita, E. Singular-Ended Spline Interpolation for 2D Boundary Element Analysis. *International Journal for Numerical Methods in Engineering*, vol.47, n.5, february, pp. 951-967, 2000.
- Bycroft, G. N., Forced vibrations of a rigid plate on a semi-infinite elastic space and an elastic stratum. *Philosophical Transactions of the Royal Society of London. Series A*, Vol. 248, p. 327-342, 1956.
- Chadwick, P. and Smith, G. D. Foundations of the theory of surface waves in anisotropic elastic materials. *Advances in Applied Mechanics*, 17(**5**), 303-376, Academic Press, New York, 1977.
- Christensen, R. M. *Theory of Viscoelasticity*. New York, Dover Publications, 2010.
- Crampin, S., Chesnokov, E. M. and Hipkin, R. G. Seismic anisotropy— the state of the art. *Geophys. J., R. Astr. Soc*, 76(**1**), 1-16, 1984.
- Debnath, L. and Bhatta, D. *Integral Transforms and Their Applications*. Chapman and Hall/CRC; 2nd edition, 728p, 2006.
- Elliot, H. A. Three-dimensional stress distributions in hexagonal aeolotropic crystals. *Proc. Cambridge Philosophical Soc.*, **44**, 522-533, 1948.

- Eskandari-Ghadi, M., Mirzapour, A. and Ardeshir-Behrestaghi, A. Rocking Vibration of a Rigid Circular Disc in Transversely Isotropic Full-Space. *International Journal for Numerical and Analytical Methods in Geomechanics*, **35**; 1587–1603; 2011.
- Eubanks, R. A. and Sternberg, E. On the axisymmetric problem of elasticity theory for a medium with transverse isotropy. *J. Rational Mech. Analysis*, **3**, 89-101, 1954.
- Friedrichs, K. O. Kirchhoff's boundary conditions and the edge effects for elastic plates. *Proc. Symp. Appl. Math*, **3**, 1950.
- Fung, Y. C. and Tong, P. *Classical and Computational Solid Mechanics*, World Scientific Publishing Company, 2001.
- Fung, Y. C. *Foundations of Solid Mechanics*, Prentice-Hall, Englewood Cliffs, 1965.
- Gaul, L. The Influence of Damping on Waves and Vibrations. *Mechanical Systems and Signal Processing*. **13(1)**, 1-30, 1999.
- Graff, K. F. *Wave motion in elastic solids*, Dover Publishing Co., 1974.
- Green, A. E. and Zerna, W. *Theoretical Elasticity*, Clarendon Press, Oxford, 1968.
- Gucunski, N. and Peek, R.; Vertical Vibrations of Circular Flexible Foundations on Layered Media, *Soil Dynamics and Earthquake Engineering*, **12**, 183-192, 1993.
- Hu, H. C. On the equilibrium of a transversely isotropic elastic half-space, *Scientia Sinica*, **3**, 463-479, 1954.
- Kausel, E. and Peek, R. Dynamic loads in the interior of a layered stratum: an explicit solution, *Bull. Seism. Soc. Am.*, **72** 1459-1481, 1982.
- Kirchhoff G. Über das Gleichgewicht und die Bewegung einer elastischen Scheibe. *J. Reine und Angewandte Mathematik*, 40:51-88, 1850.
- Labaki, J., Romanini, E. and Mesquita, E. Stationary Dynamic Displacement Solutions for a Rectangular Load Applied within a 3D Viscoelastic Isotropic Full Space—Part II: Implementation, Validation, and Numerical Results. *Mathematical Problems in Engineering*, Volume 2012, 2012.

- Lekhnitskii, S. G. Theory of anisotropic elastic bodies, *Holden-Day Publishing Co.*, San Francisco, California, 1963.
- Luco, J. E. and Westmann, R. A. Dynamic response of circular footings. *J Engng Mech ASCE*, 97(5), 1381-95, 1971.
- Luco, J. E. Impedance functions for a rigid foundation on a layered medium, *Nuclear Engineering and Design*, 31, 204-217, 1974.
- Lysmer, J. *Vertical Motions of Rigid Footings*, Ph.D. Thesis, University of Michigan, Ann Harbor, United States, 1965.
- Marques de Barros, R., *Funções de Green e de Influência para meios visco-elásticos transversalmente isotrópicos no domínio da frequência* (Green's functions and influence functions for viscoelastic, transversely isotropic media, in the frequency domain). Ph.D. Thesis, State University of Campinas, Campinas, Brazil, 2001.
- Mesquita, E. *Zur Dynamischen Wechselwirkung von Fundamenten auf dem Viskoelastischen Halbraum*. (On the Dynamic Interaction of Foundations on the Viscoelastic Half-Space), Ph.D. thesis, Institut für Mechanik, Universität Hannover, Hannover, Germany, 1989.
- Mesquita, E., Adolph, M., Almeida Barros, P. L. and Romanini, E. Transient Green and Influence Functions For Plane Strain Visco-Elastic Half-Spaces. *Proceedings of the IABEM SYMPOSIUM 2002*, The University of Texas at Austin, Texas, May 28-31, 2002, pp.1-1, 2002.
- Mesquita, E., Adolph, M. Barros, P. L. A and Romanini, E. Transient Green's Functions and Distributed Load Solutions for Plane Strain, Transversely Isotropic Viscoelastic Layers. *Latin American Journal of Solids and Structures*, 1:75-100, 2003.
- Mesquita, E. and Romanini, E. Green's function approach versus direct boundary element scheme to model the dynamic interaction of foundations resting on a viscoelastic layer over a bedrock. *Proc. IABEM (International Conference on Boundary Element Methods)*, 3-6 november, Seville, Spain, vol.2, pp. 107-121, 1992.
- Mesquita, E., Romanini, E. and Labaki, J. Stationary Dynamic Displacement Solutions for a Rectangular Load Applied within a 3D Viscoelastic Isotropic Full Space—Part I: Formulation. *Mathematical Problems in Engineering*, Volume 2012, 2012.

- Mitchell, J. K. and Soga, K. *Fundamentals of Soil Behavior*. 3rd Edition. Wiley, 2005.
- Muki, R. Asymmetric problems of the theory of elasticity for a semi-infinite solid and a thick plate. I.N. Sneddon, R. Hill (Eds.), *Progress in Solid Mechanics*, Vol. 1 North Holland, Amsterdam, pp. 399–439, 1960.
- Nash, S. G. *Penalty and Barrier Methods*, Wiley Encyclopedia of Operations Research and Management Science, 2010.
- Pak, R. Y. S and Gobert, A. T. Forced Vertical Vibration of Rigid Discs with Arbitrary Embedment, *J. Eng. Mech*, **117**, issue 11, 2527, 1991.
- Payton, R. G., *Elastic Wave Propagation in Transversely Isotropic Media*. The Hague: Martinus Nijho, 1983.
- Piessens, R, Doncker-Kapenga, E. D. and Überhuber, C. W. *QUADPACK: a subroutine package for automatic integration*. Springer, 1983.
- Rajapakse, R. K. N. D; Wang. Y. Green's Functions for Transversely Isotropic Elastic Half Space. *Journal of Engineering Mechanics*, **119**, No. 9, pp. 1724-1746, 1993.
- Rajapakse, R. K. N. D. The Interaction Between a Circular Elastic Plate and a Transversely Isotropic Elastic Half-Space. *International Journal for Numerical and Analytical Methods in Geomechanics*, **12**, 419-436, 1988.
- Romanini, E. *Síntese de funções de influência e Green para o tratamento da interação dinâmica solo-estrutura através de equações integrais de contorno*. Ph.D. Thesis, State University of Campinas, Campinas, Brazil, 1995.
- Seale, S. H. and Kausel, E. Point loads in cross-anisotropic layered half-spaces, *J. Engrg. Mech. ASCE*, **115**, 509-524, 1989.
- Senjuntichai, T. and Sapsathiarn, Y. Forced Vertical Vibration of Circular Plate in Multilayered Poroelastic Medium, *J. Eng. Mech.*, 129(11), 1330–1341, 2003.
- Selvadurai, A. P. S. *Elastic Analysis of Soil-Foundation Interaction*, Elsevier, Amsterdam, 1979a.
- Selvadurai, A. P. S. The interaction between a uniformly loaded circular plate and an isotropic elastic halfspace: A variational approach. *J. Struct. Mech.*, 7, 231-246, 1979b.

- Selvadurai, A. P. S.; An energy estimate of the flexural behaviour of a circular foundation embedded in an isotropic elastic medium. *International Journal of Numeric and Analytic Methods in Geomechanics*, **3**, 285-292, 1979c.
- Selvadurai, A. P. S. The eccentric loading of a rigid circular foundation embedded in an isotropic elastic medium, *International Journal for Numerical and Analytical Methods in Geomechanics*, **4**, Issue 2, 121-129, 1980.
- Selvadurai, A. P. S. Elastic contact between a flexible circular plate and a transversely isotropic elastic half-space, *Int. J. Solids Struct.*, **16**, 167-176, 1980b.
- Selvadurai, A. P. S. and Singh, B. M. Some Annular Disc Inclusion Problems in Elasticity, *International Journal of Solids and Structures*, **20**, n 2, 129-139, 1984.
- Slaughter, W. S. *The Linearized Theory of Elasticity*, Birkhäuser Boston, **16**, 543 p, 2002.
- Sommerfeld, A., *Partial Differential Equations*, Academic Press, New York, 1949.
- Stoneley, R. Elastic waves at the surface of separation of two solids. *Proc. R. Soc.*, **106**, Issue 738, pp. 416-428, 1924.
- Thomazo, L. H. *Formulação do Método dos Elementos de Contorno Indireto para Resposta Transiente de Meios Visco-elásticos* (Formulation of Transient Response in 2D Viscoelastic Medium using Indirect Boundary Element Method). M.Sc. Dissertation, State University of Campinas, Campinas, Brazil, 2004.
- Timoshenko, S. and Woinowsky-Krieger, S. *Theory of Plates and Shells*, McGraw-Hill Classic Textbook Series, 1964.
- Van der Heijden, A. M. A. *On modified boundary conditions for the free edge of a shell*, Delft University Press, 1976.
- Wan, F. Y. M. Stress boundary conditions for plate bending. *International Journal of Solids and Structures*, **40**, 4107–4123, 2003.
- Wang, Y. *Fundamental Solutions for Multi-Layered Transversely Isotropic Elastic Media and Boundary Element Applications*. Ph.D. Thesis, University of Manitoba, Winnipeg, Canada, 1992.

- Wood, D. M. Soil Behaviour and Critical State Soil Mechanics. Cambridge University Press, 1990.
- Wass, G. *Linear two-dimensional analysis of soil dynamics problems in semi-infinite layered media*. Ph.D thesis, University of California, Berkeley, California, 1972.
- Wass, G. *Dynamics Belastete Fundamente auf Geschichteten Baugrund*, VDI Berichte, **381**, 185-180 (in German), 1980.
- Wu, D. Z, Cai, Y. G, Xu, C. J. and Zhan, H. Torsional vibrations of rigid circular plates on transversely isotropic saturated soil, *Applied Mathematics and Mechanics*, 27(**11**):1541–1548, 2006.
- Zeng, X. and Rajapakse, R. K. N. D. Vertical vibrations of a rigid disk embedded in a poroelastic medium, *International Journal for Numerical and Analytical Methods in Geomechanics*, **23**, 2075-2095, 1999.